Investigation of the Time-Dependent Longitudinal Flexural Behavior of the Varina-Enon Bridge

Seth Michael Lindley

Thesis submitted to the faculty of the Virginia Polytechnic Institute and State University in partial fulfillment of the requirements for the degree of

Master of Science

In

Civil Engineering

Carin L. Roberts-Wollmann (Chair)

Ioannis Koutromanos

Matthew H. Hebdon

June 6th, 2019

Blacksburg, VA

Keywords: Prestressed concrete, Prestress loss, Creep, Shrinkage, Varina-Enon,

Investigation of the Time-Dependent Longitudinal Flexural Behavior of the Varina-Enon Bridge

Seth M. Lindley

ACADEMIC ABSTRACT

Prestress loss due to creep, shrinkage, and relaxation can cause serviceability issues, and in the case of externally post-tensioned structures, can reduce the flexural capacity. The accurate estimation of these prestress losses is vital for making good decisions about the remaining life of a structure.

The Varina-Enon Bridge is a post-tensioned concrete box-girder bridge in Richmond Virginia. Flexural cracks in the bridge prompted an investigation into the magnitude of prestress loss experienced by the structure. Long-term prestress losses are estimated using two methods. First, a finite element model is created, and multiple code expressions for creep and shrinkage are applied to a time-step analysis of the structure. The code expressions investigated in this thesis are taken from the CEB-FIP 1978, CEB-FIB 1990, and AASHTO codes. The second method utilizes data from sensors previously installed on the bridge to back-calculate the effective prestressing force.

The analysis utilizing the CEB-FIP 78 code expression for creep and shrinkage estimated prestress loss of 41.9 ksi. This represents the model code used in the original design of the Varina-Enon Bridge. The analyses utilizing the CEB-FIP ’90 and AASHTO code expressions estimated prestress losses of 43.3 ksi and 38.1 ksi respectively. Lastly the average prestress loss calculated from the field data was found to be 47.3 ksi. It can be seen that all three finite element analyses underestimated prestress loss compared to the results of field data estimations, but given the level of uncertainty in each estimation method, the results are considered to match well. Flexural capacity using the prestress loss estimated by the field measurement system meets AASHTO Strength I Load Combination demands, with demand-to-capacity ratios of 0.95 and 0.147, for positive and negative critical sections respectively.

Investigation of the Time-Dependent Longitudinal Flexural Behavior of the Varina-Enon Bridge

Seth M. Lindley

GENERAL ABSTRACT

Post-tensioned concrete is a building technology which provides a compressive force to concrete via steel tendons. This combination of steel and concrete allows for the construction of lighter and stiffer structures. Post-tensioned concrete is widely utilized throughout the United States highway system and bridge construction. Over time, the force in the prestressing strands is reduced by delayed strains in the concrete. The accurate estimation of this *prestress loss* is vital for making good decisions about the remaining capacity of a structure and the infrastructure system at large.

The Varina-Enon Bridge is a post-tensioned concrete box-girder bridge in Richmond Virginia. Cracks in the bridge prompted an investigation into the magnitude of prestress loss experienced by the structure. To estimate prestress loss, a computer model of the structure was created. In addition, data from sensors previously installed on the bridge were used to back calculate prestress loss.

It was found that the estimation of losses from the field closely matched those estimated at the construction of the bridge. Additionally, more updated loss models estimated similar, or slightly smaller values for prestress loss.

ACKNOWLEDGEMENTS

I would like to thank the Virginia Department of Transportation for their support on this project, providing documentation on the design and construction of the Varina-Enon Bridge. I would also like to thank Nishant Tamakuwala who's work and report on the Varina-Enon Bridge, though unpublished, provided preliminary information for this thesis. Thank you also to Drs. Roberts-Wollmann and Koutromanos for your guidance and support throughout this process. I learned a great deal from both of your expertise.

Lastly, I would like to thank Leah. Your support brings completeness to my life in the most difficult of times.

TABLE OF CONTENTS

LIST OF FIGURES

LIST OF TABLES

Chapter 1.
Introduction

In this chapter, the major concepts, motivation, and project purpose are introduced. In the first section, the concepts of prestressed concrete, and prestress losses are introduced, and the motivation for this research project is presented. In the second section, the Varina-Enon Bridge is described. And in the third section, the project goals and scope are outlined.

1.1 Motivation

Prestressed concrete is a composite material which utilizes steel strands to provide a pre-compression to concrete elements. This technique produces lighter and stiffer concrete structures. Patents for prestressed technology were filed as early as 1886, but wide use of prestressed concrete was limited throughout the early 20th century because prestress losses were significant in relation to the ultimate strength of the steel strands. With the advent of high-strength steels, however, the use of prestressed concrete became widespread in Europe and America starting in the 1940s. (Naaman 2012).

Since its inception, prestressed concrete has been adopted in every major building sector. It has been exceptionally effective in the Federal Highway System, where it is a predominant method for constructing short to mid-length bridge spans. As this infrastructure ages, however, it is important that professionals are able to accurately assess the remaining service life of prestressed bridges. One key aspect of the structural evaluation of prestressed bridges is the accurate prediction of *prestress losses*. Significant prestress losses can affect the serviceability of structures by causing cracking and excessive deflections, while, in post-tensioned structures with un-bonded tendons, prestress losses can also reduce the structures' ultimate strength.

1.1.1 Prestress Loss

Prestress losses in concrete structures come from multiple sources, but the long-term losses caused by creep and shrinkage are the most difficult to predict. Creep is a volumetric change which occurs, primarily, due to loading applied over an extended period of time. Shrinkage is a volumetric change which occurs due to the loss of water in the pore structure of the concrete. These phenomena result in a shortening of the prestressed member causing long-term losses in the prestressing strands. These long-term losses are estimated using analytical models which describe the development of creep and shrinkage with time.

The most striking example of the consequences of long-term losses is the collapse of the Koror Babeldaob Bridge, seen in Figure 1.1. After 18 years in service, the bridge had a mid-span deflection of 5.3

ft caused, in large part, by creep and shrinkage. This deflection did not constitute a structural concern, but the remedial prestressing carried out to reduce the mid-span sag ultimately compromised the integrity of the structure. On September 26th, 1996 the bridge collapsed catastrophically, killing two people.

Figure 1.1. (Left) Koror-Babeldaob Bridge prior to collapse. (right) Koror-Babeldaob Bridge after collapse. (OPAC 2000)

1.2 Varina-Enon Bridge

The Varina-Enon Bridge (VEB) is a cable-stayed, segmentally-constructed, post-tensioned box-girder bridge. The VEB spans the James River, connecting Chester and Henrico Virginia at mile marker 18 along Interstate 295. Figure 1.2 shows an aerial view of VEB which carries six lanes of traffic via two parallel box girders. The VEB was designed by Figg and Muller Engineers beginning in 1985 and was opened to traffic on July 18, 1990.

Figure 1.2. Aerial view of the Varina-Enon Bridge over the James River.

The total length of the bridge is 4,680 ft, and it is composed of 28 spans. Seven of these spans make up the cable-stayed, *main span* of the structure. The remaining 21 spans make up the *approach units* of the bridge. On the South end of the bridge, two six-span-continuous approach units make up the southernmost 12 spans of the bridge. The focus of this study is on the Eastern box-girder in the southernmost approach unit, as shown in Figure 1.3. This approach unit is made up of six 150-ft spans, resulting in a total length of 900 ft. Piers and spans are numbered sequentially, beginning with the southernmost elements, as seen in Figure 1.3.

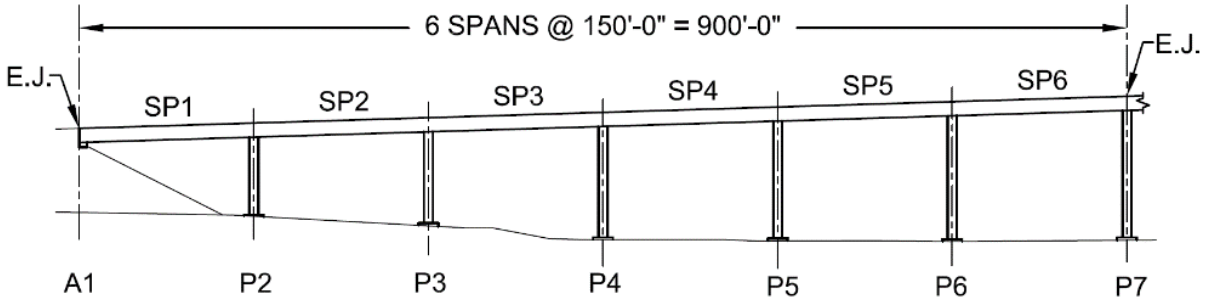

Figure 1.3. Elevation of the southernmost approach unit.

The approach unit of the VEB is composed of seven 20-ft precast segments. These segments were match-cast in a long-run configuration and placed using steel launch trusses (seen in Figure 1.4). Segments were epoxied at the joints as each was placed, then the span was post-tensioned. Typical precast segments are shown in Figure 1.4 and Figure 1.5 and are located between piers. *Pier segments*, which are located atop each pier, have the same outer dimensions as the *typical segments* but contain diaphragms on the interior which act as anchorages for the longitudinal post-tensioning.

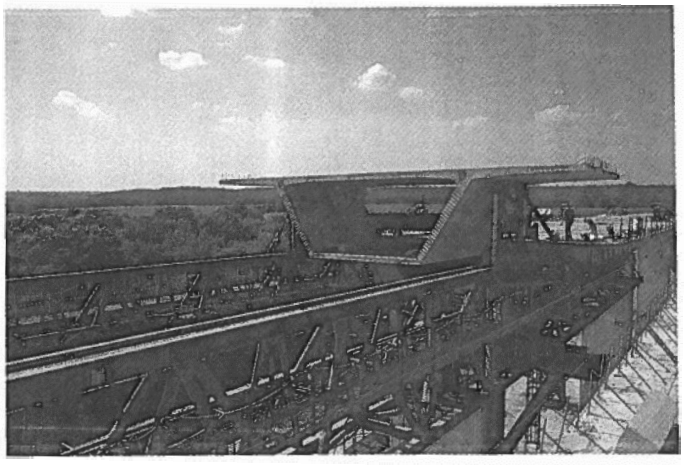

Figure 1.4. Construction of approach spans (F&M Engineers 1993).

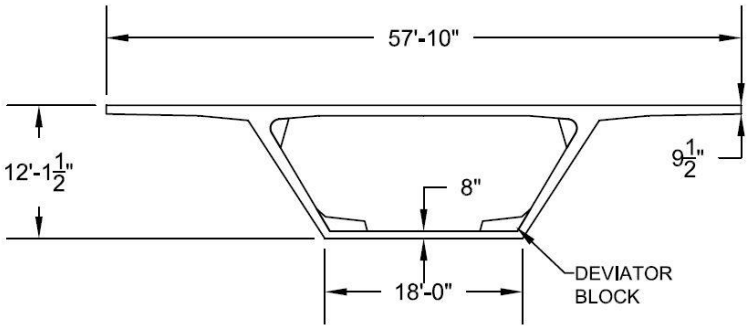

Figure 1.5. Typical approach-unit, precast section.

Longitudinal post-tensioning of the VEB consists of eight external tendons in each span. Each tendon contains (19) 0.6 in. diameter strands. Tendons are located in the interior of the box girder cell and are deviated via blocks at the bottom of the section as seen in Figure 1.5. Figure 1.6 shows the configuration of tendons in Span 6, as well as the longitudinal locations of deviator blocks. Figure 1.6 also illustrates how the tendons provide continuity to the structure over pier supports. At the location of Pier 6, the tendons in Span 5 and Span 6 overlap in the diaphragm of the pier segment. As each span was constructed, this overlap provided continuity to the structure. As-built drawings of the two sections in the approach structure and the three unique tendon layouts can be found in Appendix C.

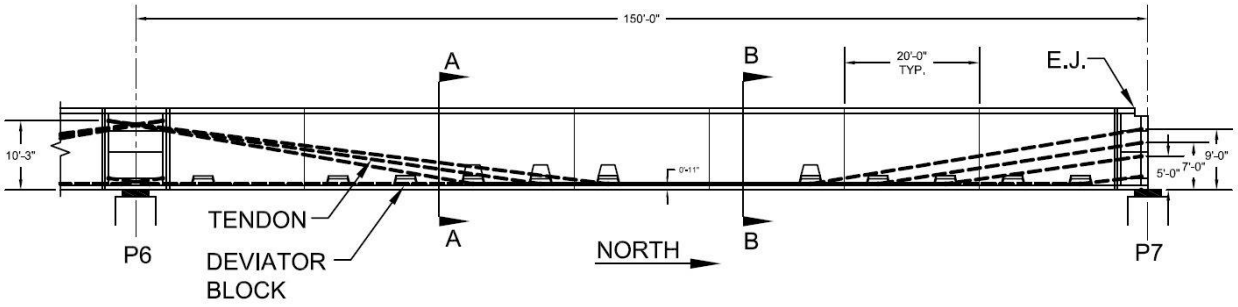

Figure 1.6. Section view of Span 6, (tendons shown by the dashed line).

Tension cracks on the bottom flange of the VEB were identified by the Virginia Department of Transportation in 2012. Though these cracks were partially attributed to large thermal gradients, the literature suggests that large segmentally-constructed box girders are known to experience larger-than-expected creep deflections (Bažant et al. 2011). With this in mind, it is vital that the remaining service life of the VEB be assessed. At 27 years old, the VEB should remain in service for decades to come. Left unchecked, however, excessive prestress loss can shorten the life of the bridge and cause safety risks.

1.3 Purpose, and Scope

The purpose of this research is to investigate the time-dependent longitudinal flexural behavior of the Varina-Enon Bridge. The final goal of which is to estimate the longitudinal prestress loss using existing flexural cracks, and to compare these losses to those estimated by a finite element model of the six-span approach unit. The scope of this research includes the following:

- Estimating longitudinal prestress losses using data gathered from field measurements.
- Developing a finite element model, and evaluating prestress loss using multiple code expressions for creep and shrinkage.
- Evaluating, reinstalling and expanding instrumentation on the VEB.
- Providing recommendations for continued research on the VEB.

Chapter 2.

Literature Review

The literature surrounding prestressed concrete and long-term prestress losses is extensive. This chapter provides a review of this literature, as well as several other areas which inform this research project. First, the topics of creep, shrinkage and prestress loss are covered. Second, the experimental methods of prestress loss measurement are reviewed. Third, the relevant literature on stresses induced by thermal gradients is summarized. Last, the previous research on the VEB is outlined.

2.1 Creep and Shrinkage

Creep and shrinkage cause delayed strains in concrete which result in deflections and prestress losses in bridge structures. These strains progress at a decreasing rate over time, as seen in Figure 2.1. A number of analytical models have been developed over the years to describe this process, all of which take into account material properties and environmental conditions. Each model, however, considers slightly different aspects of the material and uses different functions to describe the progression of creep and shrinkage with time.

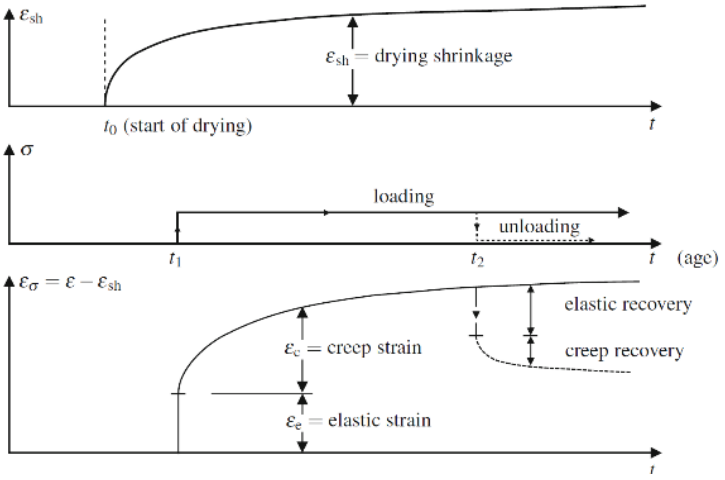

Figure 2.1. Creep and shrinkage response with respect to time (Bažant and Jirasek 2018).

Creep is described analytically by a stress-independent term called the *compliance function*, $J(t,t_o)$. This function describes creep strain for unit stress and thus can be used to model creep strains for any given stress. A generalized version of the compliance function is shown in Equation (2.1), where $\phi(t,t_o)$ represents the *creep coefficient*, and E_x represents some variation of the elastic modulus. Additionally, the term, t represents the time of interest, and t_o represents the time when the structure was loaded, both in units of

days. The compliance function for each model code varies, depending on what value of elastic modulus is used, and how the creep coefficient is calculated.

$$J(t,t_o) = \frac{1+\phi(t,t_o)}{E_x} \tag{2.1}$$

Because shrinkage does not depend on the stress in the concrete, strains due to shrinkage are simply a function of the time of drying and the material properties. Total shrinkage strains, $\varepsilon_{sh}(t,t_o)$, are defined in all models by a bounded function which approaches some ultimate value.

2.1.1 Review of Creep and Shrinkage Models

For the purposes of this thesis, CEB-FIP '78, CEB-FIP '90, ACI 209, AASHTO and B3 creep and shrinkage models are reviewed and compared. CEB-FIP '78 is the model code used for the design of the VEB, while the remaining four represent the most widely used models in current use.

CEB-FIP '78 model code was published by the Comité Euro-International Du Béton in 1978. The CEB-FIP '78 code expression for creep and shrinkage was adopted in the commentary of the AASHTO Guide Specifications for Design and Construction of Segmental Concrete Bridges, 1st edition. This model was widely used in the United States throughout the 1980s. The creep coefficient, in this model code, depends on ambient relative humidity, volume-to-surface ratio of the section, and concrete strength development. The time development of creep is defined graphically by a bounded asymptotic function which approaches an ultimate value and is defined for an age up to 10,000 days (CEB-FIP 1978).

The CEB-FIP '90 is an updated version of the 1978 code expression for creep and shrinkage which includes provisions for high-strength concretes. Again, the time-development of both creep and shrinkage are defined by a bounded function which approaches an ultimate value. The graphical depictions of these functions, however, are replaced with the functions themselves. The ultimate value of the creep coefficient depends on the ambient relative humidity, volume-to-surface ratio of the section, concrete strength development, cement type, and aggregate type (ACI 209 2008).

The ACI 209R-92 model was developed by Branson and Christianson (1971) and was adopted by the American Concrete Institute in 1992. Like both CEB-FIP models, the ACI time-development of creep and shrinkage is defined by an asymptotic function. The ultimate value of this function depends on ambient relative humidity, volume-to-surface ratio of the section, type of curing process, fine-aggregate content, and air content (ACI 209 2008).

The AASHTO 2012 code expression for creep and shrinkage is based on the ACI model with modification suggested by more recent research on the subject (AASHTO 2012). This model only takes

into account ambient relative humidity, volume-to-surface ratio of the section, and concrete strength. Like all previous models, the time-development of creep and shrinkage are defined by asymptotic functions.

The B3 model was proposed by Bažant and Baweja (1995). This model is the most detailed of the five models, and breaks creep compliance into basic and drying creep functions. A large number of material properties are considered in the B3 model including cement content, water-to-cement ratio, and aggregate-to-cement ratio. In addition to these values the cement type, curing conditions, and ambient relative humidity are also considered. The B3 model differs from the previous models by its use of the asymptotic elastic modulus in the formulation of the compliance function, and by its use of a logarithmic function for the time-development of creep. The B3 model defines the asymptotic modulus as $E_{cm28}/0.6$. This variable represents the modulus for an instantaneously applied stress.

2.1.2 Comparison of Creep Compliance Functions

In order to convey the relative behavior of the creep described in these models, the compliance function of each has been graphed in Figure 2.2. These compliance functions have been computed for the typical section of the VEB which is pictured in Figure 1.5. A theoretical concrete mix which consisted of type III cement, limestone aggregate, and a water-to-cement ratio of 0.45 was assumed.

Several important notes can be made in Figure 2.2 which, it should be noted, is plotted on a semi-log scale. First, the slope of the compliance functions at 10,000 days can be seen to vary widely. With that said, CEB-FIP, ACI, and AASHTO models appear to be relatively flat, while the B3 model has a constant positive slope. This difference is due to the different time-development functions which describe creep. Second, the compliance from the B3 model is significantly higher than that of the other models. A more detailed description of each creep and shrinkage model can be found in Appendix A.

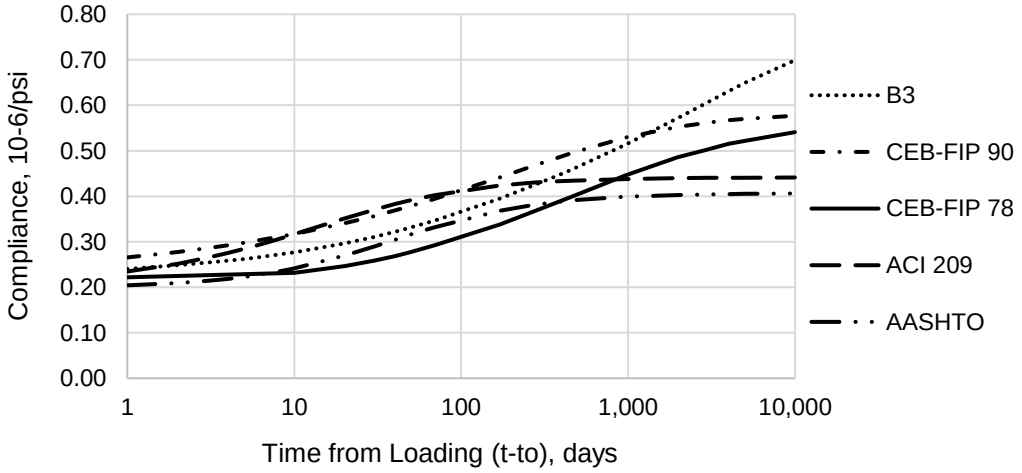

Figure 2.2. Comparison of compliance functions.

2.2 Prestress Losses

Total prestress loss for a post-tensioned concrete structure is categorized, generally, into *Instantaneous losses* and *long-term losses*, as seen in Equation (2.2). Instantaneous losses occur during the construction process, or shortly thereafter, and include friction and seating losses (Δf_{pFS}), and elastic shortening losses (Δf_{pES}). The mechanics of these losses are well known and will not, therefore, be explained at length in this thesis. Long-term losses, which are the focus of this study, begin at the moment of stressing, and continue throughout the life of the structure. These Long-term losses are made up of *creep losses* (Δf_{pCR}), *shrinkage losses* (Δf_{pSH}), and *relaxation losses* (Δf_{pRE}). The seminal document which outlines the methods for calculating prestress loss is ACI 423.10R *Guide to Estimating Prestress Losses* (ACI 423 2016).

$$\Delta f_{pT} = \underbrace{\Delta f_{pFS} + \Delta f_{pES}}_{\text{Short-term losses}} + \underbrace{\Delta f_{pCR} + \Delta f_{pSH} + \Delta f_{pRE}}_{\text{Long-term losses}} \tag{2.2}$$

Several methods for calculating long-term prestress losses have been developed over the years. At the beginning of code development, long-term losses were calculated as a lump-sum value which depended only on the level of stress in the steel and concrete. These calculations were first outlined by the Bureau of Public Roads in 1954 and can be seen in Equation (2.3). This method, however, does not take into account any of the properties of the concrete itself and is only used today for preliminary design.

$$\Delta f_{pT} = 3000 + 11 f_{cps} + 0.04 f_{pi} \text{ (psi)} \tag{2.3}$$

Where:

f_{cps} is the concrete stress at the center of gravity of the prestressing force due to all loads.

f_{pi} is the initial stress in the prestressing steel.

A simplified method for estimating long-term losses is allowed for structures under normal design conditions. This method is more accurate than the lump-sum method and is accepted in modern design but makes many simplifying assumptions about material properties. This method intends to "reasonably estimate" the losses due to creep, shrinkage, and relaxation individually. Losses depend primarily on *K* factors for creep, shrinkage, and relaxation which are taken from tables and depend on the type of concrete, the age at load application, and the type of prestressing steel.

The most accurate methods of estimating prestress loss directly consider the creep, shrinkage, and relaxation models for the materials being used. These methods can generally be categorized into time-step

methods and age-adjusted effective modulus methods. The age-adjusted effective modulus method modifies the modulus of elasticity using the creep coefficient and a term called the aging coefficient (χ) to calculate the total long-term strains due to a load. This age-adjusted modulus can be seen in Equation (2.4).

$$E''_c = \frac{E_c}{1 + \chi\phi(t, t_0)} \tag{2.4}$$

The time-step method, like the age-adjusted effective modulus method, directly utilizes creep and shrinkage models as described in Chapter 2.1. This method is unique in that it breaks the life of the structure down into discrete periods of time and calculates the creep and shrinkage strains at each discrete time step. The time-dependent strains are then added to the mechanical strains to determine the total change in length and curvature of the structure. The prestress losses are then used to update the stresses for use in the next time-step calculation. This incremental process accounts for the fact that the rate of prestress loss due to one effect such as creep, is altered by losses due to the other two effects, relaxation and shrinkage (Naaman 2012).

2.3 Measuring Effective Prestress Force

Effective prestress force is defined as the remaining prestress force at some specific time of interest in the life of a structure. Measuring effective prestress force is an integral part of assessing a bridge's remaining service life. Many methods of measuring effective prestress have been studied throughout the years. The most relevant of these studies are summarized in the ACI committee *423 Guide to Estimating Prestress Losses* (2016). The two most well-established methods of measuring effective prestress force in the literature are the use of embedded vibrating wire gages (VWGs) and the use of crack-reopening load tests.

2.3.1 Embedded Vibrating Wire Gage Measurement

The measurement of effective prestress by the use of embedded VWGs involves tracking the forces in the prestressing strands from the time of initial stressing. These forces are calculated from strains measured via VWGs adhered directly to the prestressing strands or to other bars in the structure. These gages are then cast into the members, and track the loss of prestressing over time. This method requires the involvement of researchers from the time of casting and has been historically used to validate prestress loss estimation formulas. Since most structures are not cast with embedded VWGs, this is not a viable method of measuring effective prestress force for the majority of bridges.

Garber et al. (2015) instrumented 30 precast specimens with VWGs to investigate prestress losses over a period of 3 years. The goals of this research were to investigate the effect of various parameters on prestressed loss and to compare service load methods of loss calculations to VWG methods. Specimens were either 40 in. standard AASHTO I-girders, or 46 in. bulb-T cross-sections. All beams were 45 ft long. VWGs were embedded into the cross sections of the specimens at the time of casting and set in storage for up to 3 years. After this period of time, the specimens were tested to cracking loads. The effective prestress was then calculated using these crack reopening test, and the results were compared to the effective prestress measured from VWGs. Researchers determined from this study that effective prestress can be measured accurately using service-load tests as well as the embedded VWG method (Garber et al. 2015).

2.3.2 Method Utilizing Crack Re-opening

The most well-established method for measuring effective prestress is by means of loading and re-loading the beam to the point of cracking and re-cracking. The load and the geometry of the beam at the instant of crack re-opening are then used to calculate effective prestressing force by assuming zero stress at the extreme tension fiber. Prestress loss can then easily be calculated from the effective prestress force if initial jacking force is known.

The configuration for the crack re-opening test method, as conducted by Pessiki et al. (1996), can be seen in Figure 2.3. The test procedure consisted of loading a simply-supported beam in three-point bending. First, the beam was loaded to the point of the first occurrence of flexural cracking as identified by visual inspection. After the cracks were located and marked, the beam was unloaded. The beam was then instrumented with electric-resistance strain gages adjacent to cracks, LVDT spanning cracks, or a combination of both. The beams were then repeatedly loaded to the point of crack re-opening as measured by strain gages, LVDTs, and visual inspection. (Pessiki et al. 1996). Though some variation exists, this set-up represents the general procedure of tests employing this method.

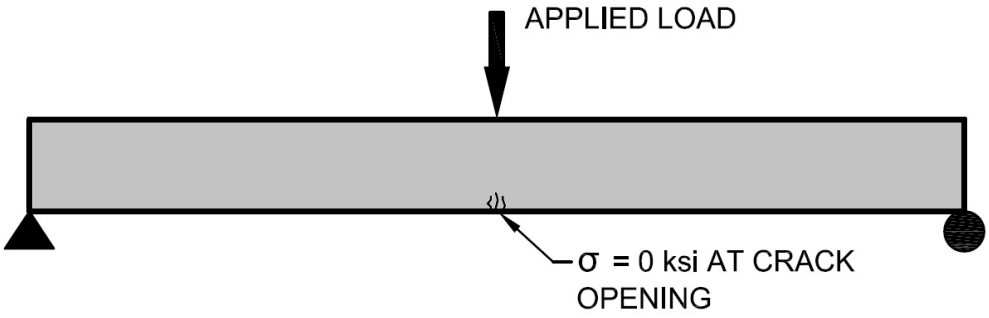

Figure 2.3. Testing configuration employed by Pessiki et al. (1996).

The applied load measured at the occurrence of crack re-opening is then used in Equation (2.5). At the instant of crack re-opening, the stress in the extreme tension fiber is zero. This fact is used to simplify and rearrange Equation (2.5), to solve for the prestress force at mid-span of the beam, as seen in Equation (2.6).

$$\sigma = -\frac{P_e}{A} - \frac{P_e e y}{I} + \frac{M_{sw} y}{I} + \frac{M_{applied}\, y}{I} \tag{2.5}$$

Where P is the effective prestress force
A is the cross-sectional area
e is the prestressing eccentricity
y is the distance from the neutral axis to the depth in question
I is the beam moment of inertia
M_{sw} is the moment due to self-weight
$M_{applied}$ is the moment due to the applied load

$$P_e = \frac{(M_{sw} + M_{applied})y}{I}\left(A + \frac{I}{ey}\right) \tag{2.6}$$

2.3.3 Research Employing Crack Re-opening Tests

A number of studies which utilize equation (2.6) have been conducted. This research is summarized by ACI committee 423 in the 2016 document *423.10R Guide to Estimating Prestress Losses*. This summary includes studies which employed a variety of measurement methods, beam ages, and span lengths. Table 2.1 summarizes the relevant research conducted using methods similar to Pessiki et al.

Table 2.1. Summary of research employing crack re-opening tests.

Researchers	Number of beams tested	Age of beams, yr	Length of beams, ft
Shenoy and Frantz 1991	2	27	54
Tabatabai and Dickson 1993	1	34	43
Pessiki et al. 1996	2	28	89
Halsey and Miller 1996	2	40	29
Azizinamini et al. 1996	1	25	55
Labia et al. 1997	2	20	70
Greuel et al. 2000	1	0.5	115.5
Eder et al. 2005	2	45	50
Kukay et al. 2010	8	40	34.5
Attanayake and Aktan 2011	1	49	48
Osborn et al. 2012	7	42	24
Garber et al. 2015	30	3	45.5

The majority of the tests summarized in Table 2.1 were conducted on pre-tensioned I-girders and box girders. All of the tests were conducted in simple span configurations in lab settings. To-date, no studies have employed crack re-opening tests on continuous-span structures or on in-service bridge girders. The following is a detailed summary of the relevant studies which have been conducted using crack re-opening tests.

The test setup employed by Pessiki et al. (1996) is described above. Researchers found that strain gages adjacent to flexural cracks typically measured decompression at lower loads than LVDTs, and likewise, that LVDTs measured decompression at lower loads than did visual observations. It was also found that the gage length of strain gages had no effect on the determination of decompression load (Pessiki et al. 1996). In total, it was found that the AASHTO Bridge Specifications (1992) as well as the PennDOT design manual, overestimated prestress losses by as much as 60%. (Pessiki et al. 1996)

Tabatabai and Dickson (1993) conducted load testing on a 34-year-old, 43 ft. long, post-tensioned I-girder. The purpose of this study was to evaluate the remaining prestressing force in the tendons as well as to measure the cracking and ultimate flexural strengths of the beams. The girder was loaded in a four-point bending, simple-span configuration. The first cracking event was measured by an accelerometer. The girder was then unloaded and instrumented with a crack gage to measure decompression at the mid-span crack. Data resulting from these tests indicated actual prestress loss of 29 ksi. Prestress loss calculations at the time of design estimated a loss of 25 ksi, which translates to a 14% underestimation. Calculations conducted using Section 9.16 of the fifteenth edition of the AASHTO Specifications resulted in losses of 33.2 ksi, which translates to a 14% over-estimation. (Tabatabai and Dickson 1993)

Shenoy and Frantz (1991) conducted structural testing on two 27-year-old prestressed concrete box girders. Among other things, the tests were conducted to measure the remaining prestress force in the girders. The beams were 36 in. wide by 27 in. deep and measured a length of 54 ft. The girders were tested in a simple-span configuration and were loaded at third points. Results from these tests were used to calculate effective prestress. This study indicated that the calculations from code expressions for creep and shrinkage generated a conservative estimation of losses, and that the actual prestress losses were as low as 50% of what was expected (Shenoy and Frantz 1991).

Halsey and Miller (1996) conducted load testing on two 40-year-old pre-tensioned inverted T-beam specimens. The beams were loaded in three-point bending to the cracking moment, after which clip gages were mounted across cracks. The beams were then loaded until the first crack was identified, unloaded, and reloaded to failure. Prestress loss calculated from these tests was measured to be 29.3 ksi (20%) and 34.5

ksi (23%) for beams 1 and 2 respectively. Loss calculations which were conducted using the 1989 AASHTO specifications, were found to be 40 ksi (27%). This is a conservative estimation compared to the measured loss values from the crack re-opening method. (Halsey and Miller 1996)

Osborn et al. (2012) conducted load testing on a total of seven pre-tensioned AASHTO Type II I-beams. Cracking-moment tests were conducted on the first five beams which consisted of loading the beams until the first visual cracks were identified. The cracks were then marked and the beams were unloaded. Next, foil gages were mounted across the marked crack locations and load was re-applied to each beam twice to induce crack re-opening. Decompression of the crack was identified by a deviation of the strain gage strain-load graph from a straight line. The effective prestress force in the girders was then calculated, taking into account the small amount of composite action due to the cast in place deck. These measured values of effective prestress force were then compared to values calculated using the AASHTO approximate, and refined methods, as well as the original bridge span values. All loss-estimation methods yielded conservative results, compared to the measured values. The AASHTO approximate method yielded effective prestress force of 188.4 kips (15% higher than measured), while AASHTO refined method yielded 179.8 kips (10% higher than measured. Lastly, the effective prestress force calculated in bridge plan specifications was 176 kips (8% higher than measured). (Osborn et al. 2012)

Labia et al. (1997) conducted structural testing of two 20-year-old box girders. The box girders were 70 ft. long with width and depth dimensions of 48 in and 33 in. respectively. The girders were loaded to cracking, then unloaded, instrumented with LVDTs across flexural cracks, and reloaded to crack opening. The average measured prestress loss was found to be 62 ksi. Original shop drawings estimated a lump-sum loss of 35 ksi, while the more detailed methods of estimation found in ACI 318R-89, AASHTO specification 15th edition, and the PCI manual calculated losses of 50 ksi, 46 ksi, and 43 ksi respectively. Losses were also calculated using Naaman's time-step method. Assuming a moist cured condition, the upper bound of loss for this time-step analysis was 54 ksi. Researchers attributed the larger measured losses to the use of high-strength concrete as well as the large temperature and humidity fluctuations in Reno, Nevada. (Labia et al. 1997)

2.4 Creep in Long-Span Structures

The CEB-FIP, ACI and AASHTO code expressions for creep and shrinkage, described above, have been utilized in a wide range of structures over the years. In 2008 however, several researchers began investigating whether these models were appropriate for use in large-span bridge structures which are highly sensitive to creep and shrinkage. Motivated by the release of litigated data from the collapse of the

Koror-Babeldaob Bridge, Bažant et al. (2010) created a finite element model of the bridge and evaluated deflections and prestress losses using the most common code expressions for creep and shrinkage. Researchers found that the current code expressions did an insufficient job of estimating long-term mid-span deflections and long-term prestress losses. Measurements taken shortly before the collapse indicated a 50% loss of prestressing force in the Koror-Babeldaob Bridge. This greatly exceeded the design value of 22%, and the value from the finite element analysis utilizing the CEB-FIP ’90 code expression for creep and shrinkage (24%). Figure 2.4 shows the prestress loss predictions utilizing each model along with the actual measured values (Bažant et al. 2010).

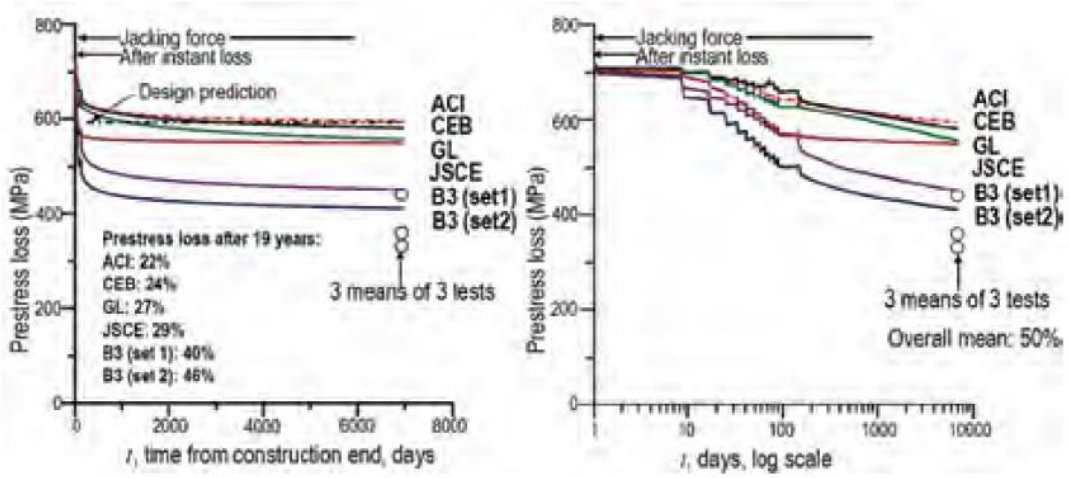

Figure 2.4. Prestress loss estimations on the Koror-Babeldaob Bridge.

The following year, Bažant et al. (2011) published data on a total of 56 large box-girder bridge spans which were experiencing excessive deflections. Most of the spans were balanced cantilevers with midspan hinges and were experiencing very similar behavior to the collapsed Koror-Babeldaob Bridge. Namely, the progression of deflections was significantly greater than those predicted by ACI and CEB models after multiple decades. Researchers concluded that these excessive deflections were far more prevalent than originally suspected and that the blame likely rests, not on poor construction, but on design recommendations.

2.5 Thermal Gradients

Thermal gradients play an important role in understanding the flexural behavior of large, box-girder bridges. Furthermore, in the VEB specifically, the stresses induced by non-linear thermal gradients have been shown to be significant (Maguire et al. 2015).

Throughout a given day, the temperature through the depth of a concrete box girder may vary. This temperature differential is termed a thermal gradient and can be influenced by many factors, as seen in Figure 2.5. Energy is absorbed on the top surface by radiation from the sun, while energy is gained and lost to the surrounding environment through convection and conduction (NCHRP 1985). Thermal gradients can be linear or non-linear depending on environmental and geometric conditions. These two types of gradients are picture in the first column of Table 2.2. Thermal gradients cause differential expansion and contraction through the depth of the section, which result in deflections and rotations in the member if not restrained.

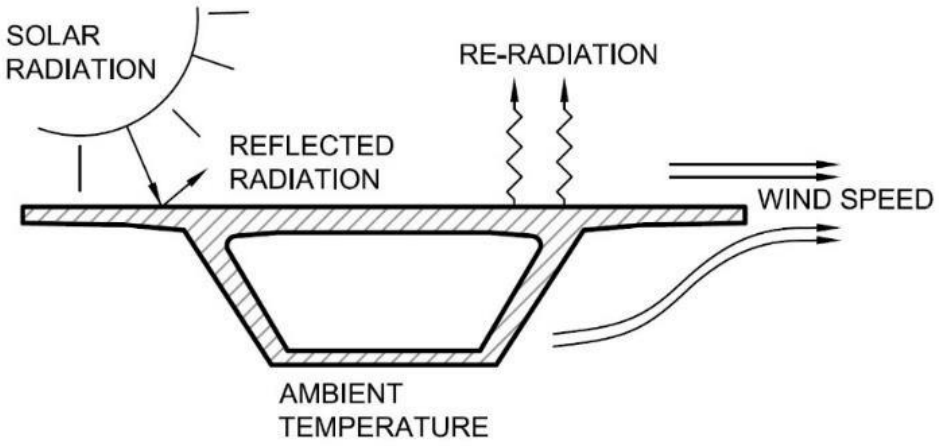

Figure 2.5. Factors which affect thermal gradients.

Large box girders tend to experience non-linear thermal gradients on days with high temperature fluctuations. This is the result of their large top flange which is exposed directly to solar radiation and which tends to shade the webs and bottom flange. The effect of non-linear thermal gradients is shown in the second row of Table 2.2 and is compared to the effect of linear thermal gradients shown in the first row.

In a simply-supported configuration, this non-linear thermal gradient will not induce internal moment or axial forces but will induce stresses in the beam section. This scenario can be seen in the third row and second column of Table 2.2. The stresses induced in a simply supported beam from a non-linear thermal gradient are termed self-equilibrating stresses. These stresses should be thought of as the difference between the free deformations of section fibers due to the non-linear thermal gradient, and the linear strain profile assumed by the Navier-Bernoulli assumption that plane sections remain plane. The calculation of these temperature-induced stresses is outlined by the National Cooperative Highway Research Program (NCHRP) in their 1985 Report-276, and detailed in Chapter 3.3 of this thesis.

Table 2.2. Summary of temperature induced thermal stresses.

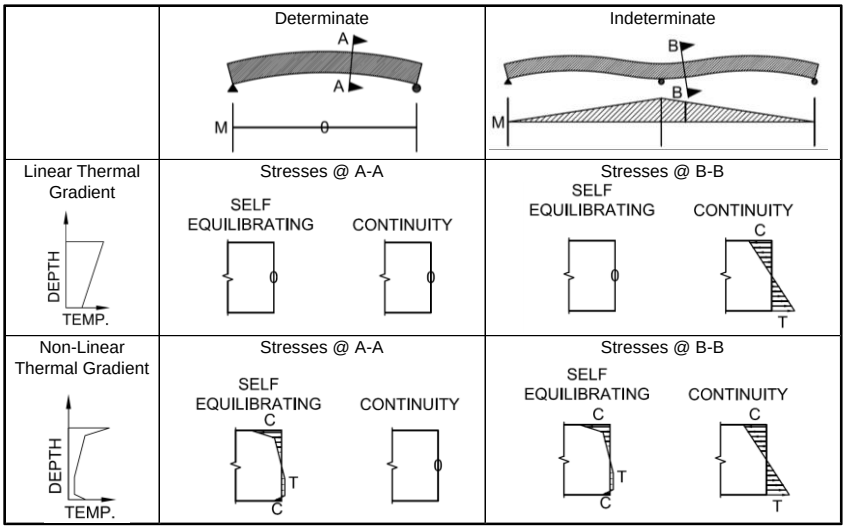

Additionally, when redundancies are added into the structure, continuity stresses will be induced in addition to self-equilibrating stresses. This scenario can be seen in the third row and third column of Table 2.2. The state of stress, therefore, in an indeterminate beam from non-linear thermal gradients can be calculated by superimposing the self-equilibrating stresses and continuity stresses (NCHRP 1985).

2.6 The Varina-Enon Bridge

Maguire et al. (2014) investigated the longitudinal behavior of the VEB under live-load testing. This study was funded by the Virginia Department of Transportation beginning in 2012 after a 1/16-in. crack was identified in the bottom flange of one of the southern-most approach units of the VEB.

In addition to live-load testing, a long-term monitoring system was set up on the VEB. The purpose of the long-term monitoring system was to log crack opening events, and the thermal gradients associated with these events. The long-term monitoring system consisted of 27 thermocouples spread throughout the top flange, web, and bottom flange of the box girder, two strain transducers, and two LVDTs. Researchers concluded from this study that crack openings were generally correlated with large non-linear thermal gradients in the bridge (Maguire et al. 2018).

In addition to thermal gradients, the issue of crack openings could also be the result of larger-than-expected prestress force losses in the longitudinal post-tensioning strands. In 2017, the long-term monitoring data was re-evaluated in an effort to calculate the effective prestress force. This study resulted in a preliminary report but was never published.

2.7 Summary of the Literature

Properly estimating long-term prestress loss in prestressed concrete requires the accurate assessment of creep and shrinkage strains. For this purpose, multiple analytical models to describe the time-development of creep and shrinkage have been developed. Most of these models describe creep by an asymptotic function which approaches an ultimate value, but recent research has shown that creep does not behave in this manner. As a result, more recent models describe the progression of creep by a logarithmic function.

The measurement of long-term prestress loss has been accomplished through several experimental testing protocols. The purpose of measuring prestress loss has generally been to validate analytical models for long-term loss, but another purposes has been to assess the remaining service life of beams similar to those being tested. Crack reopening tests have generally been accepted as the most reliable method of measuring prestress loss, but all of these tests have been conducted on simply supported beams under laboratory conditions.

The evaluation of prestress loss on the VEB has become important to researchers because of cracks identified on the bridge's bottom flange. Data gathered from the monitoring system installed on the VEB allows researchers to measure prestress loss by evaluating the state of stress in the section at the time of crack opening. This method is complicated by the presence of thermal gradients and redundant supports in the structure.

Chapter 3.
Methodology

The performance of the Varina-Enon Bridge (VEB) came into question after the discovery of cracking in Span 6 of the northbound approach unit. Sensors were installed at the crack location by Maguire et al. (2014) to monitor thermal gradients and crack openings. Data from this monitoring system is used in this study to calculate the effective prestress force in Span 6. This is done by modifying Equation (2.6) at events when the crack in the bottom flange opens. Alongside this back-calculation of the effective prestress force, a finite element (FE) model is created to evaluate effective prestress using multiple code expressions for creep and shrinkage.

The purpose of this chapter is to describe the methods used and activities performed in completing these tasks. First, the long-term monitoring system is described, and the method of data processing is briefly outlined. Second, the FE model and associated time-step analysis is described. Last, the method of calculating effective prestress from field data is detailed.

3.1 Long-Term Monitoring System

The long-term monitoring system was deployed by Maguire et al. (2014) for the purpose of measuring the number and magnitude of crack-opening events in Span 6. These sensors measured crack displacement, temperature, and live-load strains throughout Span 6. Data from this long-term monitoring system was used to correlate thermal gradients, and live-load strains to crack opening events in order to calculate effective prestress.

An elevation view of the sensors which make up the long-term monitoring system can be seen in Figure 3.1. Section A-A represents the location of the transverse crack being monitored, while Section B-B represents the location of live-load strain measurements. Thermocouples and linear variable differential transformers (LVDTs) measured temperatures and crack opening widths at Section A-A respectively. Two strain transducers measured live-load strains at Section B-B and crack decompression at Section A-A.

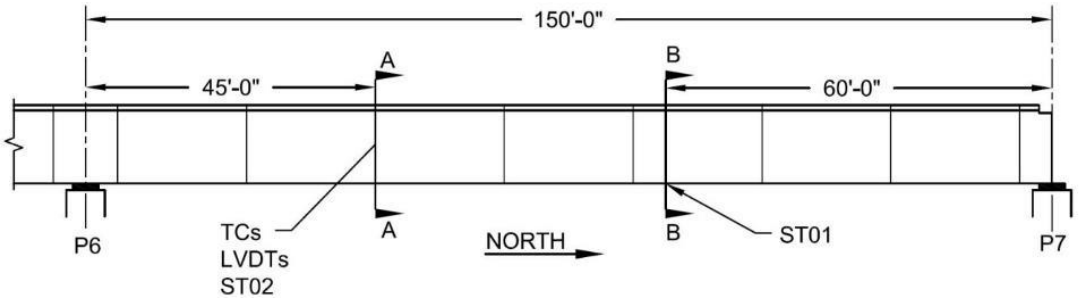

Figure 3.1. Span 6 longitudinal sensor layout.

3.1.1 LVDTs

Two LVDTs were installed at Section A-A of Span 6. These LVDTs were oriented longitudinally and measured crack displacement. These LVDTs were located on the top face of the bottom flange of the box-girder section, as seen in Figure 3.2.

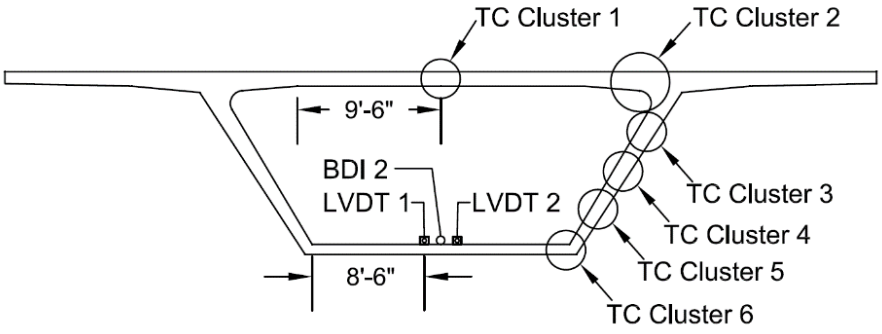

Figure 3.2. Section A-A sensor layout.

3.1.2 Thermocouples

Thermocouples were installed throughout the depth of the box-girder section, as seen in Figure 3.2. Each cluster of thermocouples represents several sensors installed through the thickness of the flange or web. Each thermocouple was assigned a tributary area over which the temperature of the section was taken to be constant. Table 3.1 shows the location of each thermocouple from the top of the wearing surface, the tributary area, and the location of the centroid of that area from the bottom of the section. Each of the values in Table 3.1 is used in the calculation of the thermal moment and axial force in Chapter 3.3.

Several thermocouples were located at approximately the same depth in the section. Because of this, these temperature measurements were averaged and treated as one measurement for subsequent calculations. Thermocouples averaged because of proximity include 4/5, 6/7, and 8/9 in the web and thermocouples 16/21, 17/22, and 18/23 in the top flange. Thermocouple 99 represents an estimated

temperature at 3/4 in. from the top of the wearing surface. This temperature was interpolated from the existing temperature measurements using the fifth-order curve approximation presented by Priestley (1978).

Table 3.1. Location and tributary areas of thermocouples.

TC	Elev. from top of wearing surface, in.	CG from the bottom, in.	Tot area, $in.^2$	Area*cg, $in.^3$
1	140.0	8.1	1,086.8	8,838.8
2	142.3	3.2	496.5	1,602.6
3	144.5	1.1	457.5	481.4
4,5	108.8	35.8	754.9	27,043.1
	110.8			
6,7	78.0	66.2	848.4	56,156.3
	80.6			
8,9	48.5	97.5	1,030.0	100,394.8
	51.1			
10	15.8	122.9	667.5	82,040.1
11	13.8	131.8	317.2	41,810.9
12	11.8	133.9	673.2	90,158.4
13	9.8	135.3	713.9	96,594.5
19	9.5	136.2	692.9	94,363.8
14	7.8	137.6	1,041.0	143,241.6
15	6.5	138.9	798.1	110,876.0
16,21	5.5	140.0	694.0	97,160.0
	5.5			
17,22	4.5	141.0	694.0	97,854.0
	4.5			
18,23	3.5	142.0	694.0	98,548.0
	3.5			
24	2.5	143.7	957.7	137,614.8
99	0.8	145.6	1,131.2	164,666.0

3.1.3 Strain Transducers

In addition to LVDTs and thermocouples, two strain transducers were installed to measure stain in the bottom flange of the section. ST01 was located at the top of the bottom flange at Section B-B which is 60 ft from the center of Pier 7 and represents the location of the maximum moment in Span. ST01 was used to trigger the data acquisition system and was also used to measure strain due to live loads. The second strain transducer, ST02, was located at the top of the bottom flange adjacent to Section A-A, as seen in

Figure 3.2. This sensor was used to measure decompression of the bottom flange during crack opening events.

More detailed information regarding the types and locations of sensors installed on the VEB can be found in the Final Contract Report to the Virginia Department of Transportation (Maguire et al. 2015).

3.1.4 Data Collection

Data was collected using two Campbell Scientific CR1000 data loggers. One data logger collected strain and displacement data at a rate of 33 Hz. However, data was only stored on this data logger each time ST01 measured a strain of 12 με or more. The 3.6 seconds of data which was stored is termed a *load event* for the remainder of this paper. The second data logger collected temperature data via an analog multiplexer which sampled every 2 minutes. All of the temperature data was stored continuously in a file separate from the strain data.

3.1.5 Data Processing

Data files were collected from the two data loggers at one-month intervals. Data was then separated into discrete events by comparing the timestamp on adjacent samples. A new event was defined when the timestamp increased by a value greater than 3/100ths of a second. A thermal gradient was then matched to each event by comparing the timestamp of that event to the timestamps of the temperature data. Finally, descriptive values were extracted from the event and used to characterize it. These values included the timestamp, maximum and minimum values of ST01, the maximum value of ST02, and the maximum values of both LVDTs,

In some cases, events were recorded which did not represent a load passing over the crack. This may have been due to drift in ST01, or malfunction of one of the sensors. Figure 3.3 shows an example of a load event which represents a single load passing over the crack location, while Figure 3.4 shows an example of a registered event which represents drift in ST01. It was necessary to review the data and filter out events which did not represent a load event. A small percentage of events were visually inspected as seen in Figure 3.3 and Figure 3.4. From this inspection, exclusionary criteria were calibrated and applied to all the data to filter out events which did not constitute a true load event.

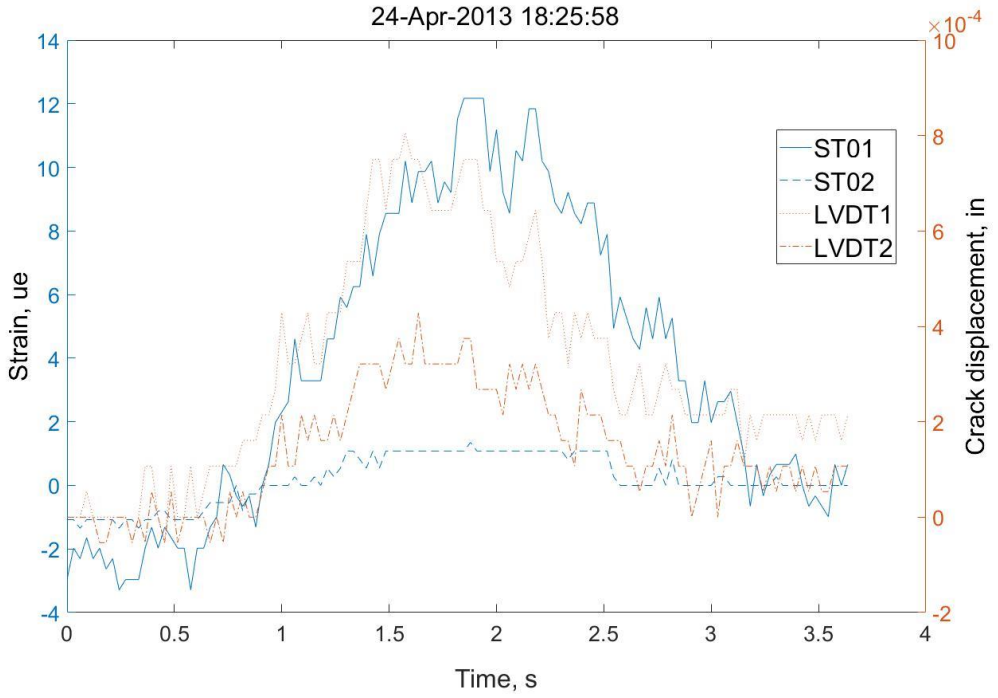

Figure 3.3. Example of data for a typical load event.

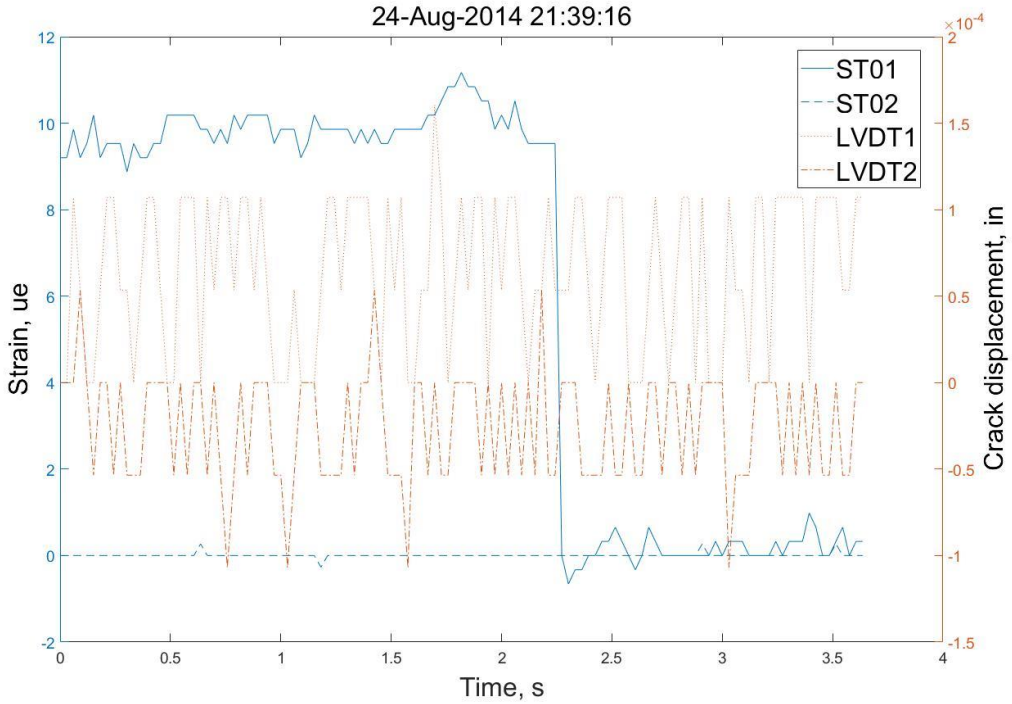

Figure 3.4. Example of data which was filtered out.

3.2 Finite Element Model

In addition to the data collected in the field, an FE model of the approach unit was developed. LARSA 4D was used to create this FE model, which can be seen in Figure 3.5. There are two purposes for developing this model. First, it is used to calculate prestress losses in the bridge, utilizing multiple creep and shrinkage models. Second, it is used to calculate dead-load moment, prestressing moment, and general moment distributions necessary to calculate effective prestress from the field data. All salient features of the FE model are reported in Appendix B.

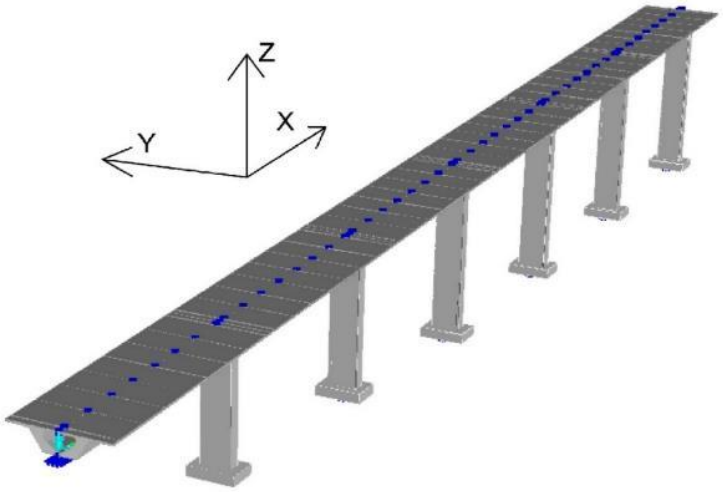

Figure 3.5. Overview of the FE model.

3.2.1 Finite Element Model Overview

The bridge superstructure is modeled as a six-span-continuous beam. Each pre-cast segment is modeled as an individual beam element which ensures that information at each joint is available. The mean, elastic modulus of concrete at 9,500 days is taken as 5,000 ksi. This value was validated by live-load tests conducted by Maguire (2013). The mean, 28-day ultimate strength, $f`_{cm28}$ is assumed to be 6,600psi. Cross-section dimensions of the superstructure are shown in Figure 1.5. The depth of the top slab varies from wing tip to center-line between 9 1/2 in. and 11 1/2 in., and includes a 1 1/2-in. concrete wearing surface.

Rigid links are used at pier locations to connect joints on the reference line to joints located at the bottom of the superstructure section. Springs are used to model the neoprene bearing pads at the joint between these rigid links and the substructure. These springs have translational stiffness in the Z and X-axes, and rotational stiffness about the Y-axis as referenced by Figure 3.5. For the remaining three degrees

of freedom, the superstructure is rigidly connected to the substructure. Bearing pad stiffnesses for the VEB were characterized by Maguire (2013) and are recorded in Appendix B.

Prestressing tendons are modeled from dimensions found in the as-built drawings. Tendon material is A416 steel which has an ultimate tensile strength of 270 ksi, and an apparent modulus of elasticity of 27,400 ksi. The apparent modulus was calculated using benchmark elongation tests during the construction of the VEB (F&M Engineers 1993). Actual jacking forces varied slightly for each tendon and can be found in as-built drawings which are recorded in Appendix C.

Self-weight loads are included in the FE model and applied as each span is activated. In addition to the gross cross section of the box girder, tendon deviation blocks and barrier rails are incorporated into the model as point and distributed loads respectively. The stiffness due to barrier rails is not considered in the overall stiffness of the section.

3.2.2 Staged Construction Analysis

Segmental construction of the VEB is modeled using a *time-dependent construction stage analysis*. This analysis method accounts for the placement and stressing of each span during construction, as well as the long-term behavior of the structure due to creep, shrinkage, and relaxation. Several definitions are key to understanding this staged construction analysis. First, construction *activities* are defined as events which may include placement of an element, addition of a support, or stressing of a tendon. Second, construction *steps* are defined as an individual analysis and may include several construction *activities*. Last, construction *stages* are each defined as a group of construction *steps* and represent one day of construction for purposes of calculating time-dependent behavior.

The construction of the approach unit is modeled in six stages, each consisting of the construction of one span. Construction of each span consists of nine construction steps. In the first step, the substructure and superstructure of each span are activated, and the self-weight is applied. In Steps, 2 through 9, each of the eight tendons in the span are stressed. It is necessary to analyze the structure after stressing each tendon to account for elastic shortening losses. The deflected shape for Steps 1 and 9 in Stages 1 and 2 are pictured in Table 3.2.

Table 3.2. Staged construction analysis for Spans 1 and 2.

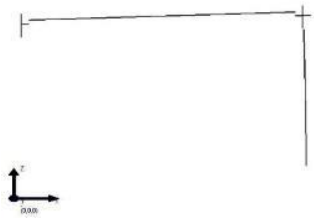	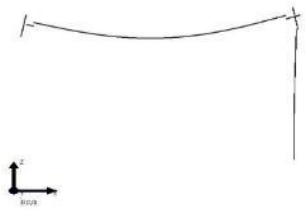
Stage1, Step 1: Span 1 is activated	Stage 1, Step 1: Span 1 self-weight is applied
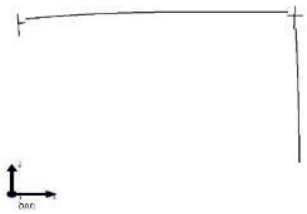	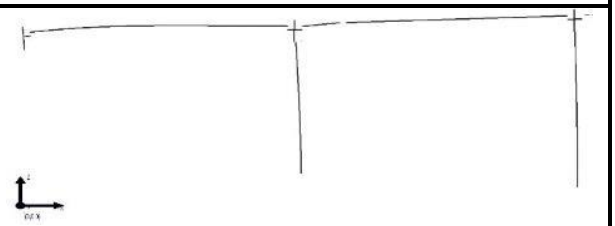
Stage 1, Step 9: Span 1 is prestressed	Stage 2, Step 1: Span 2 is activated
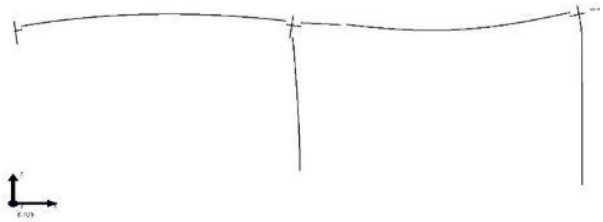	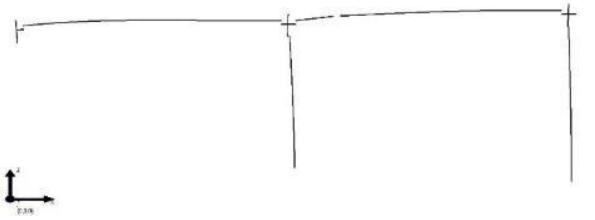
Stage 2, Step 1: Span 2 self-weight is applied	Stage 3, Step 9: Span 2 is prestressed

A day-of-casting is assigned to each beam element in the staged construction analysis. This casting day is used to define the age of the element at loading and each subsequent construction stage. Casting dates for each element are obtained from erection logs recorded in the VEB Inspection and Maintenance Manual (F&M Engineers 1993). Day zero is defined as the day that the first segment of the approach structure was cast which occurred on August 8th, 1987.

The first six construction stages take place from day 88 to 184. After the construction of the approach unit, empty construction stages are placed at 100-day increments up to day 500, then at 1,000-day increments up to day 9,500. These construction stages do not represent any construction activity but are placed as time steps for the time-step analysis. The final construction stage represents the structure in the year 2013 and is used to generate FE model results which can be compared to field data of that year.

3.2.3 Short-Term Prestress Losses

Short-term prestress losses are incorporated into the FE model prior to the construction stage analysis. These losses are calculated as the sum of friction, seating, and elastic shortening losses. These losses depend on the stressing operation as well as the modulus of elasticity of the concrete at the time of stressing.

Curvature friction losses are caused by friction between prestressing strands and the inside of the tendon duct at any location that the strand changes direction. The curvature friction coefficient, μ was measured to be 0.25 during construction (F&M Engineers 1993). No wobble friction is present in the structure Since the tendons are external to the cross section. An example of a tendon force profile after curvature friction losses is shown by the solid line in Figure 3.6.

Seating losses result from slippage that occurs when the strand is released from the stressing jack. In the case of the VEB, this slippage is given in as-built documents as 3/8 in. (F&M Engineers 1993). The amount of curvature friction influences how far seating losses extend through the length of the tendon. The dashed line in Figure 3.6 illustrates the loss in force due to seating.

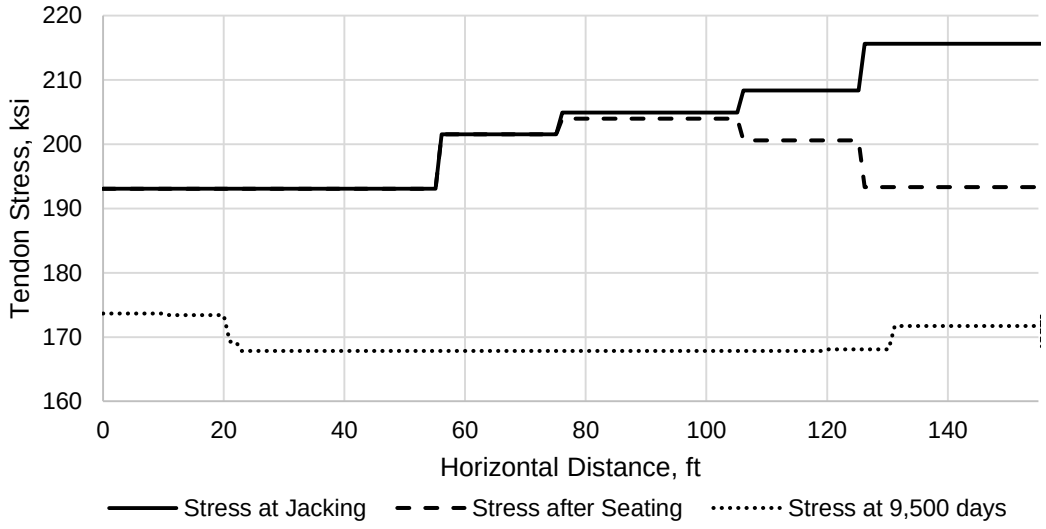

Figure 3.6. Tendon S6-T9L stress profile.

Lastly, losses due to elastic shortening of concrete occur in post-tensioned structures when tendons are stressed sequentially. As the first tendon in a span is stressed, the surrounding concrete is put into compression. When the second tendon is stressed, the first tendon experiences elastic shortening loss as the concrete is put into further compression. When the third tendon is stressed, the first and second tendons

experience elastic shortening loss, and so on. Elastic shortening loss in each tendon is assumed to be uniform through the length of the span.

3.2.4 Long-Term Prestress Loss

Long-term prestress losses are accounted for in the FE model through the time-step analysis conducted as part of the time-dependent construction stage analysis. This time-step analysis is conducted using code expressions for creep and shrinkage from the CEB-FIP ’79, CEB-FIP ’90, and AASHTO 2012 model codes. Creep losses depend on the change in creep strain over each time step. Change in creep strains vary through the depth of the section depending on the distribution of stress, but prestress losses due to creep are calculated from the average change in creep strain over the depth of the cross-section. Shrinkage strains are computed and prestress losses are simply calculated from these strain. Long-term prestress losses can be seen by the dotted line in Figure 3.6.

3.3 Effective Prestress from Field Data

3.3.1 Overview

The method which evaluates the stress at crack re-opening is used to calculate the effective prestress force in Span 6 of the VEB. A pre-existing crack, which had been observed to open under service live loads, was used as the location of crack monitoring. The long-term monitoring system was used to gather data.

Employing this method in a continuous structure, under service conditions presents several challenges to the calculation of prestressing force. First, non-linear thermal gradients cause continuity and self-equilibrating stresses in the structure. Second, the redundancies in the structure cause secondary prestressing moments and moments due to creep and shrinkage deformations. Third, the bridge is subject to service live loads that need to be accounted for. All of these aspects are incorporated into the effective prestress force calculation in Equation (3.1). The terms in this equation are outlined below and an example of the calculation procedure is presented in Appendix D.

$$P_e = \left(-\sigma_{SE} + \sigma_{con} + \frac{\left(M_{sw} + M_{live} + M_{other}\right) y}{I_{cr}} + \frac{P_{sw} + P_{other}}{A_{cr}} \right) \left(A_{cr} + \frac{I_{cr}}{e_{cr} y_{cr}} \right) \quad (3.1)$$

Where:

P_e is the effective prestress force.
σ_{SE} is the self-equilibrating stress at the bottom flange due to thermal gradients.
σ_{con} is the continuity stress associated with thermal moments.
M_{sw} is the self-weight moment.
M_{live} is the live-load moment.
M_{other} is the moment due to secondary effects from prestressing, creep and shrinkage.

I_{cr} is the cracked transformed moment of inertia of the box girder.
P_{sw} is the axial force due to the self-weight of the structure.
P_{other} is the axial force due to secondary effects from prestressing, creep, and shrinkage.
A_{cr} is the cracked transformed area of the box girder.
e_{cr} is the tendon eccentricity from the cracked centroid.
y_{cr} is the distance from the cracked centroid to the top of the bottom flange of the section.

3.3.2 Section Properties

Transformed, partially-cracked section properties are used in the calculation of effective prestress force. Mild steel is not considered in the transformed section because it does not extend through epoxy joints. A partially-cracked section was considered because of the location of ST01, and the crack-monitoring LVDTs on the top of the bottom flange. All live-load strain and crack-opening data is recorded at the point at which the bottom flange is entirely decompressed, as seen in Figure 3.7.

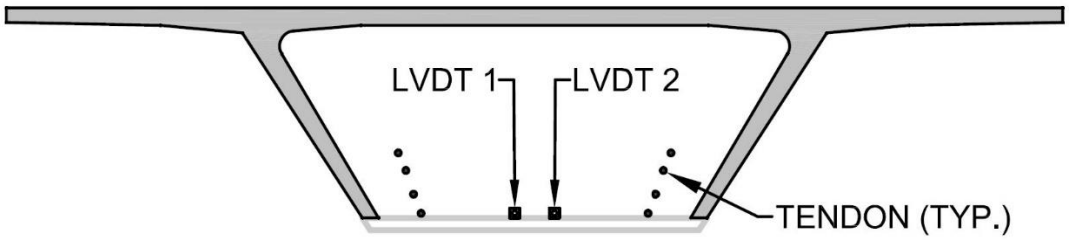

Figure 3.7. Cracked section used in the analysis.

3.3.3 Self-Weight Moment

The self-weight moment is calculated through the staged construction analysis of the FE model. The self-weight of the superstructure consists of the section of the box girder as shown in Figure 1.5, and also includes deviator blocks, and concrete guardrails. Deviator blocks are applied as point loads to the structure at their respective locations while the rest of the self-weight is incorporated as a distributed load totaling 15.86 klf. Figure 3.8 shows the moment in Span 6 due to self-weight and displays the moment calculated at Section A-A.

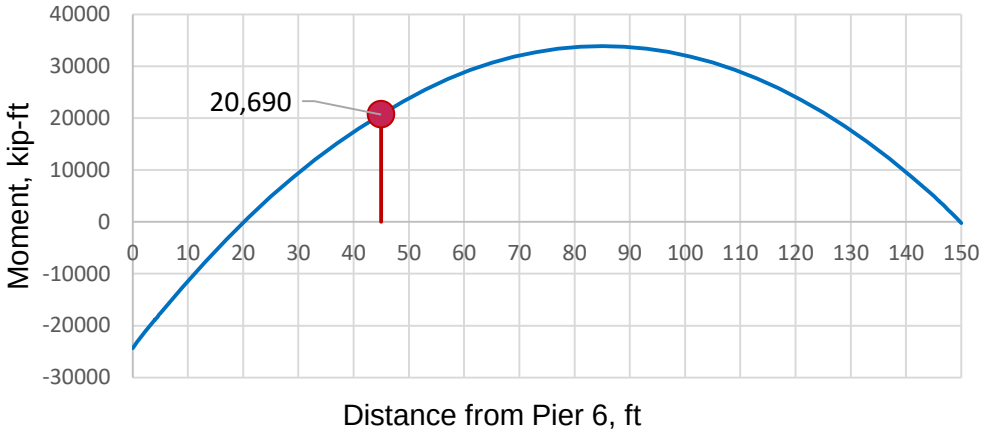

Figure 3.8. Dead-load moment in Span 6.

3.3.4 Live Load Moment

The live-load moment at Section A-A is calculated from the strain measured by the ST01 strain transducer at Section B-B. This is accomplished by calculating the moment at Section B-B associated with the strain in the bottom flange, then correlating the maximum moment at Section B-B to a maximum moment at Section A-A. This correlation is made by conducting an influence line analysis on Span 6 of the VEB. The maximum moment envelope from this analysis is shown in Figure 3.9 as a fraction of the moment at Section B-B. The ratio used to correlate moment at A-A to moment at B-B is 0.689.

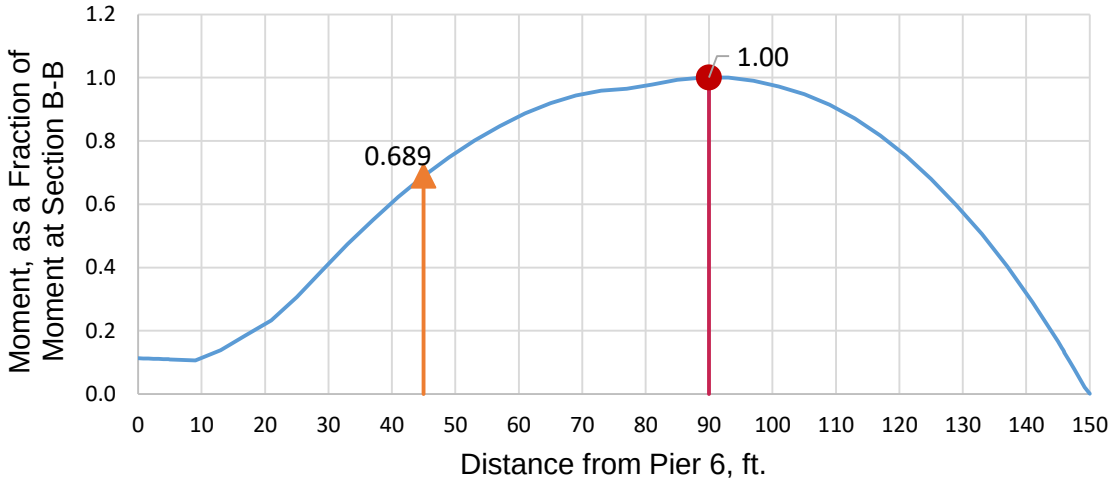

Figure 3.9. Span 6, max moment envelope.

3.3.5 Self-Equilibrating Stresses

Stresses, resulting from non-linear thermal gradients are divided into self-equilibrating (SE) stresses and continuity stresses as outlined in Report 276 (NCHRP 1985). Once these values are calculated, the

principle of superposition is used to sum them together to get the total stress distribution due to the thermal gradient. First, the method of calculating SE stresses is described, then the method of calculating continuity stresses is outlined.

SE stresses arise from the difference between thermal strains which would result from a free expansion of the section fibers, and the strains in the resultant plane section (NCHRP 1985). This concept of strain difference is illustrated in Figure 3.10.

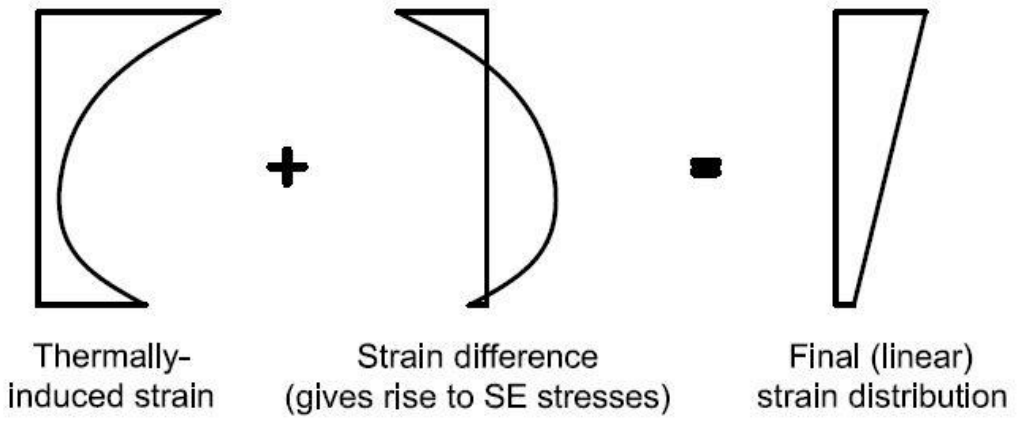

Figure 3.10. Strain difference that results in self-equilibrating stress.

SE stresses can also be conceptualized as the stresses due to the thermal gradient in an artificially restrained structure plus the stresses resulting from the axial load and moment that would be required to remove the artificial restraints (NCHRP 1985). By this method, calculating SE stresses at the top of the bottom flange begins by removing all of the interior supports and then artificially restraining the approach structure at Piers 1 and 7. The thermally-induced stress at the bottom flange is then calculated using Equation (3.2).

$$\sigma_{t1} = -E\,\alpha\Delta T_1 \tag{3.2}$$

Where:

E is the modulus of elasticity
α is the coefficient of thermal expansion
ΔT_1 is the difference in temperature between the coolest location, and TC_1.

Next, the restraining axial force and moment are calculated using Equations (3.3) and (3.4). Equal and opposite forces and moments are then applied to the structure to restore deflections and rotations.

$$P = \sum_{i=1}^{18} E\,\alpha \Delta T_i A_i \tag{3.3}$$

$$M = \sum_{i=1}^{18} E\,\alpha \Delta T_i A_i Y_i \tag{3.4}$$

Where:
ΔT_i is the difference in temperature between TC_i, and TC_{cool}
A_i is the tributary Area of thermocouple *i*, as presented in Table 3.1.
Y_i is the distance of thermocouple *i* from the center-of-gravity of the section.

The final SE stress at Section A-A, at the depth of the bottom flange, is calculated by adding the stresses due to the axial force and the bending moment, to the stress due to the thermal gradient in the artificially restrained structure. This calculation can be seen in Equation (3.5).

$$\sigma_{SE} = \sigma_t + \frac{P}{A} + \frac{My}{I} \tag{3.5}$$

3.3.6 Thermal Continuity Forces

As outlined in Chapter 2.5, thermal continuity forces arise from the application of a thermal gradient to a redundant structure. In Chapter 3.3.5, the redundancies of the VEB are removed, and the SE stresses are calculated. To calculate continuity forces at Section A-A for a thermal gradient, the interior supports are reinstated, and the thermal moment and axial force are applied to the structure. The resulting bending moment and axial force at Section A-A are then found. Since a large number of thermal gradients are being considered, the structure was analyzed for an applied constant unit moment and axial force, and the unit internal forces of 0.878, and 0.017 were found for bending moment and axial force respectively. These values are then used to scale Equations (3.4) and (3.5), and the continuity forces at Section A-A are calculated. A graph illustrating the calculation of the unit bending moment is shown in Figure 3.11.

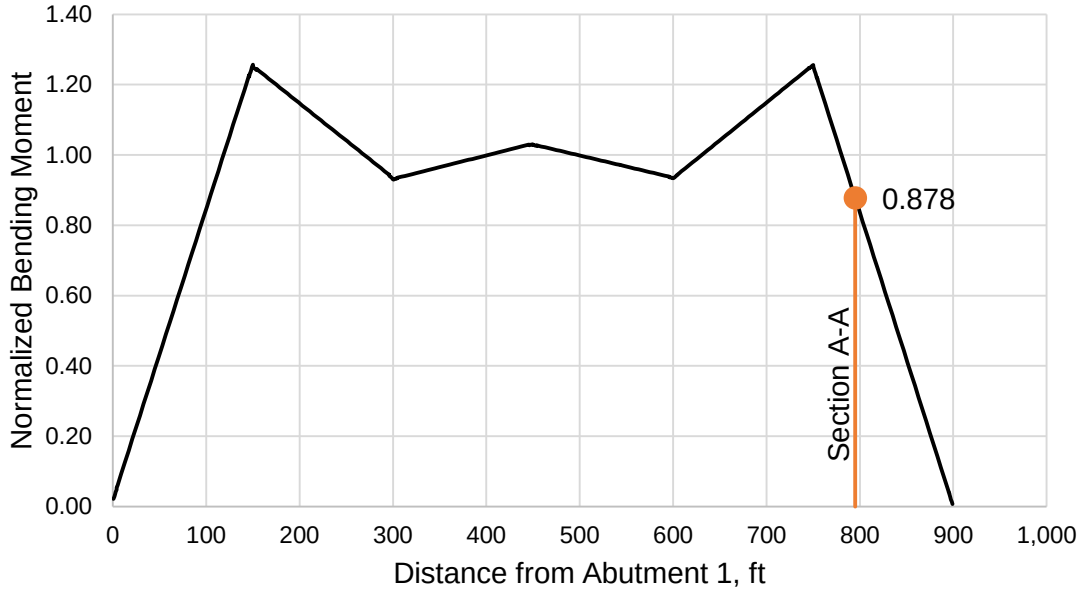

Figure 3.11. Thermal continuity moments normalized by the applied thermal moment.

3.3.7 Secondary Prestress, creep, and shrinkage effects

Prestressing, creep and shrinkage are all applied deformations to the structure. These deformations result in forces due to the redundancies within the approach unit which are termed secondary prestress, creep and shrinkage forces respectively. Both moments and axial forces are caused by these three applied deformations.

Secondary prestress effects are caused when the structure is stressed. In the simply supported case, the superstructure would tend to shorten and camber upward. When redundancies are present, however, these deformations are restrained by the superstructure's own self-weight, and the stiffness of the bearing supports. At Section A-A, the secondary prestressing moment, M_2 is 14,456 kip-ft while the secondary prestressing axial force, P_2 is 14.5 kip (T).

Creep and shrinkage effects are caused by the restrained deformation over the life of the structure. The axial forces and moments due to these imposed deformations are tabulated in the FE model separately from other forces. Creep causes axial shortening and bending in both the superstructure and the substructure. At Section A-A, the bending moment due to creep, M_{cr} is taken to be 1,483 kip-ft while the axial force, P_{cr} is -133 kip (C). The compressive nature of the creep axial force is a result of the restrained bending of the substructure. Shrinkage only causes shortening of the superstructure and substructure without any bending. This results in an axial force at Section A-A, P_{sh} is calculated as 197 kip (T) and a bending moment, M_{sh} is 148 kip-ft. The small amount of bending moment due to shrinkage results from differential shortening of the substructure.

3.4 Re-Installation of the Long-Term System

In March of 2019, the long-term monitoring system was re-installed in Span 6 of the VEB. This purpose of this system is to gather more up-to-date data on effective prestress force and to gather data in adjacent spans. The sensor layout in the new installation is the same as described in Chapter 3.1 with the addition of several sensors described below. Thermocouples were left installed in the superstructure when the original long-term monitoring system was decommissioned in 2014. These thermocouples were re-connected to the data logger and found to be operational.

In addition to the strain gages and LVDTs described in Chapter 3.1, several sensors were installed to gather more data in Span 6 as well as Span 5. An additional strain transducer was installed at Section B-B on the bottom of the top flange to record localized strains due to individual axles. This information will be used to better estimate the distribution of loads for the calculation of the live-load moment. Also, an LVDT was installed at the mid-span of Span 5, on the top of the bottom flange to investigate crack opening at that location. Last, two additional LVDTs are to be installed at Section A-A on the bottom of the bottom flange to measure first crack opening at the extreme fiber in tension. These LVDTs were not installed along with the rest of the sensors due to the difficulty of access to this location. The locations of these additional sensors, as well as the sensors re-installed in Span 6, are pictured in Figure 3.12.

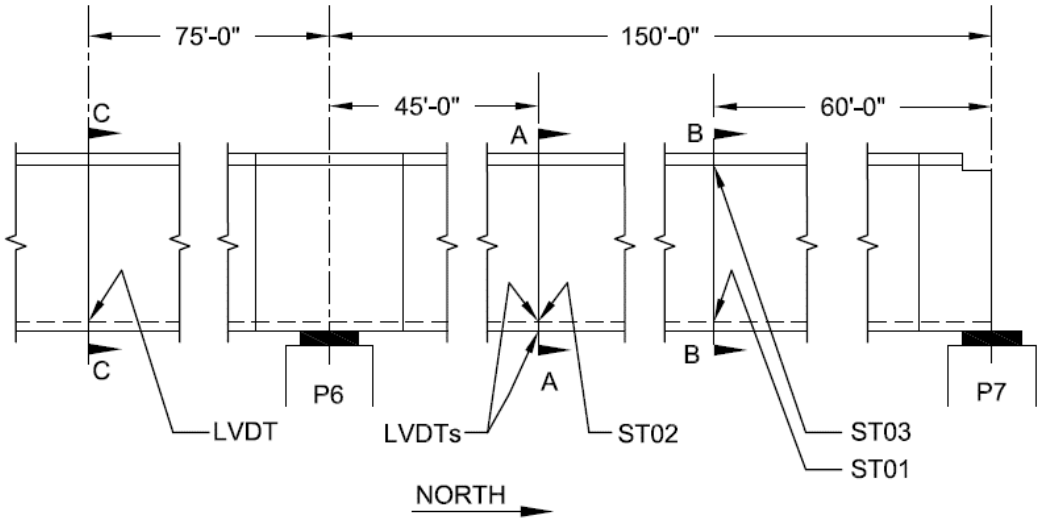

Figure 3.12. Sensors re-installed on to the Span-6, long-term monitoring system.

Chapter 4.
Results and Discussion

This Chapter presents analysis results, aimed to estimate the effective prestress force using field monitoring data and to comparatively evaluate, by means of finite element (FE) analyses, the effective prestress force obtained with different code expressions for long-term losses. First, the FE model presented in the previous chapter is validated, by comparing the analytically calculated deflections to corresponding live-load test data obtained in 2012. After that, the effective-prestress estimates obtained from the model are presented, followed by an estimate of the same value using field data. The chapter is completed with a calculation of the flexural capacity of the bridge girder.

4.1 Validation of the Finite Element Model

The FE model is validated, by verifying its capability to reproduce deflections obtained during live-load testing on the Varina-Enon Bridge (VEB), conducted by Maguire (2013) in August of 2012. During these tests, two load trucks crossed the approach unit at highway speeds in three different *load configurations*. The first load configuration consisted of one truck driving in the center lane, the second consisted of the same truck driving in the left lane, and the third consisted of both load trucks side-by-side. Vertical deflections were measured at the mid-span of Span 5 by a deflectometer mounted on the bottom flange of the section.

The axle loads were applied to the FE model as static loads, without any dynamic amplification factors. The analytically-obtained and field-recorded maximum mid-span deflections for Span 5 are compared in Table 4.1. The FE model satisfactorily reproduces the live-load test values of deflection, with the normalized difference ranging from 0.2% for load configuration 2, to 21.1% for load configuration 3.

Table 4.1. Comparison of vertical deflections at mid-span of Span 5.

Load Configuration	Span 5, Mid-Span Deflection, in.		Normalized Difference
	Live-Load Test Results	FE Model Results	
LC1	-0.03	-0.035	16.9%
LC2	-0.035	-0.035	0.2%
LC3	-0.062	-0.075	21.1%

4.2 Finite Element Results

Three time-dependent, staged-construction analyses were conducted on the FE model. Results are obtained from these analyses over the life-span of the structure. For each analysis, one of three code expressions for creep and shrinkage were used to estimate long-term prestress losses. For the purposes of this project, CEB-FIP ’78, CEB-FIP’90, and AASHTO codes were used. The average tendon-stress profiles for these three analyses are shown in Figure 4.1 along with the average tendon profile before any long-term losses occur. The average jacking force in Span 6 was 879 kips resulting in average jacking stress of 213.1 ksi.

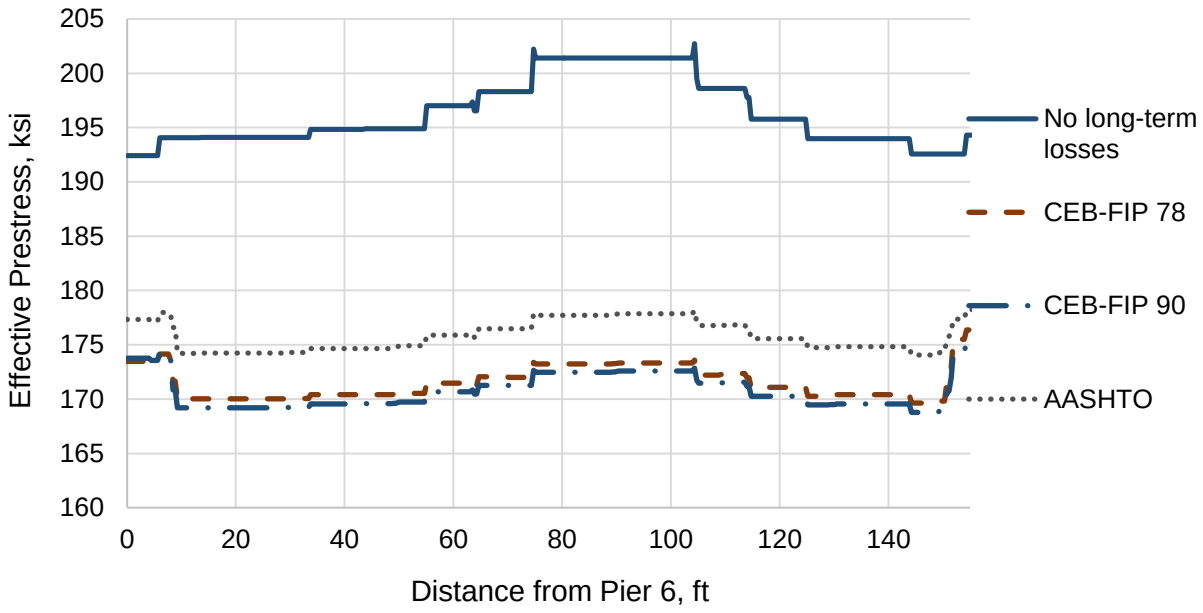

Figure 4.1. Span 6 tendon-stress profiles taken at 9,500 days.

The original design of the VEB utilized the CEB-FIP ’78 model code expression for creep and shrinkage to estimate long-term prestress losses. The average total prestress loss at Section A-A using this code expression is 41.9 ksi. This represents what designers would have expected of the bridge’s long-term performance in 1986. The prestress loss estimation from the analysis utilizing the CEB-FIP ’90 code expression is 43.3 ksi at Section A-A. This is the largest loss estimate of the FE analyses. The lowest estimate is calculated from the analysis utilizing the AASHTO specification expression for creep and shrinkage, at 38.1 ksi.

The FE model was also used to estimate the projected prestress loss at the age of 50 and 100 years. This progression of prestress loss over time can be seen in Figure 4.2 for ages up to 20,000 and 36,000 days

(approximately 50 and 100 years respectively). In addition, the prestress loss is estimated for the time frame from 2013 to 2019. The estimated average prestress loss over this 6-year period is 0.7 ksi, 0.9 ksi, and 0.7 ksi, for the analysis utilizing the CEB-FIP ’78, ’90 and AASHTO code expressions, respectively.

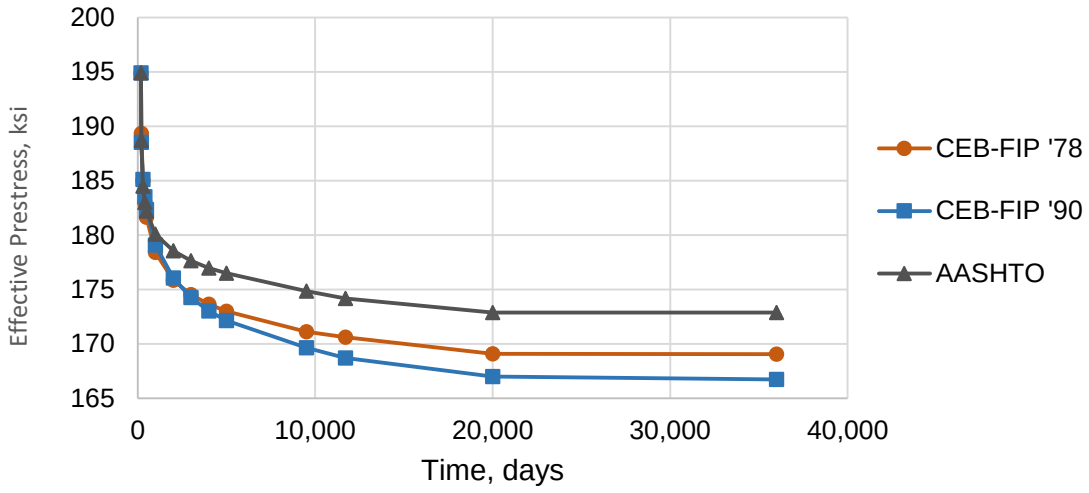

Figure 4.2. Progression of prestress loss with time, at Section A-A of Span 6.

In addition to prestress loss, the progression of deflection is calculated by the FE analyses. These deflections give a good picture of the serviceability performance of the structure. Significant long-term deflections may cause future serviceability concerns. The deflections at mid-span of Span 6 were calculated using the FE model, and are shown in Figure 4.3. The analysis utilizing the CEB-FIP ’90 creep and shrinkage code expressions calculates the largest deflection at 9,500 days of -0.297 in., while the analysis utilizing AASHTO creep and shrinkage code expressions calculates the smallest deflection of -0.12 in.

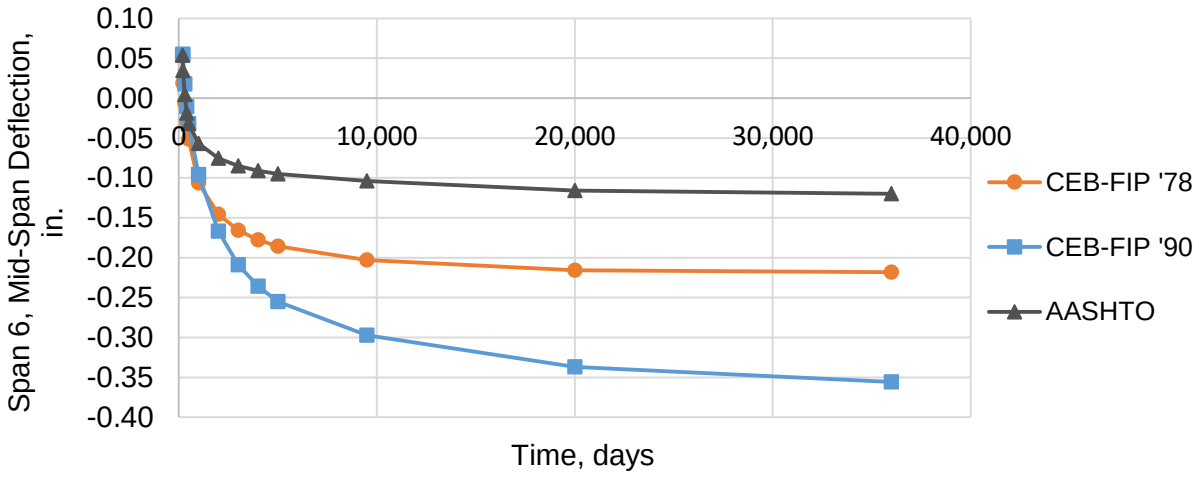

Figure 4.3. Progression of mid-span deflections in Span 6.

4.3 Field Measurement Results

In addition to FE model results, data from the long-term monitoring system was used to calculate values of effective prestress for each crack-opening event. A total of 6,697 events were recorded over a one-year period in 2013. The average effective-prestress value of these events is 153.9 ksi and the standard deviation is 6.7 ksi. The maximum crack width recorded was 0.0274 in., but the large majority of crack openings were significantly smaller than this maximum value. Effective-prestress values are plotted against their corresponding crack displacements in Figure 4.4. The distribution of prestress values can be seen by the histogram in Figure 4.5.

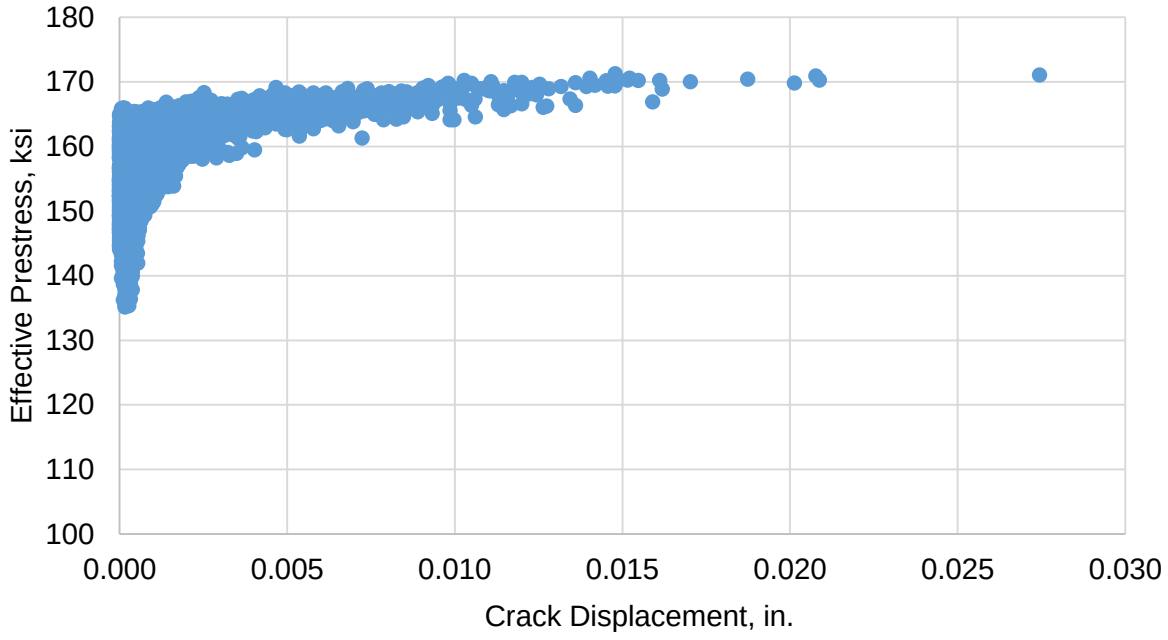

Figure 4.4. Effective prestress vs. crack opening for all 2013 events.

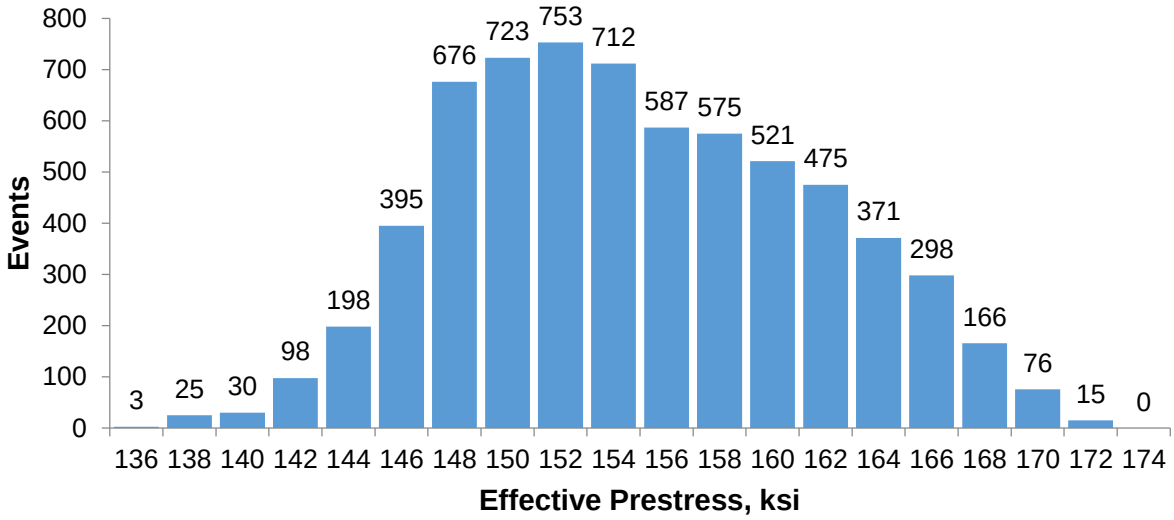

Figure 4.5. Histogram of prestress values for all 2013 events.

The plot in Figure 4.4 indicates that the scatter of prestress estimates increases as the corresponding crack widths decrease. As crack openings approach zero, the scatter in the prestress value exceeds 30 ksi. Furthermore, there appears to be an upper bound to the prestress estimates which increases linearly with crack width. The variation in prestress values at these small crack widths is consistent with the idea that the flange may not have fully decompressed when small crack are registered. The presence of compressive stress is in contrast with the basic assumption employed in the derivation of Equation (3.1) and would be expected to result in low prestress estimates. For this reason, events for which the crack displacements are less than 0.002 in. were disregarded.

As can be seen in Figure 4.6, this 0.002 in. threshold significantly reduces the size of the data set. After applying the threshold, a total of 576 events remain for further analysis. The distribution of prestress estimates, for these 576 events, is shown by the histogram in Figure 4.7. It can be seen that the data resembles a normal distribution. The mean prestress value is 166 ksi, and the standard deviation is 2.5 ksi. Figure 4.8 presents the relationship between effective-prestress values and crack width for the 576 events.

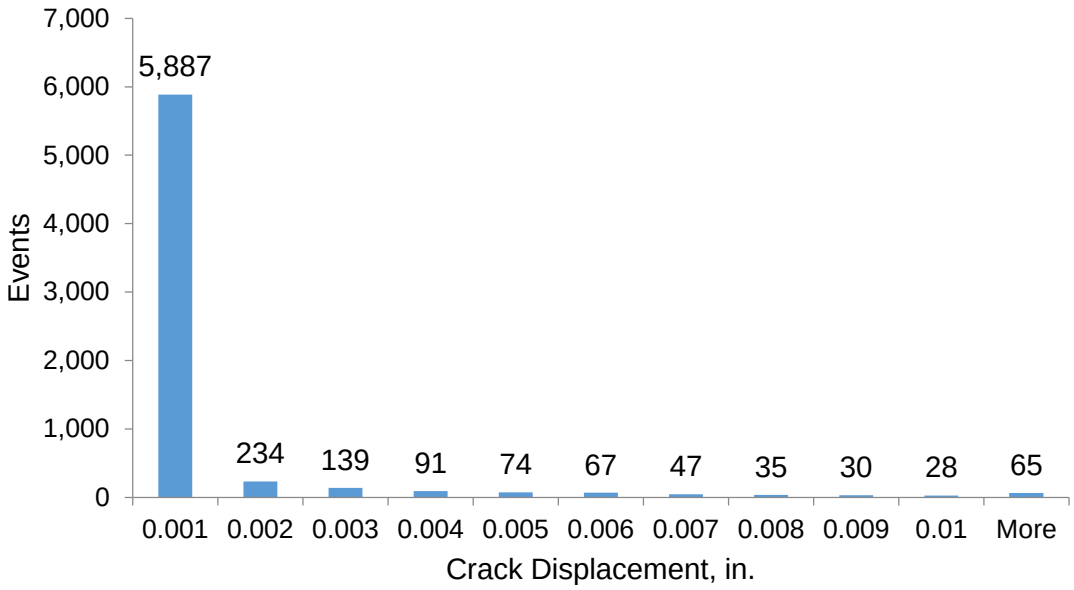

Figure 4.6. Frequency of crack displacement widths for all 2013 events.

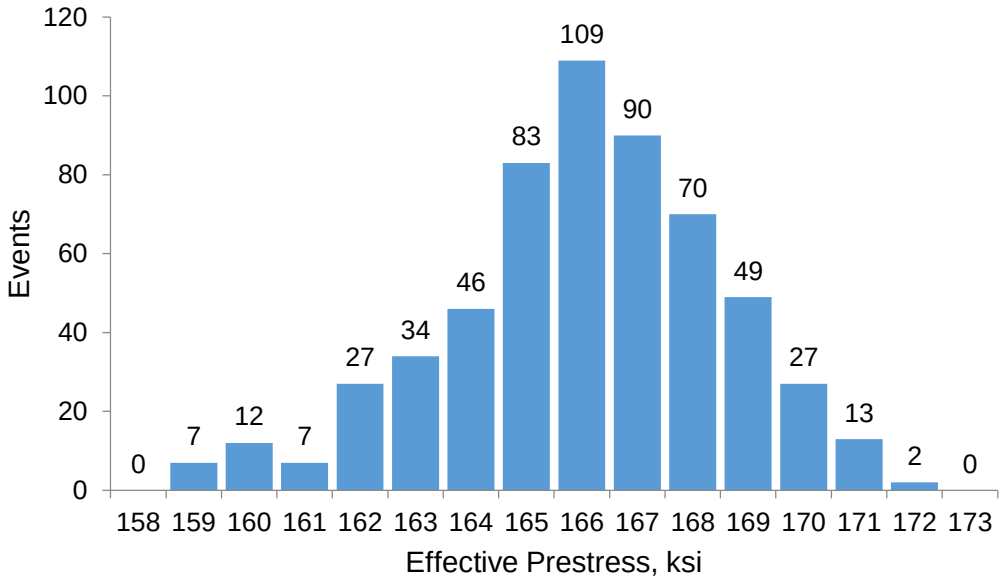

Figure 4.7. Histogram of effective prestress for 2013 events with corresponding crack openings of 0.002 in. or greater.

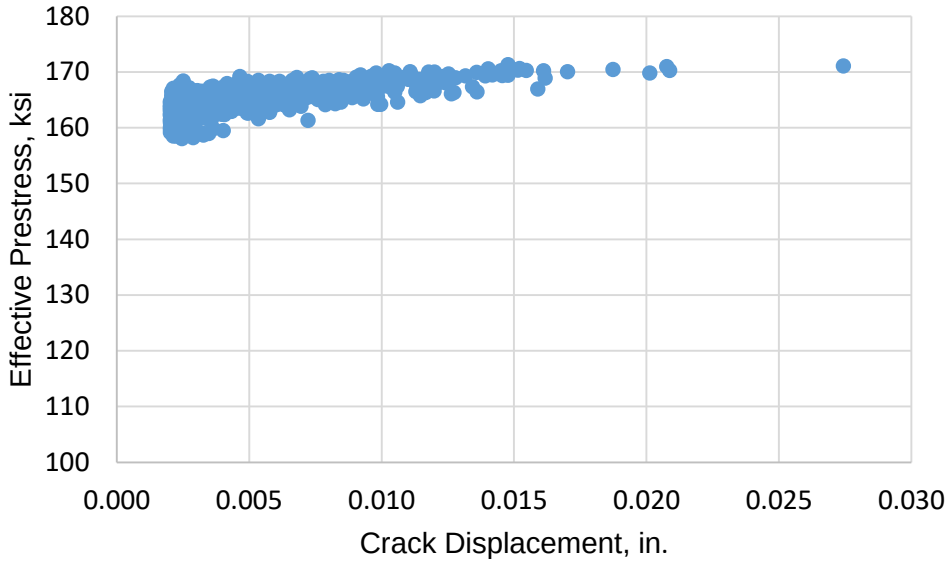

Figure 4.8. Effective prestress vs. crack opening for 2013 events with corresponding crack openings of 0.002 in. or greater.

4.3.1 Comparison of Prestress Values Calculated from 2013 and 2019 Data Sets

As mentioned in Chapter 3.4, the long-term monitoring system was reinstalled in Span 6. Data has been gathered from this new system over a one-month from April to May of 2019. The preliminary results from this data set are presented herein.

A comparison of effective-prestress values calculated from one-month data sets collected in 2013 and 2019 is shown in Figure 4.9. A similar number of events, 1,275 and 1,044 for 2013 and 2019 respectively, were recorded in the two data sets. It can be seen that data from both time frames appears to follow the same relationship between crack-opening widths and effective-prestress values, though crack openings in excess of 0.002 in. have not yet been recorded in 2019. Descriptive statistics for the data gathered in 2013 and 2019 can also be visualized by the box plots shown in Figure 4.10. The average measured prestress for data gathered in 2013 and 2019 is 150.7 ksi and 149.2 ksi respectively.

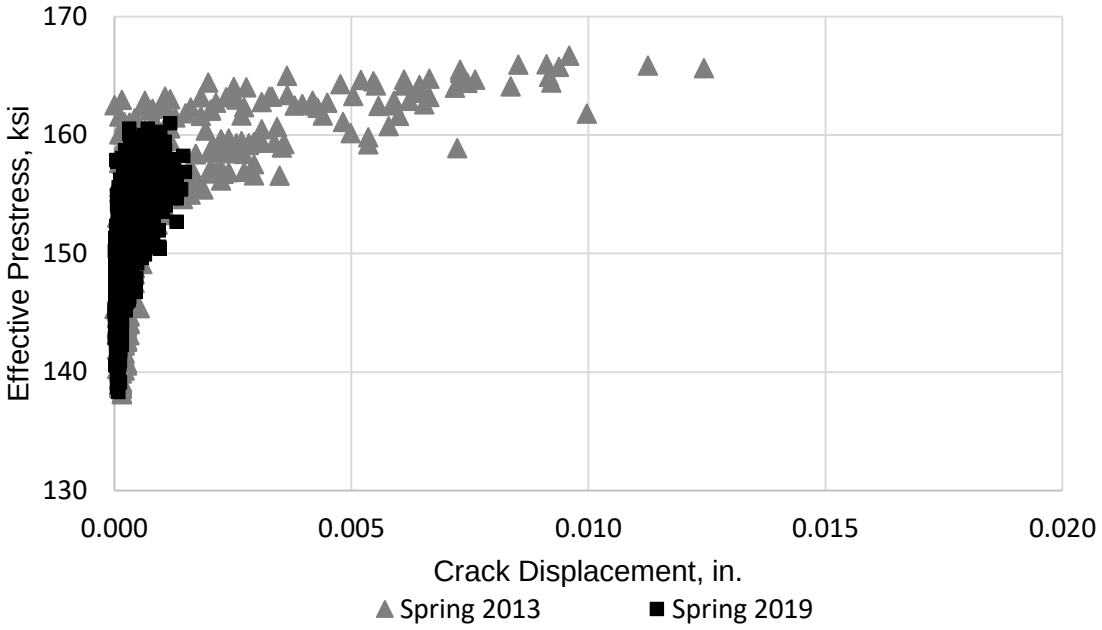

Figure 4.9. Effective prestress vs. crack opening for 2013 and 2019.

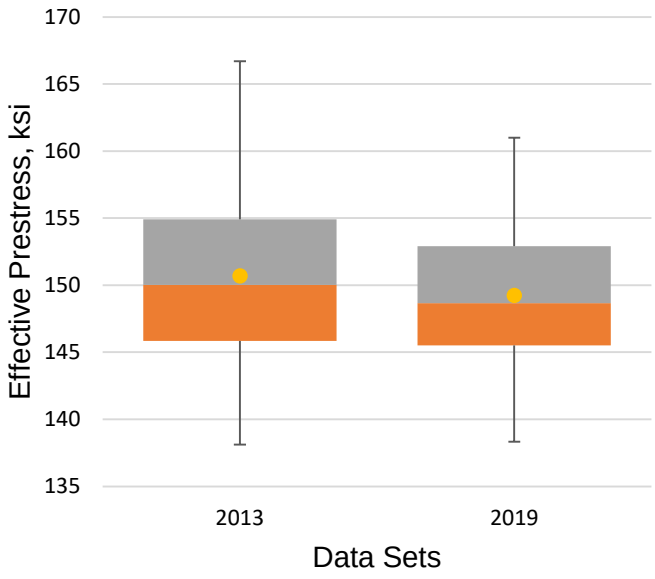

Figure 4.10. Box plots of effective-prestress estimates from April to May of 2013 and 2019.

4.4 Finite Element and Field Data Comparison

The FE model was developed to verify the accuracy of the assumptions made in calculating effective prestress from field data. A comparison of the results from the FE analyses as well as the field-data calculations is shown in Table 4.2. Total losses are calculated by subtracting the effective prestress from the original jacking stress. The jacking stress was assumed to be 213 ksi for all analyses. Both short-term and long-term losses are included in the total loss.

Table 4.2. Comparison of prestress-loss estimations from field data and FE analysis.

	Average prestress loss at 9,500 days, ksi	Percent difference from field estimates
Field Measurements	47.3	n.a.
FE model - CEB-FIP '78	41.9	11.5%
FE model - CEB-FIP '90	43.3	8.4%
FE model - AASHTO	38.1	19.4%

4.5 Flexural strength

It is well-known and documented, e.g. AASHTO 2012 and Naaman 2012, that the ultimate flexural strength of prestressed concrete members with unbonded tendons depends on the effective prestress, rather than the ultimate strength of the prestressing strands. Table 4.3 tabulates the sectional, flexural strength at Section B-B (M_n^+) and at the inside face of Pier 6 (M_n^-). The demands from the AASHTO Strength I Load Combination are 67,970 kip-ft, and -5,642 kip-ft for the positive and negative critical sections respectively.

Table 4.3. Flexural strength resulting from various effective-prestress estimations.

	t = 9,500 days			t = 50 years			t = 100 years		
	fpe (ksi)	φM_n^+ (kip-ft)	$\underline{\varphi M_n^-}$ (kip-ft)	f_{pe} (ksi)	φM_n^+ (kip-ft)	$\underline{\varphi M_n^-}$ (kip-ft)	f_{pe} (ksi)	φM_n^+ (kip-ft)	$\underline{\varphi M_n^-}$ (kip-ft)
Measured mean (total)	154	71,880	38,270	NA	NA	NA	NA	NA	NA
Measured mean (cr > 0.002 in.)	166	75,710	40,490	NA	NA	NA	NA	NA	NA
CEB-FIP '78	173	78,160	41,910	171	77,470	41,510	171	77,470	41,510
CEB-FIP '90	170	76,990	41,240	167	76,130	40,740	167	76,050	40,690
AASHTO	175	78,680	42,210	173	78,040	41,840	173	78,040	41,840

Chapter 5.
Summary, Conclusions, and Recommendations for Future Work

5.1 Summary

The Virginia Department of Transportation identified flexural cracking in the bottom flange of the Varina-Enon Bridge (VEB) in the summer of 2012. This cracking may be the result of several factors, including inadequate effective prestress force. The purpose of this thesis was to investigate the time-dependent, longitudinal flexural behavior of the VEB and estimate the effective prestress. Data from a previous project on the VEB was utilized along with a finite element (FE) model to evaluate the structure. The field data was used to calculate prestress force by assuming that the concrete stress at the time of crack opening was zero. The FE model was used to verify the field-data results by conducting time-step analyses which utilized multiple code expressions for creep and shrinkage.

Field-data results were refined to exclude crack opening events of less than 0.002 in., to ensure the validity of the assumptions employed to estimate the effective prestress. The average prestress calculated from the remaining 576 events is 166 ksi. The FE model utilizes code expressions for creep and shrinkage from the CEB-FIP 1978 and 1990 model codes, as well as the AASHTO LRFD Design Specification. The average effective prestress from these analyses were 173.3, 169.7, and 174.9 ksi respectively.

This Chapter summarizes the main conclusions of the present study and presents recommendations for future research on the VEB.

5.2 Conclusions

5.2.1 Expected and measured prestress

Estimates resulting from raw, field data suggests significantly larger prestress losses than predicted by the FE analyses. Results more closely align with estimates from the FE analyses, however, when events with crack openings less than 0.002 in. are excluded. Even after this threshold is applied, field-data estimates still differ from the FE analysis results, but to a less significant degree.

The analysis using the CEB-FIP ’78 cod expressions results in underestimation of prestress losses by 11.5% as compared to field-data estimates. This is considered to be within a reasonable margin of error considering the complexity of the structure and the uncertainty inherent in creep and shrinkage calculations. The analysis using the CEB-FIP ’90 code expressions most closely matches field-data estimates, only

underestimating losses by 8.4%. This is considered to be a very good agreement, and well within the margin of error. Lastly, the analysis using the AASHTO code expressions underestimates losses by the largest margin at 19.4%. Though this error is considerably larger than the previous two, This may be attributed to relative simplicity of the AASHTO code expressions which take no consideration of the of material properties beyond concrete strength.

In summary, the results from the FE analyses are found to be in good agreement with the results from the field data. Thus, the FE model successfully verifies the assumptions and methods used to calculate effective prestress via crack opening observations on in-service structures. Furthermore, the VEB does not appear to be experiencing significantly larger prestress losses than would have been originally considered at the design of the structure.

5.2.2 Future bridge performance.

Future prestress loss in the VEB may be of concern, but results from the FE model and the field data conflict. Finite element analysis results indicate that the vast majority of prestress loss had already occurred by 2013. The largest additional losses (beyond 2013) are estimated when using the CEB-FIP ’90 code expression for creep and shrinkage. In this analysis the losses in 2013 represent 93.7% of the total 100-year losses. Further research is needed, however, to validate this claim for two reasons. First, the literature suggests that our current code expressions for creep and shrinkage do not adequately represent the progression of these phenomena at old ages. All of the code expressions used in this study assumed a bounded time-development of creep, but Research by Bazant et al. has shown that this is not the case. Second, preliminary results from the long-term monitoring system indicate that the change in average prestress from 2013 to 2019 is nearly twice that which was expected by the analysis utilizing the CEB-FIP ’90 code expressions.

When considering prestress loss, two major serviceability concerns arise. The first concern is that cracking of the structure will cause accelerated deterioration due to moisture infiltration. In the case of the VEB this is of little concern because the tendons are fully grouted and encapsulated in PVC ducts. The second concern is that of deflections. In this regard also, there are not concerns with the VEB itself. In the worst case FE analysis, deflection results indicate that the VEB has experience less than 1/2 in. of deflection from its original camber.

Flexural strength is a concern when considering the effective prestress force in a prestressed concrete member with unbonded tendons. In considering the worst-case estimate of flexural strength in the VEB, the lowest estimate of effective prestress is taken. This estimate is calculated from the raw field data without correction for small crack openings. The flexural strength is adequate for this effective-prestress value when

considering the AASHTO Strength I Load Combination. The demand-to-capacity ratios for this prestress value are and 0.147 the positive and negative moments respectively.

5.3 Recommendations for Future Work

This research has investigated the estimation of effective prestress in Span 6 of the VEB. To better assess the condition of the VEB as a whole, the following recommendations are made for continued work.

1. The literature suggests that current code expressions for creep and shrinkage underestimate prestress losses as structures age beyond 10,000 days. The prestress loss in Span 6 should continue to be monitored in order to assess, the rate at which prestress loss progresses. This progression should then be compared to current model codes.
2. The literature also indicates that the Model B4 provides a more accurate estimation of prestress loss at ages beyond 10,000 days. This analytical model should be incorporated into the FE model, and the results should be compared to the CEB-FIP and AASHTO model codes.
3. LVDTs were originally installed on the top of the bottom flange to measure first crack opening because of access constraints. For the purpose of this thesis, it was assumed, at the time of registered crack opening, that the entire bottom flange had decompressed, and cracked section properties were used as such. To investigate the validity of this assumption, LVDTs should be installed on the bottom of the bottom flange in addition to the top of the bottom flange and results should be compared.
4. Though an estimate of prestress loss has been made in Span 6, similar cracking has been identified at other locations throughout the bridge. These crack locations should be monitored in a similar fashion, to Span 6, to determine if larger than expected losses are found at these additional locations.
5. A more detailed analysis should be conducted to determine how the progression of prestress loss affects the future load rating of the VEB.

BIBLIOGRAPHY

AASHTO (2012). "AASHTO LRFD Bridge Design Specifications." American Association of State Highway and Transportation Officials, Washington, DC.

ACI 209 (2008). "Buide for Modeling and Calculating Shrinkage and Creep in Hardened Concree." American Concrete Institute, Farmington Hills, MI.

ACI 423 (2016). "ACI 423.10R-16 Guide to Estimating Prestress Losses." American Concrete Institute.

Bažant, Ž. P., and Baweja, S. (1995). "Creep and Shrinkage Prediction Model for Analysis and Design of Concrete Structures: Model B3."Farmington Hills, MI.

Bažant, Ž. P., Hubler, M. H., and Yu, Q. (2011). "Pervasiveness of excessive segmental bridge deflections: Wake-up call for creep." *ACI Structural Journal*, 108(6), 766-774.

Bažant, Ž. P., and Jirasek, M. (2018). *Creep and Hygrothermal Effects in Concrete Structures*, Springer Science+Business Media B.V., Dordrecht, The Netherlands.

Bažant, Ž. P., Yu, Q., Li, G.-H., Klein, G. J., and Křístek, V. (2010). "Excessive Deflection of Record-Span Prestressed Box Girder." *Concrete International*, 32(6), 8.

CEB-FIP (1978). *Model Code for Concrete Structures*.

F&M Engineers, I. (1993). "Owner's Manual for Inspection and Maintenance of Segmental Concrete Approach and Main Span." *Varina Enon Bridge*Prepared for: Virginia Department of Transportation.

Garber, D. B., Gallardo, J. M., Deschenes, D. J., and Bayrak, O. (2015). "Experimental investigation of prestress losses in full-Scale bridge girders." *ACI Structural Journal*, 112(5), 553-564.

Halsey, J. T., and Miller, R. (1996). "Destructive testing of two forty-year-old prestressed concrete bridge beam." *PCI Journal*, 41(5), 84-93.

Labia, Y., Saiidi, M. S., and Douglas, B. (1997). "Full-scale testing and analysis of 20-year-old pretensioned concrete box girders." *ACI Structural Journal*, 94(5), 471-482.

Maguire, M. (2013). "Transverse and Longitudinal Bending of Segmental Concrete Box Girder Bridges." Doctor of Philosophy, Virginia Tech, Blacksburg, VA.

Maguire, M., Moen, C. D., Roberts-Wollmann, C., and Cousins, T. (2015). "Field Verification of Simplified Analysis Procedures for Segmental Concrete Bridges." *Journal of Structural Engineering*, 141(1), D4014007 (4014011 pp.).

Maguire, M., Roberts-Wollmann, C., and Cousins, T. (2018). "Live-Load Testing and Long-Term Monitoring of the Varina-Enon Bridge: Investigating Thermal Distress." *Journal of Bridge Engineering*, 23(3).

Maguire, M., Roberts-Wollmann, C. L., and Cousins, T. (2014). "Live Load Test and Long Term Monitoring of the Varina-Enon Bridge." Virginia Tech, Blacksburg, VA.

Naaman, A. E. (2012). *Prestressed Concrete Analysis and Design*, Techno Press 3000, Ann Arbor, MI.

NCHRP (1985). "Thermal Effects in Concrete Bridge Superstructures." T. R. Board, ed., National Research Council, Washington, D.C.

OPAC (2000). "Koror-Babeldoab Bridge." <https://www.opacengineers.com/projects/Koror>.

Osborn, G. P., Barr, P. J., Petty, D. A., Halling, M. W., and Brackus, T. R. (2012). "Residual prestress forces and shear capacity of salvaged prestressed concrete bridge girders." *Journal of Bridge Engineering*, 17(2), 302-309.

Pessiki, S., Kaczinski, M., and Wescott, H. H. (1996). "Evaluation of effective prestress force in 28-year-old prestressed concrete bridge beams." *PCI Journal*, 41(6), 78-89.

Priestley, M. J. N. (1978). "Design of Concrete Bridges for Temperature Gradients." *Journal Proceedings*, 75(5).

Shenoy, C., V., and Frantz, G. C. (1991). "Structural Tests of 27-Year-Old Prestressed Concrete Bridge Beams." *PCI Journal*, 36(5), 11.

Tabatabai, H., and Dickson, T. J. (1993). "Structural Evaluation of a 34-Year-Old Precast Post-Tensioned Concrete Girder." *PCI Journal*, 38(5), 14.

Appendix A. Creep and Shrinkage Models

This thesis utilized several creep and shrinkage models for the purpose of measuring effective prestress force in the finite element model. The following is a detailed description of the calculation procedure for the five creep and shrinkage models reviewed in this research, CEB-FIP '78, CEB-FIP '90, ACI 209R, AASHTO 2012, and Model B3.

CEB-FIP 1978 Creep Calculations

The creep coefficient in the CEB-FIP '78 code is calculated using Equation (A-1). The second term includes a constant φ_d = 0.4, and the function β_d, the product of which represent the *delayed elasticity* of the concrete. The function β_d can is defined graphically, and can be seen in Figure A-1. The third, and last, term of the creep coefficient includes the product of the constant φ_f and the function β_f, which represents the *flow*, or *irreversible delayed deformation* of the concrete. The term φ_f is itself a product of the terms φ_{f1} and φ_{f2} which can be found from Table A-1 and Figure A-2 respectively. β_f is a function which is defined graphically in CEB-FIP 78, and can be seen in Figure A-3. All of the following equations are expressed in terms of SI units.

$$\varphi(t,t_o) = \beta_a(t_o) + \varphi_d \beta_d(t - t_o) + \varphi_f[\beta_f(t) - \beta_f(t_o)] \quad \text{(A-1)}$$

Where β_a, which represents the irreversible deformation is calculated by Equation (A-2). And the notional thickness is calculate by Equation

$$\beta_a = 0.8\left(1 - \frac{f_c(t_0)}{f_{c\infty}}\right) \quad \text{(A-2)}$$

$$h_o = \lambda \frac{A_c}{u} \quad \text{(A-3)}$$

Where:

Ac is the area of the gross cross-section
u is the perimeter in contact with the atmosphere
λ is taken from Table A-1

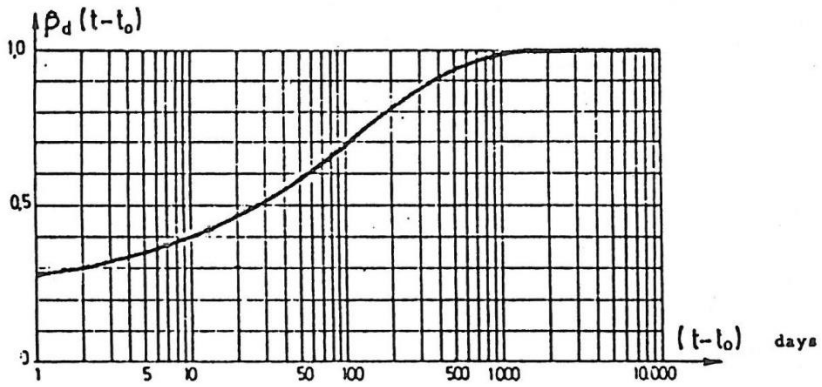

Figure A-1: Development with time of the delayed elastic strain

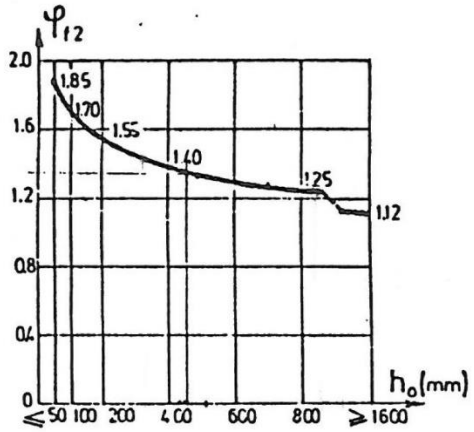

Figure A-2: Influence of notional thickness on creep

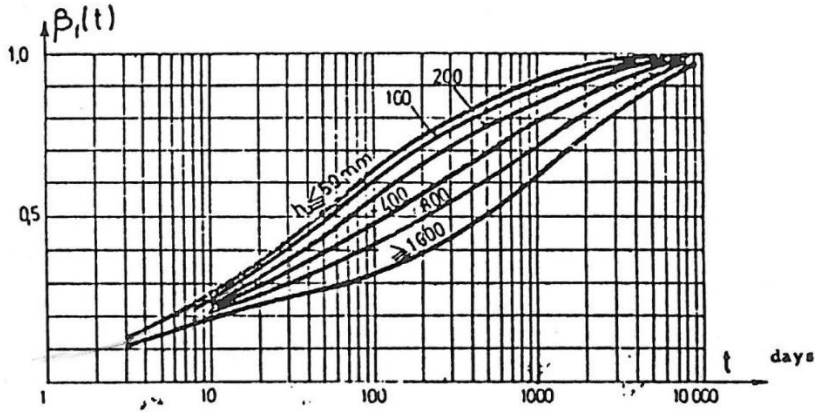

Figure A-3: Development with time of the delayed plastic strain

Table A-1: Basic coefficients of creep and shrinkage.

Ambient Environment	Relative humidity	coefficients of		Coefficient λ (e.1.6)	
		creep φ_{f1}	shrinkage ε_{s1} (e.1.4)		
1	2	3	4	5	
Water		0,8	+0,00010	30	
Very damp atmosphere	90%	1,3 1,0	−0,00013	5	
Outside in general	80% 70%	1,5 2,0	−0,00023 −0,00032	2,5 1,5	
Very dry atmosphere	40%	3,0	−0,00052	1	

CEB-FIP 1978 Shrinkage Calculations

Shrinkage strain, as formulated in the CEB-FIP 78 code, depends primarily on ambient environment and notional thickness. Equation (A-4) shows the calculation of shrinkage strain, which is added to the elastic and creep strains to calculate the total long-term strain in the concrete. The term, β_d is a function which is defined graphically in CEB-FIP 78, and is shown in Figure A-4.

$$\varepsilon_s(t,t_o) = \varepsilon_{so}\left[\beta_s(t) - \beta_s(t_o)\right] \tag{A-4}$$

Where the basic shrinkage coefficient, ε_{so} is calculated by Equation (A-5)

$$\varepsilon_{so} = \varepsilon_{s1}\varepsilon_{s2} \tag{A-5}$$

Where:

ε_{s1} is found in Table A-1

ε_{s2} is taken from Figure A-5

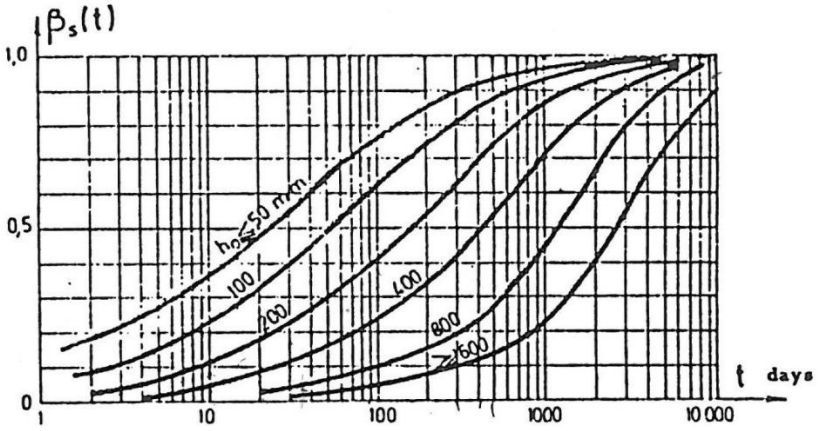

Figure A-4: Influence of the notional thickness on shrinkage

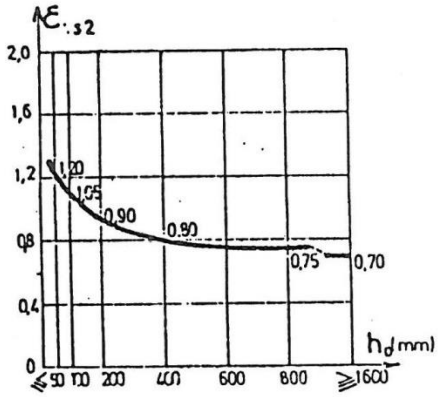

Figure A-5: Influence of the notional thickness on shrinkage

CEB-FIP 1990 Creep Calculations

In the CEB-FIP '90 formulation of creep and shrinkage models, the creep compliance function which describes the stress dependent strain, per unit stress is calculated using Equation (A-10). All of the following calculations are in terms of lb. and in.

$$J(t,t_o) = \frac{1}{E_{cmto}} + \frac{\Phi_{28}(t,t_o)}{E_{cm28}} \tag{A-6}$$

$$E_{cmt} = E_{cm28} e^{\left[\frac{s}{2}\left(1-\sqrt{\frac{28}{t/t_1}}\right)\right]} \tag{A-7}$$

Where t is the age of concrete at the time of interest, and $t_1 = 1\ day$. And the coefficient, s is taken from Table A-2.

$$E_{cm28} = \alpha_E 3{,}118310 \sqrt[3]{\frac{f_{cm28}}{f_{cmo}}} \tag{A-8}$$

Where $f_{cmo} = 1450\ psi.$ and α_E is taken from Table A-3

$$f_{cm28} = f`_c + 1160\text{psi} \tag{A-9}$$

Where $f`_c$ is the specified compressive cylinder strength defined as the strength below which 5% of all possible strength measurements for the specified concrete may be expected to fall.

$$\phi_{28}(t,t_o) = \phi_o \beta_c (t - t_o) \tag{A-10}$$

Where

$$\phi_o = \phi_{RH}(h)\beta(f_{cm28})\beta(t_o) \tag{A-11}$$

$$\phi_{RH}(h) = \left[1 + \frac{1 - h/h_o}{\sqrt[3]{0.1[(V/S)/(V/S)_o]}}\alpha_1\right]\alpha_2 \tag{A-12}$$

Where (V/S) is the volume to surface ratio of the section, and h is the relative humidity as a decimal. $(V/S)_o = 2\ in.$ and $h_o = 1$.

$$\beta(f_{cm28}) = \frac{5.3}{\sqrt{f_{cm28}/f_{cmo}}} \tag{A-13}$$

$$\beta(t_o) = \frac{1}{0.1 + (t_o/t_1)^{0.2}}$$

$$\alpha_1 = \left[\frac{3.5 f_{cmo}}{f_{cm28}}\right]^{0.7} \tag{A-14}$$

$$\alpha_2 = \left[\frac{3.5 f_{cmo}}{f_{cm28}}\right]^{0.2} \quad \text{(A-15)}$$

And (A-16)

$$\beta_c(t\text{-}t_o) = \left[\frac{(t-t_o)/t_1}{\beta_H + (t-t_o)/t_1}\right]^{0.3}$$

$$\beta_H = 150\left[1+(1.2h)^{18}\right](V/S) + 250\alpha_3 \le 1500\alpha_3 \quad \text{(A-17)}$$

$$\alpha_3 = \left[\frac{3.5 f_{cmo}}{f_{cm28}}\right]^{0.5} \quad \text{(A-18)}$$

Table A-2: Coefficient s, which depends on cement type.

f_{cm28}	Type of cement	s
≤60 MPa (8700 psi)	RS (rapid hardening high-strength cement)	0.20
	N or R (normal or rapid hardening cements)	0.25
	SL (slowly-hardening cement)	0.38
>60 MPa (8700 psi)*	All types	0.20

*Case not considered in CEB MC90.

Table A-3: Coefficient α_E, Effect of aggregate type on modulus of elasticity..

Aggregate type	α_E
Basalt, dense limestone aggregates	1.2
Quartzitic aggregates	1.0
Limestone aggregates	0.9
Sandstone aggregates	0.7

CEB-FIP 1990 Shrinkage Calculations

Shrinkage strains in CEB-FIP model code ‘90 are calculated very similarly to shrinkage strains in the ‘78 model code. Total shrinkage strains are the product of a notional shrinkage coefficient and a function of shrinkage development with time, as shown in Equation (A-19).

$$\varepsilon_{sh}(t,t_c) = \varepsilon_{cso}\beta_s(t-t_c) \quad \text{(A-19)}$$

Where t_c is the age that drying ends (day).

$$\varepsilon_{cso} = \varepsilon_s\left(f_{cm28}\right)\beta_{RH}(h) \quad \text{(A-20)}$$

$$\varepsilon_s\left(f_{cm28}\right) = \left[160 + 10\beta_{sc}\left(9 - f_{cm28}/f_{cm0}\right)\right]\cdot 10^{-6} \quad \text{(A-21)}$$

Where β_{sc} is found in Table A-4.

$$\beta_{RH}(h) = -1.55[1-(h/h_o)^3] \quad \text{for } 0.4 \le h < 0.99 \quad \text{(A-22)}$$

$$\beta_{RH}(h) = 0.25 \quad \text{for } h \geq 0.99$$

$$\beta_s(t - t_c) = \left[\frac{(t - t_c)/t_1}{350[(V/S)/(V/S)_o]^2 + (t - t_c)/t_1} \right]^{0.5} \tag{A-23}$$

Table A-4: Coefficient β_{sc}, which depends on cement type.

Type of cement according to EC2	β_{sc}
SL (slowly-hardening cements)	4
N and R (normal or rapid hardening cements)	5
RS (rapid hardening high-strength cements)	8

ACI 209R-92 Creep Compliance

The ACI 209R-92 creep compliance function is shown in Equation (A-24).

$$J(t,t_o) = \frac{1+\phi\left(t,t_o\right)}{E_{cmto}} \tag{A-24}$$

$$E_{cmto} = 33\gamma_c^{1.5}\sqrt{f_{cmto}} \tag{A-25}$$

$$f_{cmt} = \left[\frac{t}{a+bt}\right] f_{cm28} \tag{A-26}$$

Where a and b are taken from Table A-5

$$\phi(t,t_o) = \frac{\left(t-t_o\right)^{\psi}}{d+\left(t-t_o\right)^{\psi}}\phi_u \tag{A-27}$$

Where And d and ψ are typically taken as 10 and 0.6 respectively.

$$\phi_u = 2.35\gamma_c \tag{A-28}$$

$$\gamma_c = \gamma_{c,to}\gamma_{c,RH}\gamma_{c,vs}\gamma_{c,s}\gamma_{c,\psi}\gamma_{sh,\alpha} \tag{A-29}$$

For steam cured concrete,

$$\gamma_{c,to} = 1.13t_o^{-0.094} \tag{A-30}$$

$$\gamma_{c,RH} = 1.27 - 0.67h \text{ for h} \geq 0.40 \tag{A-31}$$

$$\gamma_{c,vs} = \frac{2}{3}\left(1+1.13e^{\{-0.54(V/S)\}}\right) \tag{A-32}$$

Where h is the relative humidity, and V/S is the volume-to-surface ratio.

$$\gamma_{c,s} = 0.82 + 0.067s \tag{A-33}$$

Where s is the slump of fresh concrete.

$$\gamma_{c,\psi} = 0.88 + 0.0024\psi \tag{A-34}$$

Where ψ is the ratio of fine aggregate to total aggregate by weight.

$$\gamma_{c,\alpha} = 0.46 + 0.09\alpha \geq 1 \tag{A-35}$$

Where α is the air content of the concrete expressed as a percent, and $\gamma_{sh,\alpha}$ is taken from the shrinkage calculation.

Table A-5: Values of the constants *a* and *b*

Type of cement	Moist-cured concrete		Steam-cured concrete	
	a	b	a	b
I	4.0	0.85	1.0	0.95
III	2.3	0.92	0.70	0.98

ACI 209R-92 Shrinkage Calculation

The total shrinkage strain calculated by ACI 209R-92 is shown in Equation (A-36).

$$\varepsilon_{shu} = 780\gamma_{sh} \cdot 10^{-6} \quad \text{(in./in.)} \tag{A-36}$$

$$\gamma_{sh} = \gamma_{sh,tc}\gamma_{sh,RH}\gamma_{sh,vs}\gamma_{sh,s}\gamma_{sh,\psi}\gamma_{sh,c}\gamma_{sh,\alpha} \tag{A-37}$$

$$\gamma_{sh,tc} = 1.0 \quad \text{for steam cured concrete} \tag{A-38}$$

$$\gamma_{sh,RH} = 140 - 1.02h \quad \text{for } 0.40 \le h \le 0.80 \tag{A-39}$$

$$\gamma_{sh,vs} = 1.2e^{\{-0.12(V/S)\}} \tag{A-40}$$

$$\gamma_{sh,s} = 0.89 + 0.0161s \tag{A-41}$$

$$\gamma_{sh,\psi} = 0.30 + 0.014\psi \quad \text{for } \psi \le 50\% \tag{A-42}$$

$$\gamma_{sh,\psi} = 0.90 + 0.002\psi \quad \text{for } \psi > 50\%$$

$$\gamma_{sh,c} = 0.75 + 0.00036c \tag{A-43}$$

Where c is the cement content in lb/yd^3

$$\gamma_{sh,\alpha} = 0.95 + 0.008\alpha \quad \ge 1 \tag{A-44}$$

AASHTO 2012 Creep Calculation

Creep calculations are given in the AASHTO LRFD design specifications 6th edition, in section 5.4.2.3.2. No equation for creep compliance is given in the AASHTO specification. Rather, the creep coefficient is simply calculated, as seen in Equation (A-45).

$$\psi(t,t_i)=1.9k_s k_{hc} k_f k_{td} t_i^{-0.118} \tag{A-45}$$

Where t_i is the age of concrete at the time of load application (day)

$$k_s = 1.45 - 0.13(V/S) \geq 1.0 \tag{A-46}$$

$$k_{hc} = 1.56 - 0.008H \geq 1.0 \tag{A-47}$$

Where H is the ambient relative humidity. The time-development of both creep and shrinkage are:

$$k_{tc} = \left(\frac{t}{61 - 4f`_{ci} + t} \right) \tag{A-48}$$

AASHTO 2012 Shrinkage Calculation

Shrinkage strains in the AASHTO specification are calculated directly by Equation (A-49). If the concrete is exposed to drying before 5 days of curing have elapsed, the shrinkage strain should be increased by 20 percent.

$$\varepsilon_{sh} = k_s k_{hs} k_f k_{td} 0.48 \times 10^{-3} \tag{A-49}$$

Where the humidity factor for shrinkage is:

$$k_{hs} = 2.00 - 0.014H \tag{A-50}$$

Model B3 Creep Calculation

The creep compliance function for the Model B3 consists of three parts which can be seen in Equation (A-51). q_1 represents the instantaneous strain due to the unit stress, $C_o(t,t_o)$ is the compliance function for basic creep, and $C_d(t,t_o)$ is the compliance function for drying creep.

$$J(t,t_o) = q_1 + C_o\left(t,t_o\right) + C_d\left(t,t_o,t_c\right) \tag{A-51}$$

Where q_1 is taken as the instantaneous strain due to a unit stress, and is calculated by Equation (A-52)

$$q_1 = \frac{0.6}{E_{cm28}} \tag{A-52}$$

and

$$E_{cm28} = 57{,}000\sqrt{f_{cm28}}\,. \tag{A-53}$$

The compliance function for basic creep is composed of an aging viscoelstic term, a non-aging viscoelastic term, and an aging flow term, as seen in Equation (A-54)

$$C_o\left(t,t_o\right) = q_2 Q(t,t_o) + q_3 \ln[1+\left(t-t_o\right)^n] + q_4 \ln(t/t_o) \tag{A-54}$$

Where t_o is the age of concrete when the load is applied (days).

$$q_2 = 86.814\cdot 10^{-6} c^{0.5} f_{cm28}{}^{-0.9} \tag{A-55}$$

Where c is the cement content of the concrete (lb/yd^3)

$$Q(t,t_o) = Q_f(t_o)\left[1+\left(\frac{Q_f\ t_o}{Z\ t,t_o}\right)^{r\ t_o}\right]^{-1/r\ t_o} \tag{A-56}$$

$$Q_f\ t_o = \left[0.086\ t_o{}^{2/9} + 1.21\ t_o{}^{4/9}\right]^{-1} \tag{A-57}$$

$$Z\ t,t_o = t_o{}^{-m}\cdot\ln\left[1+\ t-t_o{}^{\ n}\right] \tag{A-58}$$

Where m and n are empirical parameters who's values can be taken as 0.5 and 0.1 respectively for all normal weight concretes.

$$r\ t_o = 1.7\ t_o{}^{0.12} + 8 \tag{A-59}$$

$$q_3 = 0.29\ \ w/c\ {}^4 q_2 \tag{A-60}$$

$$q_4 = 0.14\cdot 10^{-6}\ \ a/c\ {}^{-0.7} \tag{A-61}$$

Where w/c and a/c are the water-to-cement and aggregate-to-cement ratios respectively. The compliance function for drying creep is shown in Equation (A-62), and can be seen to include drying from before loading begins.

$$C_d\ \ t,t_o,t_c\ \ = q_5\Big[\exp\ \ -8H\ \ t\ \ \ -\exp\ \ -8H(t_o\ \ \Big]^{1/2} \tag{A-62}$$

Where t_c is the age that drying commences (days).

$$q_5 = 0.757\, f_{cm28}{}^{-1}\left|\varepsilon_{sh\infty}\cdot 10^6\right|^{-6} \tag{A-63}$$

Where $\varepsilon_{sh\infty}$ is the ultimate shrinkage strain as calculated in Equation (A-68).

$$H\ \ t\ \ = 1-\ \ 1-h\ \ S\ \ t-t_c \tag{A-64}$$

$$H\ \ t_o\ \ = 1-\ \ 1-h\ \ S\ \ t_o-t_c \tag{A-65}$$

Where $S(t\text{-}t_c)$ represents the time function for shrinkage as seen in Equation (A-66).

$$S(t-t_c) = \tanh\left[\left(\frac{t-t_c}{\tau_{sh}}\right)^{1/2}\right] \tag{A-66}$$

Model B3 Shrinkage Calculation

The mean shrinkage strain in the cross section at a concrete age of t (days) is calculated using Equation (A-67).

$$\varepsilon_{sh}\ \ t,t_c\ \ = -\varepsilon_{sh\infty}k_h S\ \ t-t_c \tag{A-67}$$

Where k_h is taken from Table A-6.

$$\varepsilon_{sh\infty} = -\varepsilon_{s\infty}\frac{E_{cm607}}{E_{cm\ \ t_c+\tau_{sh}}} \tag{A-68}$$

$$\varepsilon_{s\infty} = -\alpha_1\alpha_2\left[0.02565w^{2.1}f_{cm28}{}^{-0.28}+270\right]\cdot 10^{-6} \tag{A-69}$$

Where α_1 and α_2 are taken from Table A-7 and Table A-8 respectively.

$$E_{cmt} = E_{cm28}\left(\frac{t}{4+0.85t}\right)^{0.5} \tag{A-70}$$

$$\tau_{sh} = 190.8t_c{}^{-0.08}f_{cm28}{}^{-0.25}\Big[2k_s\ \ V/S\ \ \Big]^2 \tag{A-71}$$

Where k_s is taken from Table A-9.

Table A-6: Values for humidity dependent, k_h

Relative humidity	k_h
$h \leq 0.98$	$1 - h^3$
$h = 1.00$	–0.2
$0.98 < h < 1.00$	Linear interpolation: $12.74 - 12.94h$

Table A-7: Values for α_1 as a function of cement type

Type of cement	α_1
Type I	1.00
Type II	0.85
Type III	1.10

Table A-8: Values of α_2 as a function of cement type

Curing method	α_2
Steam cured	0.75
Cured in water or at 100% relative humidity	1.00
Sealed during curing or normal curing in air with initial protection against drying	1.20

Table A-9: Values of k_s as a function of cross section shape

Cross section shape	k_s
Infinite slab	1.00
Infinite cylinder	1.15
Infinite square prism	1.25
Sphere	1.30
Cube	1.55

Note: The analyst needs to estimate which of these shapes best approximates the real shape of the member or structure. High accuracy in this respect is not needed, and $k_s \approx 1$ can be used for simplified analysis.

Appendix B. Finite Element Model Report

INPUT PROPERTIES	Count	INPUT GEOMETRY	Count	Load Cases	Count
Universal Restraints	NONE	Joints	101	Load Cases	24
Materials	3	Members	91	Combination Cases	NONE
Sections	7	Plates	NONE	Construction Stages	16
User Coordinate System	NONE	Springs	21	Linked Databases	2
Spring Curves	NONE	Isolaters	NONE		
Isolater Property	NONE	Mass Elements	NONE		
Creep Definitions	1	Slave / Masters	NONE		
		Tendons	48		

INPUT : Material Properties

Name	Modulus of Elasticity (lb/in²)	Poisson Ratio	Shear Modulus (lb/in²)	Unit Weight (lb/in³)	Thermal Expansion (1/ °F *10^-6)	Assigned
Fc_5500	5,000,000.00	0.1704	2,135,946.42	0.0897	5.500000	Yes
Rigid Material	400,000.00	0.0000	200,000.00	0.0000	0.000000	Yes
A416	2.74e7	0.2946	1.06e7	0.2836	6.500000	Yes

INPUT : Joints

ID	X (ft)	Y (ft)	Z (ft)	Translation DOF	Rotation DOF	Displacement UCS	Assignment
1	0.0000	0.0000	100.9000	all free	all free	Global	Yes
2	4.0000	0.0000	101.0200	all free	all free	Global	Yes
3	5.0000	0.0000	101.0500	all free	all free	Global	Yes
4	25.0000	0.0000	101.6498	all free	all free	Global	Yes
5	45.0000	0.0000	102.2496	all free	all free	Global	Yes
6	65.0000	0.0000	102.8494	all free	all free	Global	Yes
7	85.0000	0.0000	103.4492	all free	all free	Global	Yes
8	105.0000	0.0000	104.0490	all free	all free	Global	Yes
9	125.0000	0.0000	104.6488	all free	all free	Global	Yes
10	145.0000	0.0000	105.2486	all free	all free	Global	Yes
11	146.0000	0.0000	105.2785	all free	all free	Global	Yes
12	150.0000	0.0000	105.3985	all free	all free	Global	Yes
13	154.0000	0.0000	105.5185	all free	all free	Global	Yes
14	155.0000	0.0000	105.5485	all free	all free	Global	Yes
15	175.0000	0.0000	106.1483	all free	all free	Global	Yes
16	195.0000	0.0000	106.7481	all free	all free	Global	Yes
17	215.0000	0.0000	107.3479	all free	all free	Global	Yes
18	235.0000	0.0000	107.9477	all free	all free	Global	Yes
19	255.0000	0.0000	108.5475	all free	all free	Global	Yes
20	275.0000	0.0000	109.1473	all free	all free	Global	Yes
21	295.0000	0.0000	109.7471	all free	all free	Global	Yes
22	296.0000	0.0000	109.7770	all free	all free	Global	Yes
23	300.0000	0.0000	109.8970	all free	all free	Global	Yes
24	304.0000	0.0000	110.0170	all free	all free	Global	Yes
25	305.0000	0.0000	110.0470	all free	all free	Global	Yes
26	325.0000	0.0000	110.6468	all free	all free	Global	Yes
27	345.0000	0.0000	111.2466	all free	all free	Global	Yes
28	365.0000	0.0000	111.8464	all free	all free	Global	Yes
29	385.0000	0.0000	112.4462	all free	all free	Global	Yes
30	405.0000	0.0000	113.0460	all free	all free	Global	Yes
31	425.0000	0.0000	113.6458	all free	all free	Global	Yes
32	445.0000	0.0000	114.2456	all free	all free	Global	Yes
33	446.0000	0.0000	114.2755	all free	all free	Global	Yes
34	450.0000	0.0000	114.3955	all free	all free	Global	Yes
35	454.0000	0.0000	114.5155	all free	all free	Global	Yes
36	455.0000	0.0000	114.5455	all free	all free	Global	Yes
37	475.0000	0.0000	115.1453	all free	all free	Global	Yes
38	495.0000	0.0000	115.7451	all free	all free	Global	Yes
39	515.0000	0.0000	116.3449	all free	all free	Global	Yes
40	535.0000	0.0000	116.9447	all free	all free	Global	Yes
41	555.0000	0.0000	117.5445	all free	all free	Global	Yes
42	575.0000	0.0000	118.1443	all free	all free	Global	Yes
43	595.0000	0.0000	118.7441	all free	all free	Global	Yes
44	596.0000	0.0000	118.7740	all free	all free	Global	Yes
45	600.0000	0.0000	118.8940	all free	all free	Global	Yes
46	604.0000	0.0000	119.0140	all free	all free	Global	Yes
47	605.0000	0.0000	119.0440	all free	all free	Global	Yes
48	625.0000	0.0000	119.6438	all free	all free	Global	Yes
49	645.0000	0.0000	120.2436	all free	all free	Global	Yes

50	665.0000	0.0000	120.8434	all free	all free	Global	Yes
51	685.0000	0.0000	121.4432	all free	all free	Global	Yes
52	705.0000	0.0000	122.0430	all free	all free	Global	Yes
53	725.0000	0.0000	122.6428	all free	all free	Global	Yes
54	745.0000	0.0000	123.2426	all free	all free	Global	Yes
55	746.0000	0.0000	123.2725	all free	all free	Global	Yes
56	750.0000	0.0000	123.3925	all free	all free	Global	Yes
57	754.0000	0.0000	123.5125	all free	all free	Global	Yes
58	755.0000	0.0000	123.5425	all free	all free	Global	Yes
59	775.0000	0.0000	124.1423	all free	all free	Global	Yes
60	795.0000	0.0000	124.7421	all free	all free	Global	Yes
61	815.0000	0.0000	125.3419	all free	all free	Global	Yes
62	835.0000	0.0000	125.9417	all free	all free	Global	Yes
63	855.0000	0.0000	126.5415	all free	all free	Global	Yes
64	875.0000	0.0000	127.1413	all free	all free	Global	Yes
65	895.0000	0.0000	127.7411	all free	all free	Global	Yes
66	896.0000	0.0000	127.7710	all free	all free	Global	Yes
67	900.0000	0.0000	127.8910	all free	all free	Global	Yes
101	0.0000	0.0000	88.2667	all fixed	all fixed	Global	Yes
102	-0.6333	0.0000	88.9000	all free	all free	Global	No
103	0.0000	0.6330	88.9000	all free	all free	Global	No
104	0.0000	0.0000	88.9000	x fixed	x, z fixed	Global	Yes
201	150.0000	0.0000	21.2102	all fixed	all fixed	Global	Yes
202	150.0000	0.0000	27.2102	all free	all free	Global	Yes
203	150.0000	0.0000	89.0402	all free	all free	Global	Yes
204	150.0000	0.0000	93.0402	y fixed	x, z fixed	Global	Yes
205	150.0000	0.0000	93.3985	y fixed	x, z fixed	Global	Yes
301	300.0000	0.0000	13.8170	all fixed	all fixed	Global	Yes
302	300.0000	0.0000	19.8170	all free	all free	Global	Yes
303	300.0000	0.0000	93.6470	all free	all free	Global	Yes
304	300.0000	0.0000	97.6470	y fixed	x, z fixed	Global	Yes
305	300.0000	0.0000	97.8970	y fixed	x, z fixed	Global	Yes
401	450.0000	0.0000	1.3155	all fixed	all fixed	Global	Yes
402	450.0000	0.0000	7.3155	all free	all free	Global	Yes
403	450.0000	0.0000	98.1455	all free	all free	Global	Yes
404	450.0000	0.0000	102.1455	y fixed	x, z fixed	Global	Yes
405	450.0000	0.0000	102.3955	y fixed	x, z fixed	Global	Yes
501	600.0000	0.0000	-0.1860	all fixed	all fixed	Global	Yes
502	600.0000	0.0000	5.8140	all free	all free	Global	Yes
503	600.0000	0.0000	102.6440	all free	all free	Global	Yes
504	600.0000	0.0000	106.6440	y fixed	x, z fixed	Global	Yes
505	600.0000	0.0000	106.8940	y fixed	x, z fixed	Global	Yes
601	750.0000	0.0000	0.2042	all fixed	all fixed	Global	Yes
602	750.0000	0.0000	6.2042	all free	all free	Global	Yes
603	750.0000	0.0000	107.0342	all free	all free	Global	Yes
604	750.0000	0.0000	111.0342	y fixed	x, z fixed	Global	Yes
605	750.0000	0.0000	111.3925	y fixed	x, z fixed	Global	Yes
701	900.0000	0.0000	0.4277	all fixed	all fixed	Global	Yes
702	900.0000	0.0000	6.4277	all free	all free	Global	Yes
703	900.0000	0.0000	111.2577	all free	all free	Global	Yes
704	900.0000	0.0000	115.2577	y fixed	x, z fixed	Global	Yes
705	900.0000	0.0000	115.8910	y fixed	x, z fixed	Global	Yes

INPUT : Members

ID	I-Joint	J-Joint	Spa	Type	Section at Start	Section at End	Material	Prestress Force	Length (ft)	Rigid Zone from	Rigid Zone from End	Orientation Angle (deg)	Casting (day	Structure Group
1	1	2	-	Beam	pier	(same as start)	Fc_5500	0.0000	4.0018	0.0000	0.0000	90.0000	17	span 1
2	2	3	-	Beam	section	(same as start)	Fc_5500	0.0000	1.0004	0.0000	0.0000	90.0000	17	span 1
3	3	4	-	Beam	section	(same as start)	Fc_5500	0.0000	20.009	0.0000	0.0000	90.0000	33	span 1
4	4	5	-	Beam	section	(same as start)	Fc_5500	0.0000	20.009	0.0000	0.0000	90.0000	32	span 1
5	5	6	-	Beam	section	(same as start)	Fc_5500	0.0000	20.009	0.0000	0.0000	90.0000	27	span 1
6	6	7	-	Beam	section	(same as start)	Fc_5500	0.0000	20.009	0.0000	0.0000	90.0000	26	span 1
7	7	8	-	Beam	section	(same as start)	Fc_5500	0.0000	20.009	0.0000	0.0000	90.0000	25	span 1
8	8	9	-	Beam	section	(same as start)	Fc_5500	0.0000	20.009	0.0000	0.0000	90.0000	24	span 1
9	9	10	-	Beam	section	(same as start)	Fc_5500	0.0000	20.009	0.0000	0.0000	90.0000	4	span 1
10	10	11	-	Beam	section	(same as start)	Fc_5500	0.0000	1.0004	0.0000	0.0000	90.0000	70	span 1
11	11	12	-	Beam	pier	(same as start)	Fc_5500	0.0000	4.0018	0.0000	0.0000	90.0000	70	span 1
12	12	13	-	Beam	pier	(same as start)	Fc_5500	0.0000	4.0018	0.0000	0.0000	90.0000	70	span 1
13	13	14	-	Beam	section	(same as start)	Fc_5500	0.0000	1.0004	0.0000	0.0000	90.0000	70	span 1
14	14	15	-	Beam	section	(same as start)	Fc_5500	0.0000	20.009	0.0000	0.0000	90.0000	46	span 2
15	15	16	-	Beam	section	(same as start)	Fc_5500	0.0000	20.009	0.0000	0.0000	90.0000	45	span 2
16	16	17	-	Beam	section	(same as start)	Fc_5500	0.0000	20.009	0.0000	0.0000	90.0000	44	span 2
17	17	18	-	Beam	section	(same as start)	Fc_5500	0.0000	20.009	0.0000	0.0000	90.0000	41	span 2
18	18	19	-	Beam	section	(same as start)	Fc_5500	0.0000	20.009	0.0000	0.0000	90.0000	40	span 2
19	19	20	-	Beam	section	(same as start)	Fc_5500	0.0000	20.009	0.0000	0.0000	90.0000	38	span 2
20	20	21	-	Beam	section	(same as start)	Fc_5500	0.0000	20.009	0.0000	0.0000	90.0000	37	span 2
21	21	22	-	Beam	section	(same as start)	Fc_5500	0.0000	1.0004	0.0000	0.0000	90.0000	6	span 2

22	22	23	-	Beam	pier	(same as start)	Fc_5500	0.0000	4.0018	0.0000	0.0000	90.0000	6	span 2
23	23	24	-	Beam	pier	(same as start)	Fc_5500	0.0000	4.0018	0.0000	0.0000	90.0000	6	span 2
24	24	25	-	Beam	section	(same as start)	Fc_5500	0.0000	1.0004	0.0000	0.0000	90.0000	6	span 2
25	25	26	-	Beam	section	(same as start)	Fc_5500	0.0000	20.009	0.0000	0.0000	90.0000	62	span 3
26	26	27	-	Beam	section	(same as start)	Fc_5500	0.0000	20.009	0.0000	0.0000	90.0000	60	span 3
27	27	28	-	Beam	section	(same as start)	Fc_5500	0.0000	20.009	0.0000	0.0000	90.0000	55	span 3
28	28	29	-	Beam	section	(same as start)	Fc_5500	0.0000	20.009	0.0000	0.0000	90.0000	54	span 3
29	29	30	-	Beam	section	(same as start)	Fc_5500	0.0000	20.009	0.0000	0.0000	90.0000	52	span 3
30	30	31	-	Beam	section	(same as start)	Fc_5500	0.0000	20.009	0.0000	0.0000	90.0000	51	span 3
31	31	32	-	Beam	section	(same as start)	Fc_5500	0.0000	20.009	0.0000	0.0000	90.0000	47	span 3
32	32	33	-	Beam	section	(same as start)	Fc_5500	0.0000	1.0004	0.0000	0.0000	90.0000	76	span 3
33	33	34	-	Beam	pier	(same as start)	Fc_5500	0.0000	4.0018	0.0000	0.0000	90.0000	76	span 3
34	34	35	-	Beam	pier	(same as start)	Fc_5500	0.0000	4.0018	0.0000	0.0000	90.0000	76	span 3
35	35	36	-	Beam	section	(same as start)	Fc_5500	0.0000	1.0004	0.0000	0.0000	90.0000	76	span 3
36	36	37	-	Beam	section	(same as start)	Fc_5500	0.0000	20.009	0.0000	0.0000	90.0000	76	span 4
37	37	38	-	Beam	section	(same as start)	Fc_5500	0.0000	20.009	0.0000	0.0000	90.0000	75	span 4
38	38	39	-	Beam	section	(same as start)	Fc_5500	0.0000	20.009	0.0000	0.0000	90.0000	74	span 4
39	39	40	-	Beam	section	(same as start)	Fc_5500	0.0000	20.009	0.0000	0.0000	90.0000	73	span 4
40	40	41	-	Beam	section	(same as start)	Fc_5500	0.0000	20.009	0.0000	0.0000	90.0000	72	span 4
41	41	42	-	Beam	section	(same as start)	Fc_5500	0.0000	20.009	0.0000	0.0000	90.0000	68	span 4
42	42	43	-	Beam	section	(same as start)	Fc_5500	0.0000	20.009	0.0000	0.0000	90.0000	66	span 4
43	43	44	-	Beam	section	(same as start)	Fc_5500	0.0000	1.0004	0.0000	0.0000	90.0000	86	span 4
44	44	45	-	Beam	pier	(same as start)	Fc_5500	0.0000	4.0018	0.0000	0.0000	90.0000	86	span 4
45	45	46	-	Beam	pier	(same as start)	Fc_5500	0.0000	4.0018	0.0000	0.0000	90.0000	86	span 4
46	46	47	-	Beam	section	(same as start)	Fc_5500	0.0000	1.0004	0.0000	0.0000	90.0000	86	span 4
47	47	48	-	Beam	section	(same as start)	Fc_5500	0.0000	20.009	0.0000	0.0000	90.0000	97	span 5
48	48	49	-	Beam	section	(same as start)	Fc_5500	0.0000	20.009	0.0000	0.0000	90.0000	96	span 5
49	49	50	-	Beam	section	(same as start)	Fc_5500	0.0000	20.009	0.0000	0.0000	90.0000	93	span 5
50	50	51	-	Beam	section	(same as start)	Fc_5500	0.0000	20.009	0.0000	0.0000	90.0000	90	span 5
51	51	52	-	Beam	section	(same as start)	Fc_5500	0.0000	20.009	0.0000	0.0000	90.0000	88	span 5
52	52	53	-	Beam	section	(same as start)	Fc_5500	0.0000	20.009	0.0000	0.0000	90.0000	87	span 5
53	53	54	-	Beam	section	(same as start)	Fc_5500	0.0000	20.009	0.0000	0.0000	90.0000	82	span 5
54	54	55	-	Beam	section	(same as start)	Fc_5500	0.0000	1.0004	0.0000	0.0000	90.0000	0	span 5
55	55	56	-	Beam	pier	(same as start)	Fc_5500	0.0000	4.0018	0.0000	0.0000	90.0000	0	span 5
56	56	57	-	Beam	pier	(same as start)	Fc_5500	0.0000	4.0018	0.0000	0.0000	90.0000	0	span 5
57	57	58	-	Beam	section	(same as start)	Fc_5500	0.0000	1.0004	0.0000	0.0000	90.0000	0	span 5
58	58	59	-	Beam	section	(same as start)	Fc_5500	0.0000	20.009	0.0000	0.0000	90.0000	117	span 6
59	59	60	-	Beam	section	(same as start)	Fc_5500	0.0000	20.009	0.0000	0.0000	90.0000	115	span 6
60	60	61	-	Beam	section	(same as start)	Fc_5500	0.0000	20.009	0.0000	0.0000	90.0000	108	span 6
61	61	62	-	Beam	section	(same as start)	Fc_5500	0.0000	20.009	0.0000	0.0000	90.0000	107	span 6
62	62	63	-	Beam	section	(same as start)	Fc_5500	0.0000	20.009	0.0000	0.0000	90.0000	103	span 6
63	63	64	-	Beam	section	(same as start)	Fc_5500	0.0000	20.009	0.0000	0.0000	90.0000	102	span 6
64	64	65	-	Beam	section	(same as start)	Fc_5500	0.0000	20.009	0.0000	0.0000	90.0000	100	span 6
65	65	66	-	Beam	section	(same as start)	Fc_5500	0.0000	1.0004	0.0000	0.0000	90.0000	44	span 6
66	66	67	-	Beam	pier	(same as start)	Fc_5500	0.0000	4.0018	0.0000	0.0000	90.0000	44	span 6
1	1	10	-	Beam	Rigid Section	(same as start)	Rigid Material	0.0000	12	0.0000	0.0000	90.0000	0	span 1
201	201	202	-	Beam	Footing	(same as start)	Fc_5500	0.0000	6.	0.0000	0.0000	90.0000	0	span 1
202	202	203	-	Beam	Substructure	(same as start)	Fc_5500	0.0000	61.83	0.0000	0.0000	90.0000	0	span 1
203	203	204	-	Beam	Pier Cap	(same as start)	Fc_5500	0.0000	4.	0.0000	0.0000	90.0000	0	span 1
12	12	205	-	Beam	Rigid Section	(same as start)	Rigid Material	0.0000	12	0.0000	0.0000	90.0000	0	span 1
301	301	302	-	Beam	Footing	(same as start)	Fc_5500	0.0000	6	0.0000	0.0000	90.0000	0	span 2
302	302	303	-	Beam	Substructure	(same as start)	Fc_5500	0.0000	73.83	0.0000	0.0000	90.0000	0	span 2
303	303	304	-	Beam	Pier Cap	(same as start)	Fc_5500	0.0000	4	0.0000	0.0000	90.0000	0	span 2
23	23	305	-	Beam	Rigid Section	(same as start)	Rigid Material	0.0000	12	0.0000	0.0000	90.0000	0	span 2
401	401	402	-	Beam	Footing	(same as start)	Fc_5500	0.0000	6	0.0000	0.0000	90.0000	0	span 3
402	402	403	-	Beam	Substructure	(same as start)	Fc_5500	0.0000	90.83	0.0000	0.0000	90.0000	0	span 3
403	403	404	-	Beam	Pier Cap	(same as start)	Fc_5500	0.0000	4	0.0000	0.0000	90.0000	0	span 3
34	34	405	-	Beam	Rigid Section	(same as start)	Rigid Material	0.0000	12	0.0000	0.0000	90.0000	0	span 3
501	501	502	-	Beam	Footing	(same as start)	Fc_5500	0.0000	6.	0.0000	0.0000	90.0000	0	span 4

50	502	503	-	Beam	Substructure	(same as start)	Fc_5500	0.0000	96.83	0.0000	0.0000	90.0000	0	span 4
50	503	504	-	Beam	Pier Cap	(same as start)	Fc_5500	0.0000	4	0.0000	0.0000	90.0000	0	span 4
50	45	505	-	Beam	Rigid Section	(same as start)	Rigid Material	0.0000	12	0.0000	0.0000	90.0000	0	span 4
60	601	603	-	Beam	Footing	(same as start)	Fc_5500	0.0000	6	0.0000	0.0000	90.0000	0	span 5
60	602	603	-	Beam	Substructure	(same as start)	Fc_5500	0.0000	100.83	0.0000	0.0000	90.0000	0	span 5
60	603	604	-	Beam	Pier Cap	(same as start)	Fc_5500	0.0000	4.	0.0000	0.0000	90.0000	0	span 5
60	56	605	-	Beam	Rigid Section	(same as start)	Rigid Material	0.0000	12	0.0000	0.0000	90.0000	0	span 5
70	701	703	-	Beam	Footing	(same as start)	Fc_5500	0.0000	6	0.0000	0.0000	90.0000	0	span 6
70	702	703	-	Beam	Substructure	(same as start)	Fc_5500	0.0000	104.83	0.0000	0.0000	90.0000	0	span 6
70	703	704	-	Beam	Pier Cap	(same as start)	Fc_5500	0.0000	4.	0.0000	0.0000	90.0000	0	span 6
70	67	705	-	Beam	Rigid Section	(same as start)	Rigid Material	0.0000	12	0.0000	0.0000	90.0000	0	span 6

INPUT : Springs

ID	I-Joint	J-Joint	Type	Direction	K Tension (kips/ft)	K Compression (kips/ft)	Maximum Tension (kips or kips-ft)	Maximum Compression (kips or kips-ft)	Hook (ft)	Gap (ft)	Properties Definition	Structure / Construction Group
101	101	104	Linear	Trans. Z	3.1200e5	3.1200e5					(none)	span 1
102	101	104	Linear	Trans. X	2,880.0000	2,880.0000					(none)	span 1
103	101	104	Linear	Rot. Y	1,700.0000	1,700.0000					(none)	span 1
201	204	205	Linear	Trans. Z	4.6200e5	4.6200e5					(none)	span 1
202	204	205	Linear	Trans. X	5,880.0000	5,880.0000					(none)	span 1
203	204	205	Linear	Rot. Y	2,500.0000	2,500.0000					(none)	span 1
301	304	305	Linear	Trans. Z	8.8320e5	8.8320e5					(none)	span 2
302	304	305	Linear	Trans. X	7,560.0000	7,560.0000					(none)	span 2
303	304	305	Linear	Rot. Y	4,900.0000	4,900.0000					(none)	span 2
401	404	405	Linear	Trans. Z	8.8320e5	8.8320e5					(none)	span 3
402	404	405	Linear	Trans. X	7,560.0000	7,560.0000					(none)	span 3
403	404	405	Linear	Rot. Y	4,900.0000	4,900.0000					(none)	span 3
501	504	505	Linear	Trans. Z	8.8320e5	8.8320e5					(none)	span 4
502	504	505	Linear	Trans. X	7,560.0000	7,560.0000					(none)	span 4
503	504	505	Linear	Rot. Y	4,900.0000	4,900.0000					(none)	span 4
601	604	605	Linear	Trans. Z	4.6200e5	4.6200e5					(none)	span 5
602	604	605	Linear	Trans. X	5,880.0000	5,880.0000					(none)	span 5
603	604	605	Linear	Rot. Y	2,500.0000	2,500.0000					(none)	span 5
701	704	705	Linear	Trans. Z	3.1200e5	3.1200e5					(none)	span 6
702	704	705	Linear	Trans. X	2,880.0000	2,880.0000					(none)	span 6
703	704	705	Linear	Rot. Y	1,700.0000	1,700.0000					(none)	span 6

INPUT : Tendons

Tendon Name	Design Group	Material	Exposure	Strand Area (per	# of Stra	Jacking Force @ Start	Jacking Force @ End	Jacking End	Anchor Set (in)	Wobble Coefficie	Curvature Fri	Peak Stress Ratio - Ends	Peak Stress Ratio	Elongation Aft	Elongation Aft	Elongation @	Elongation @	Add. Force
S1-T1L	(none)	A416	Post-Tension (External)	0.2170	19	0	861.0000	End	0.3750		0.2500	0.9000	0.9000	0	0	0	0	0
S1-T2L	(none)	A416	Post-Tension (External)	0.2170	19	0	865.0000	End	0.3750		0.2500	0.9000	0.9000	0	0	0	0	0
S1-T3L	(none)	A416	Post-Tension (External)	0.2170	19	0	871.0000	End	0.3750		0.2500	0.9000	0.9000	0	0	0	0	0
S1-T4L	(none)	A416	Post-Tension (External)	0.2170	19	0	861.0000	End	0.3750		0.2500	0.9000	0.9000	0	0	0	0	0
S1-T1R	(none)	A416	Post-Tension (External)	0.2170	19	0	861.0000	End	0.3750		0.2500	0.9000	0.9000	0	0	0	0	0
S1-T2R	(none)	A416	Post-Tension (External)	0.2170	19	0	865.0000	End	0.3750		0.2500	0.9000	0.9000	0	0	0	0	0

S1-T3R	(none)	A416	Post-Tension (External)	0.2170	19	0	871.0000	End	0.3750		0.2500	0.9000	0.9000	0	0	0	0	0
S1-T4R	(none)	A416	Post-Tension (External)	0.2170	19	0	861.0000	End	0.3750		0.2500	0.9000	0.9000	0	0	0	0	0
S2-T5L	(none)	A416	Post-Tension (External)	0.2170	19	0	879.0000	End	0.3750		0.2500	0.9000	0.9000	0	0	0	0	0
S2-T6L	(none)	A416	Post-Tension (External)	0.2170	19	0	871.0000	End	0.3750		0.2500	0.9000	0.9000	0	0	0	0	0
S2-T7L	(none)	A416	Post-Tension (External)	0.2170	19	0	865.0000	End	0.3750		0.2500	0.9000	0.9000	0	0	0	0	0
S2-T8L	(none)	A416	Post-Tension (External)	0.2170	19	0	854.0000	End	0.3750		0.2500	0.9000	0.9000	0	0	0	0	0
S2-T5R	(none)	A416	Post-Tension (External)	0.2170	19	0	879.0000	End	0.3750		0.2500	0.9000	0.9000	0	0	0	0	0
S2-T6R	(none)	A416	Post-Tension (External)	0.2170	19	0	871.0000	End	0.3750		0.2500	0.9000	0.9000	0	0	0	0	0
S2-T7R	(none)	A416	Post-Tension (External)	0.2170	19	0	865.0000	End	0.3750		0.2500	0.9000	0.9000	0	0	0	0	0
S2-T8R	(none)	A416	Post-Tension (External)	0.2170	19	0	854.0000	End	0.3750		0.2500	0.9000	0.9000	0	0	0	0	0
S3-T5L	(none)	A416	Post-Tension (External)	0.2170	19	0	879.0000	End	0.3750		0.2500	0.9000	0.9000	0	0	0	0	0
S3-T6L	(none)	A416	Post-Tension (External)	0.2170	19	0	871.0000	End	0.3750		0.2500	0.9000	0.9000	0	0	0	0	0
S3-T7L	(none)	A416	Post-Tension (External)	0.2170	19	0	865.0000	End	0.3750		0.2500	0.9000	0.9000	0	0	0	0	0
S3-T8L	(none)	A416	Post-Tension (External)	0.2170	19	0	854.0000	End	0.3750		0.2500	0.9000	0.9000	0	0	0	0	0
S3-T5R	(none)	A416	Post-Tension (External)	0.2170	19	0	879.0000	End	0.3750		0.2500	0.9000	0.9000	0	0	0	0	0
S3-T6R	(none)	A416	Post-Tension (External)	0.2170	19	0	871.0000	End	0.3750		0.2500	0.9000	0.9000	0	0	0	0	0
S3-T7R	(none)	A416	Post-Tension (External)	0.2170	19	0	865.0000	End	0.3750		0.2500	0.9000	0.9000	0	0	0	0	0
S3-T8R	(none)	A416	Post-Tension (External)	0.2170	19	0	854.0000	End	0.3750		0.2500	0.9000	0.9000	0	0	0	0	0
S4-T5L	(none)	A416	Post-Tension (External)	0.2170	19	0	879.0000	End	0.3750		0.2500	0.9000	0.9000	0	0	0	0	0
S4-T6L	(none)	A416	Post-Tension (External)	0.2170	19	0	871.0000	End	0.3750		0.2500	0.9000	0.9000	0	0	0	0	0
S4-T7L	(none)	A416	Post-Tension (External)	0.2170	19	0	865.0000	End	0.3750		0.2500	0.9000	0.9000	0	0	0	0	0
S4-T8L	(none)	A416	Post-Tension (External)	0.2170	19	0	854.0000	End	0.3750		0.2500	0.9000	0.9000	0	0	0	0	0
S4-T5R	(none)	A416	Post-Tension (External)	0.2170	19	0	879.0000	End	0.3750		0.2500	0.9000	0.9000	0	0	0	0	0
S4-T6R	(none)	A416	Post-Tension (External)	0.2170	19	0	871.0000	End	0.3750		0.2500	0.9000	0.9000	0	0	0	0	0
S4-T7R	(none)	A416	Post-Tension (External)	0.2170	19	0	865.0000	End	0.3750		0.2500	0.9000	0.9000	0	0	0	0	0
S4-T8R	(none)	A416	Post-Tension (External)	0.2170	19	0	854.0000	End	0.3750		0.2500	0.9000	0.9000	0	0	0	0	0
S5-T5L	(none)	A416	Post-Tension (External)	0.2170	19	0	879.0000	End	0.3750		0.2500	0.9000	0.9000	0	0	0	0	0
S5-T6L	(none)	A416	Post-Tension (External)	0.2170	19	0	871.0000	End	0.3750		0.2500	0.9000	0.9000	0	0	0	0	0
S5-T7L	(none)	A416	Post-Tension (External)	0.2170	19	0	865.0000	End	0.3750		0.2500	0.9000	0.9000	0	0	0	0	0
S5-T8L	(none)	A416	Post-Tension (External)	0.2170	19	0	854.0000	End	0.3750		0.2500	0.9000	0.9000	0	0	0	0	0

S5-T5R	(none)	A416	Post-Tension (External)	0.2170	19	0	879.0000	End	0.3750		0.2500	0.9000	0.9000	0	0	0	0	0
S5-T6R	(none)	A416	Post-Tension (External)	0.2170	19	0	871.0000	End	0.3750		0.2500	0.9000	0.9000	0	0	0	0	0
S5-T7R	(none)	A416	Post-Tension (External)	0.2170	19	0	865.0000	End	0.3750		0.2500	0.9000	0.9000	0	0	0	0	0
S5-T8R	(none)	A416	Post-Tension (External)	0.2170	19	0	854.0000	End	0.3750		0.2500	0.9000	0.9000	0	0	0	0	0
S6-T9L	(none)	A416	Post-Tension (External)	0.2170	19	0	889.0000	End	0.3750		0.2500	0.9000	0.9000	0	0	0	0	0
S6-T10L	(none)	A416	Post-Tension (External)	0.2170	19	0	883.0000	End	0.3750		0.2500	0.9000	0.9000	0	0	0	0	0
S6-T11L	(none)	A416	Post-Tension (External)	0.2170	19	0	874.0000	End	0.3750		0.2500	0.9000	0.9000	0	0	0	0	0
S6-T12L	(none)	A416	Post-Tension (External)	0.2170	19	0	868.0000	End	0.3750		0.2500	0.9000	0.9000	0	0	0	0	0
S6-T9R	(none)	A416	Post-Tension (External)	0.2170	19	0	889.0000	End	0.3750		0.2500	0.9000	0.9000	0	0	0	0	0
S6-T10R	(none)	A416	Post-Tension (External)	0.2170	19	0	883.0000	End	0.3750		0.2500	0.9000	0.9000	0	0	0	0	0
S6-T11R	(none)	A416	Post-Tension (External)	0.2170	19	0	874.0000	End	0.3750		0.2500	0.9000	0.9000	0	0	0	0	0
S6-T12R	(none)	A416	Post-Tension (External)	0.2170	19	0	868.0000	End	0.3750		0.2500	0.9000	0.9000	0	0	0	0	0

INPUT : CEB-FIP 78

Name	Notional Thickness Coefficient	Creep Coefficient (Environment)	Creep Coefficient (Notional Thickness)	Shrinkage Coef (Environment)	Shrinkage Coef (Notional Thickness)	Delayed Modulus of Elasticity Coef	Creep Factor	Shrinkage Factor	Relaxation Factor	Assigned
User defined C&S	1.5000	2.0000	1.5000	-0.0003	0.9000	0.4000	1.0000	1.0000	1.0000	Yes

INPUT : More Material Properties

Name	Yield Stress (lb/in²)	Post-yield to Initial Slope Ratio	Concrete Strength Specimen	Concrete fc28 or Steel Fu (lb/in²)	Concrete Cement Hardening Type	Tendon GUTS (lb/in²)	Material Time-Effect	Assigned
Fc_5500	0.00	0.020	Cylinder	6,600.00	Normal	0.00	User defined C&S	Yes
Rigid Material	0.00	0.020	Cylinder	0.00	Not Concrete	0.00	(NONE)	Yes
A416	50,000.00	0.020	Cylinder	70,300.00	Not Concrete	270,000.00	User defined C&S	Yes

INPUT : CEB-FIP 78

Name	Creep Factor	Shrinkage Factor	Relaxation Factor	Exponent of Creep Development Eqn.	Constant in Shrinkage Development Eqn.	Temp. Adjusted Concrete Age	Steel Relaxation Type	Assigned
User defined C&S	1.0000	1.0000	1.0000	0.3000	350.0000	No	Improved(Class 2)	Yes

TENDON S1-T1L

Point Type	Reference Object Type	Reference Object or Range	Offset X (ft)	Offset Y (in)	Offset Z (in)	X Reference	Y Reference	Z Reference	Curvature Type	Width
geometry	member	1	0.0000	60.0000	-128.6900	Start	-Y3 Local Edge	Reference Line	No Curve	
path only	member	2								
path only	member	3								
geometry	member	4	5.0000	11.0000	-98.5000	Start	-Y3 Local Edge	Reference Line	No Curve	
geometry	member	4	15.0000	11.0000	-90.5000	Start	-Y3 Local Edge	Reference Line	No Curve	
geometry	member	5	5.0000	11.0000	-82.5000	Start	-Y3 Local Edge	Reference Line	No Curve	
geometry	member	6	15.0000	11.0000	-82.5000	Start	-Y3 Local Edge	Reference Line	No Curve	
geometry	member	7	5.0000	11.0000	-90.5000	Start	-Y3 Local Edge	Reference Line	No Curve	
geometry	member	7	15.0000	11.0000	-98.5000	Start	-Y3 Local Edge	Reference Line	No Curve	
path only	member	8								
path only	member	9								
path only	member	10								

path only	member	11								
geometry	member	12	0.0000	123.000	-152.0000	End	-Y3 Local Edge	Reference Line	No Curve	

TENDON S1-T2L

Point Type	Reference Object Type	Reference Object or Range	Offset X (ft)	Offset Y (in)	Offset Z (in)	X Reference	Y Reference	Z Reference	Curvature Type	Width
geometry	member	1	0.0000	84.0000	-142.9400	Start	-Y3 Local Edge	Reference Line	No Curve	
path	member	2								
path	member	3								
geometry	member	4	15.0000	11.0000	-98.5000	Start	-Y3 Local Edge	Reference Line	No Curve	
geometry	member	5	5.0000	11.0000	-90.5000	Start	-Y3 Local Edge	Reference Line	No Curve	
geometry	member	6	15.0000	11.0000	-90.5000	Start	-Y3 Local Edge	Reference Line	No Curve	
geometry	member	7	5.0000	11.0000	-98.5000	Start	-Y3 Local Edge	Reference Line	No Curve	
path	member	8								
path	member	9								
path	member	10								
path	member	11								
geometry	member	12	0.0000	123.0000	-134.0000	End	-Y3 Local Edge	Reference Line	No Curve	

TENDON S1-T3L

Point Type	Reference Object Type	Reference Object or Range	Offset X (ft)	Offset Y (in)	Offset Z (in)	X Reference	Y Reference	Z Reference	Curvature Type	Width
geometry	member	1	0.0000	108.0000	-157.1250	Start	-Y3 Local Edge	Reference Line	No Curve	
path only	member	2								
path only	member	3								
path only	member	4								
geometry	member	5	5.0000	11.0000	-98.5000	Start	-Y3 Local Edge	Reference Line	No Curve	
geometry	member	6	15.0000	11.0000	-98.5000	Start	-Y3 Local Edge	Reference Line	No Curve	
path only	member	7								
path only	member	8								
path only	member	9								
path only	member	10								
path only	member	11								
geometry	member	12	0.0000	123.0000	-116.0000	End	-Y3 Local Edge	Reference Line	No Curve	

TENDON S1-T4L

Point Type	Reference Object Type	Reference Object or Range	Offset X (ft)	Offset Y (in)	Offset Z (in)	X Reference	Y Reference	Z Reference	Curvature Type	Width
geometry	member	1	0.0000	24.0000	-107.3800	Start	-Y3 Local Edge	Reference Line	No Curve	
path only	member	2								
geometry	member	3	5.0000	11.0000	-98.5000	Start	-Y3 Local Edge	Reference Line	No Curve	
geometry	member	3	15.0000	11.0000	-90.5000	Start	-Y3 Local Edge	Reference Line	No Curve	
geometry	member	4	5.0000	11.0000	-82.5000	Start	-Y3 Local Edge	Reference Line	No Curve	
geometry	member	4	15.0000	11.0000	-74.5000	Start	-Y3 Local Edge	Reference Line	No Curve	
geometry	member	5	5.0000	11.0000	-74.5000	Start	-Y3 Local Edge	Reference Line	No Curve	
geometry	member	6	15.0000	11.0000	-74.5000	Start	-Y3 Local Edge	Reference Line	No Curve	
geometry	member	7	5.0000	11.0000	-74.5000	Start	-Y3 Local Edge	Reference Line	No Curve	
geometry	member	7	15.0000	11.0000	-74.5000	Start	-Y3 Local Edge	Reference Line	No Curve	
geometry	member	8	15.0000	11.0000	-90.5000	Start	-Y3 Local Edge	Reference Line	No Curve	
path only	member	9								
path only	member	10								
geometry	member	11	2.0000	11.0000	-90.5000	Start	-Y3 Local Edge	Reference Line	No Curve	
path only	member	12								
geometry	member	12	0.0000	21.0000	-90.5000	End	-Y3 Local Edge	Reference Line	No Curve	

TENDON S1-T1R

Point Type	Reference Object Type	Reference Object or Range	Offset X (ft)	Offset Y (in)	Offset Z (in)	X Reference	Y Reference	Z Reference	Curvature Type	Width
geometry	member	1	0.0000	60.0000	128.6900	Start	-Y3 Local Edge	Reference Line	No Curve	
path only	member	2								

path only	member	3								
geometry	member	4	5.0000	11.0000	98.5000	Start	-Y3 Local Edge	Reference Line	No Curve	
geometry	member	4	15.0000	11.0000	90.5000	Start	-Y3 Local Edge	Reference Line	No Curve	
geometry	member	5	5.0000	11.0000	82.5000	Start	-Y3 Local Edge	Reference Line	No Curve	
geometry	member	6	15.0000	11.0000	82.5000	Start	-Y3 Local Edge	Reference Line	No Curve	
geometry	member	7	5.0000	11.0000	90.5000	Start	-Y3 Local Edge	Reference Line	No Curve	
geometry	member	7	15.0000	11.0000	98.5000	Start	-Y3 Local Edge	Reference Line	No Curve	
path only	member	8								
path only	member	9								
path only	member	10								
path only	member	11								
geometry	member	12	0.0000	123.0000	152.0000	End	-Y3 Local Edge	Reference Line	No Curve	

TENDON S1-T2R

Point Type	Reference Object Type	Reference Object or Range	Offset X (ft)	Offset Y (in)	Offset Z (in)	X Reference	Y Reference	Z Reference	Curvature Type	Width
geometry	member	1	0.0000	84.0000	142.9400	Start	-Y3 Local Edge	Reference Line	No Curve	
path only	member	2								
path only	member	3								
geometry	member	4	15.0000	11.0000	98.5000	Start	-Y3 Local Edge	Reference Line	No Curve	
geometry	member	5	5.0000	11.0000	90.5000	Start	-Y3 Local Edge	Reference Line	No Curve	
geometry	member	6	15.0000	11.0000	90.5000	Start	-Y3 Local Edge	Reference Line	No Curve	
geometry	member	7	5.0000	11.0000	98.5000	Start	-Y3 Local Edge	Reference Line	No Curve	
path only	member	8								
path only	member	9								
path only	member	10								
path only	member	11								
geometry	member	12	0.0000	123.0000	134.0000	End	-Y3 Local Edge	Reference Line	No Curve	

TENDON S1-T3R

Point Type	Reference Object Type	Reference Object or Range	Offset X (ft)	Offset Y (in)	Offset Z (in)	X Reference	Y Reference	Z Reference	Curvature Type	Width
geometry	member	1	0.0000	108.0000	157.1250	Start	-Y3 Local Edge	Reference Line	No Curve	
path	member	2								
path	member	3								
path	member	4								
geometry	member	5	5.0000	11.0000	98.5000	Start	-Y3 Local Edge	Reference Line	No Curve	
geometry	member	6	15.0000	11.0000	98.5000	Start	-Y3 Local Edge	Reference Line	No Curve	
path	member	7								
path	member	8								
path	member	9								
path	member	10								
path	member	11								
geometry	member	12	0.0000	123.0000	116.0000	End	-Y3 Local Edge	Reference Line	No Curve	

TENDON S1-T4R

Point Type	Reference Object Type	Reference Object or Range	Offset X (ft)	Offset Y (in)	Offset Z (in)	X Reference	Y Reference	Z Reference	Curvature Type	Width

geometry	member	1	0.0000	24.0000	107.3800	Start	-Y3 Local Edge	Reference Line	No Curve	
path only	member	2								
geometry	member	3	5.0000	11.0000	98.5000	Start	-Y3 Local Edge	Reference Line	No Curve	
geometry	member	3	15.0000	11.0000	90.5000	Start	-Y3 Local Edge	Reference Line	No Curve	
geometry	member	4	5.0000	11.0000	82.5000	Start	-Y3 Local Edge	Reference Line	No Curve	
geometry	member	4	15.0000	11.0000	74.5000	Start	-Y3 Local Edge	Reference Line	No Curve	
geometry	member	5	5.0000	11.0000	74.5000	Start	-Y3 Local Edge	Reference Line	No Curve	
geometry	member	6	15.0000	11.0000	74.5000	Start	-Y3 Local Edge	Reference Line	No Curve	
geometry	member	7	5.0000	11.0000	74.5000	Start	-Y3 Local Edge	Reference Line	No Curve	
geometry	member	7	15.0000	11.0000	74.5000	Start	-Y3 Local Edge	Reference Line	No Curve	
geometry	member	8	15.0000	11.0000	90.5000	Start	-Y3 Local Edge	Reference Line	No Curve	
path only	member	9								
path only	member	10								
geometry	member	11	2.0000	11.0000	90.5000	Start	-Y3 Local Edge	Reference Line	No Curve	
path only	member	12								
geometry	member	12	0.0000	21.0000	90.5000	End	-Y3 Local Edge	Reference Line	No Curve	

TENDON S2-T5L

Point Type	Reference Object Type	Reference Object or Range	Offset X (ft)	Offset Y (in)	Offset Z (in)	X Reference	Y Reference	Z Reference	Curvature Type	Width
geometry	member	11	0.0000	123.0000	-161.0000	Start	-Y3 Local Edge	Reference Line	No Curve	
path only	member	12								
path only	member	13								
path only	member	13								
path only	member	14								
geometry	member	15	15.0000	11.0000	-98.5000	Start	-Y3 Local Edge	Reference Line	No Curve	
geometry	member	16	5.0000	11.0000	-90.5000	Start	-Y3 Local Edge	Reference Line	No Curve	
geometry	member	16	15.0000	11.0000	-82.5000	Start	-Y3 Local Edge	Reference Line	No Curve	
path only	member	17								
geometry	member	18	5.0000	11.0000	-82.5000	Start	-Y3 Local Edge	Reference Line	No Curve	
geometry	member	18	15.0000	11.0000	-90.5000	Start	-Y3 Local Edge	Reference Line	No Curve	
geometry	member	19	5.0000	11.0000	-98.5000	Start	-Y3 Local Edge	Reference Line	No Curve	
path only	member	20								
path only	member	21								
path only	member	22								
geometry	member	23	0.0000	123.0000	-152.0000	End	-Y3 Local Edge	Reference Line	No Curve	

TENDON S2-T6L

Point Type	Reference Object Type	Reference Object or Range	Offset X (ft)	Offset Y (in)	Offset Z (in)	X Reference	Y Reference	Z Reference	Curvature Type	Width
geometry	member	11	0.0000	123.0000	-143.0000	Start	-Y3 Local Edge	Reference Line	No Curve	
path	member	12								
path	member	13								

path	member	14								
path	member	15								
geometry	member	16	5.0000	11.0000	-98.5000	Start	-Y3 Local Edge	Reference Line	No Curve	
geometry	member	16	15.0000	11.0000	-90.5000	Start	-Y3 Local Edge	Reference Line	No Curve	
path	member	17								
geometry	member	18	5.0000	11.0000	-90.5000	Start	-Y3 Local Edge	Reference Line	No Curve	
geometry	member	18	15.0000	11.0000	-98.5000	Start	-Y3 Local Edge	Reference Line	No Curve	
path	member	19								
path	member	20								
path	member	21								
path	member	22								
geometry	member	23	0.0000	123.0000	-134.0000	End	-Y3 Local Edge	Reference Line	No Curve	

TENDON S2-T7L

Point Type	Reference Object Type	Reference Object or Range	Offset X (ft)	Offset Y (in)	Offset Z (in)	X Reference	Y Reference	Z Reference	Curvature Type	Width
geometry	member	11	0.0000	123.0000	-125.0000	Start	-Y3 Local Edge	Reference Line	No Curve	
path	member	12								
path	member	13								
path	member	14								
path	member	15								
geometry	member	16	15.0000	11.0000	-98.5000	Start	-Y3 Local Edge	Reference Line	No Curve	
path	member	17								
geometry	member	18	5.0000	11.0000	-98.5000	Start	-Y3 Local Edge	Reference Line	No Curve	
path	member	19								
path	member	20								
path	member	21								
path	member	21								
path	member	22								
geometry	member	23	0.0000	123.0000	-116.0000	End	-Y3 Local Edge	Reference Line	No Curve	

TENDON S2-T8L

Point Type	Reference Object Type	Reference Object or Range	Offset X (ft)	Offset Y (in)	Offset Z (in)	X Reference	Y Reference	Z Reference	Curvature Type	Width
geometry	member	11	0.0000	21.0000	-98.5000	Start	-Y3 Local Edge	Reference Line	No Curve	
geometry	member	12	1.5000	11.0000	-98.5000	Start	-Y3 Local Edge	Reference Line	No Curve	
path	member	13								
geometry	member	14	5.0000	11.0000	-98.5000	Start	-Y3 Local Edge	Reference Line	No Curve	
geometry	member	15	5.0000	11.0000	-90.5000	Start	-Y3 Local Edge	Reference Line	No Curve	
geometry	member	15	15.0000	11.0000	-82.5000	Start	-Y3 Local Edge	Reference Line	No Curve	
geometry	member	16	5.0000	11.0000	-74.5000	Start	-Y3 Local Edge	Reference Line	No Curve	
geometry	member	16	15.0000	11.0000	-74.5000	Start	-Y3 Local Edge	Reference Line	No Curve	
path	member	17								
geometry	member	18	5.0000	11.0000	-74.5000	Start	-Y3 Local Edge	Reference Line	No Curve	
geometry	member	18	15.0000	11.0000	-74.5000	Start	-Y3 Local Edge	Reference Line	No Curve	
geometry	member	19	5.0000	11.0000	-82.5000	Start	-Y3 Local Edge	Reference Line	No Curve	
geometry	member	19	15.0000	11.0000	-90.5000	Start	-Y3 Local Edge	Reference Line	No Curve	
geometry	member	20	15.0000	11.0000	-90.5000	Start	-Y3 Local Edge	Reference Line	No Curve	
path	member	21								
geometry	member	22	2.0000	11.0000	-90.5000	Start	-Y3 Local Edge	Reference Line	No Curve	
geometry	member	23	0.0000	21.0000	-90.5000	End	-Y3 Local Edge	Reference Line	No Curve	

TENDON S2-T5R

Point Type	Reference Object Type	Reference Object or Range	Offset X (ft)	Offset Y (in)	Offset Z (in)	X Reference	Y Reference	Z Reference	Curvature Type	Width
geometry	member	11	0.0000	123.0000	161.0000	Start	-Y3 Local Edge	Reference Line	No Curve	
path	member	12								
path	member	13								
path	member	14								
geometry	member	15	15.0000	11.0000	98.5000	Start	-Y3 Local Edge	Reference Line	No Curve	
geometry	member	16	5.0000	11.0000	90.5000	Start	-Y3 Local Edge	Reference Line	No Curve	
geometry	member	16	15.0000	11.0000	82.5000	Start	-Y3 Local Edge	Reference Line	No Curve	
path	member	17								
geometry	member	18	5.0000	11.0000	82.5000	Start	-Y3 Local Edge	Reference Line	No Curve	
geometry	member	18	15.0000	11.0000	90.5000	Start	-Y3 Local Edge	Reference Line	No Curve	
geometry	member	19	5.0000	11.0000	98.5000	Start	-Y3 Local Edge	Reference Line	No Curve	
path	member	20								
path	member	21								
path	member	22								
geometry	member	23	0.0000	123.0000	152.0000	End	-Y3 Local Edge	Reference Line	No Curve	

TENDON S2-T6R

Point Type	Reference Object Type	Reference Object or Range	Offset X (ft)	Offset Y (in)	Offset Z (in)	X Reference	Y Reference	Z Reference	Curvature Type	Width
geometry	member	11	0.0000	123.0000	143.0000	Start	-Y3 Local Edge	Reference Line	No Curve	
path	member	12								
path	member	13								
path	member	14								
path	member	15								
geometry	member	16	5.0000	11.0000	98.5000	Start	-Y3 Local Edge	Reference Line	No Curve	
geometry	member	16	15.0000	11.0000	90.5000	Start	-Y3 Local Edge	Reference Line	No Curve	
path	member	17								
geometry	member	18	5.0000	11.0000	90.5000	Start	-Y3 Local Edge	Reference Line	No Curve	
geometry	member	18	15.0000	11.0000	98.5000	Start	-Y3 Local Edge	Reference Line	No Curve	
path	member	19								
path	member	20								
path	member	21								
path	member	22								
geometry	member	23	0.0000	123.0000	134.0000	End	-Y3 Local Edge	Reference Line	No Curve	

TENDON S2-T7R

Point Type	Reference Object Type	Reference Object or Range	Offset X (ft)	Offset Y (in)	Offset Z (in)	X Reference	Y Reference	Z Reference	Curvature Type	Width
geometry	member	11	0.0000	123.0000	125.0000	Start	-Y3 Local Edge	Reference Line	No Curve	
path	member	12								
path	member	13								
path	member	14								
path	member	15								
geometry	member	16	15.0000	11.0000	98.5000	Start	-Y3 Local Edge	Reference Line	No Curve	
path	member	17								
geometry	member	18	5.0000	11.0000	98.5000	Start	-Y3 Local Edge	Reference Line	No Curve	
path	member	19								
path	member	20								
path	member	21								
path	member	22								
geometry	member	23	0.0000	123.0000	116.0000	End	-Y3 Local Edge	Reference Line	No Curve	

TENDON S2-T8R

Point Type	Reference Object Type	Reference Object	Offset X	Offset Y	Offset Z	X Reference	Y Reference	Z Reference	Curvature Type	Width
geometry	member	11	0.0000	21.0000	98.5000	Start	-Y3 Local Edge	Reference Line	No Curve	
geometry	member	12	1.5000	11.0000	98.5000	Start	-Y3 Local Edge	Reference Line	No Curve	
path	member	13								

geometry	member	14	5.0000	11.0000	98.5000	Start	-Y3 Local Edge	Reference Line	No Curve	
geometry	member	15	5.0000	11.0000	90.5000	Start	-Y3 Local Edge	Reference Line	No Curve	
geometry	member	15	15.0000	11.0000	82.5000	Start	-Y3 Local Edge	Reference Line	No Curve	
geometry	member	16	5.0000	11.0000	74.5000	Start	-Y3 Local Edge	Reference Line	No Curve	
geometry	member	16	15.0000	11.0000	74.5000	Start	-Y3 Local Edge	Reference Line	No Curve	
path	member	17								
geometry	member	18	5.0000	11.0000	74.5000	Start	-Y3 Local Edge	Reference Line	No Curve	
geometry	member	18	15.0000	11.0000	74.5000	Start	-Y3 Local Edge	Reference Line	No Curve	
geometry	member	19	5.0000	11.0000	82.5000	Start	-Y3 Local Edge	Reference Line	No Curve	
geometry	member	19	15.0000	11.0000	90.5000	Start	-Y3 Local Edge	Reference Line	No Curve	
geometry	member	20	15.0000	11.0000	90.5000	Start	-Y3 Local Edge	Reference Line	No Curve	
path	member	21								
geometry	member	22	2.0000	11.0000	90.5000	Start	-Y3 Local Edge	Reference Line	No Curve	
geometry	member	23	0.0000	21.0000	90.5000	End	-Y3 Local Edge	Reference Line	No Curve	

TENDON S3-T5L

Point Type	Reference Object	Reference Object	Offset X	Offset Y	Offset Z	X Reference	Y Reference	Z Reference	Curvature Type	Width
geometry	member	22	0.0000	123.0000	-161.0000	Start	-Y3 Local Edge	Reference Line	No Curve	
path only	member	23								
path only	member	24								
path only	member	25								
geometry	member	26	15.0000	11.0000	-98.5000	Start	-Y3 Local Edge	Reference Line	No Curve	
geometry	member	27	5.0000	11.0000	-90.5000	Start	-Y3 Local Edge	Reference Line	No Curve	
geometry	member	27	15.0000	11.0000	-82.5000	Start	-Y3 Local Edge	Reference Line	No Curve	
path only	member	28								
geometry	member	29	5.0000	11.0000	-82.5000	Start	-Y3 Local Edge	Reference Line	No Curve	
geometry	member	29	15.0000	11.0000	-90.5000	Start	-Y3 Local Edge	Reference Line	No Curve	
geometry	member	30	5.0000	11.0000	-98.5000	Start	-Y3 Local Edge	Reference Line	No Curve	
path only	member	31								
path only	member	32								
path only	member	33								
geometry	member	34	0.0000	123.0000	-152.0000	End	-Y3 Local Edge	Reference Line	No Curve	

TENDON S3-T6L

Point Type	Reference Object Type	Reference Object	Offset X	Offset Y	Offset Z	X Reference	Y Reference	Z Reference	Curvature Type	Width
geometry	member	22	0.0000	123.0000	-143.0000	Start	-Y3 Local Edge	Reference Line	No Curve	
path	member	23								
path	member	24								
path	member	25								
path	member	26								
geometry	member	27	5.0000	11.0000	-98.5000	Start	-Y3 Local Edge	Reference Line	No Curve	
geometry	member	27	15.0000	11.0000	-90.5000	Start	-Y3 Local Edge	Reference Line	No Curve	
path	member	28								
geometry	member	29	5.0000	11.0000	-90.5000	Start	-Y3 Local Edge	Reference Line	No Curve	
geometry	member	29	15.0000	11.0000	-98.5000	Start	-Y3 Local Edge	Reference Line	No Curve	
path	member	30								
path	member	31								
path	member	32								
path	member	33								
geometry	member	34	0.0000	123.0000	-134.0000	End	-Y3 Local Edge	Reference Line	No Curve	

TENDON S3-T7L

Point Type	Reference Object Type	Reference Object	Offset X	Offset Y	Offset Z	X Reference	Y Reference	Z Reference	Curvature Type	Width
geometry	member	22	0.0000	123.0000	-125.0000	Start	-Y3 Local Edge	Reference Line	No Curve	
path	member	23								
path	member	24								
path	member	25								
path	member	26								
geometry	member	27	15.0000	11.0000	-98.5000	Start	-Y3 Local Edge	Reference Line	No Curve	
path	member	28								
geometry	member	29	5.0000	11.0000	-98.5000	Start	-Y3 Local Edge	Reference Line	No Curve	
path	member	30								
path	member	31								
path	member	32								
path	member	33								
geometry	member	34	0.0000	123.0000	-116.0000	End	-Y3 Local Edge	Reference Line	No Curve	

TENDON S3-T8L

Point Type	Reference Object Type	Reference Object	Offset X	Offset Y	Offset Z	X Reference	Y Reference	Z Reference	Curvature Type	Width
geometry	member	22	0.0000	21.0000	-98.5000	Start	-Y3 Local Edge	Reference Line	No Curve	
geometry	member	23	1.5000	11.0000	-98.5000	Start	-Y3 Local Edge	Reference Line	No Curve	
path	member	24								
geometry	member	25	5.0000	11.0000	-98.5000	Start	-Y3 Local Edge	Reference Line	No Curve	
geometry	member	26	5.0000	11.0000	-90.5000	Start	-Y3 Local Edge	Reference Line	No Curve	
geometry	member	26	15.0000	11.0000	-82.5000	Start	-Y3 Local Edge	Reference Line	No Curve	
geometry	member	27	5.0000	11.0000	-74.5000	Start	-Y3 Local Edge	Reference Line	No Curve	
geometry	member	27	15.0000	11.0000	-74.5000	Start	-Y3 Local Edge	Reference Line	No Curve	
path	member	28								
geometry	member	29	5.0000	11.0000	-74.5000	Start	-Y3 Local Edge	Reference Line	No Curve	
geometry	member	29	15.0000	11.0000	-74.5000	Start	-Y3 Local Edge	Reference Line	No Curve	
geometry	member	30	5.0000	11.0000	-82.5000	Start	-Y3 Local Edge	Reference Line	No Curve	
geometry	member	30	15.0000	11.0000	-90.5000	Start	-Y3 Local Edge	Reference Line	No Curve	
geometry	member	31	15.0000	11.0000	-90.5000	Start	-Y3 Local Edge	Reference Line	No Curve	
path	member	32								
geometry	member	33	2.0000	11.0000	-90.5000	Start	-Y3 Local Edge	Reference Line	No Curve	
geometry	member	34	0.0000	21.0000	-90.5000	End	-Y3 Local Edge	Reference Line	No Curve	

TENDON S3-T5R

Point Type	Reference Object Type	Reference Object	Offset X	Offset Y	Offset Z	X Reference	Y Reference	Z Reference	Curvature Type			Width
geometry	member	22	0.0000	123.0000	161.0000	Start	-Y3 Local Edge	Reference Line	No Curve			
path	member	23										
path	member	24										
path	member	25										
geometry	member	26	15.0000	11.0000	98.5000	Start	-Y3 Local Edge	Reference Line	No Curve			
geometry	member	27	5.0000	11.0000	90.5000	Start	-Y3 Local Edge	Reference Line	No Curve			
geometry	member	27	15.0000	11.0000	82.5000	Start	-Y3 Local Edge	Reference Line	No Curve			
path	member	28										
geometry	member	29	5.0000	11.0000	82.5000	Start	-Y3 Local Edge	Reference Line	No Curve			
geometry	member	29	15.0000	11.0000	90.5000	Start	-Y3 Local Edge	Reference Line	No Curve			
geometry	member	30	5.0000	11.0000	98.5000	Start	-Y3 Local Edge	Reference Line	No Curve			
path	member	31										
path	member	32										
path	member	33										
geometry	member	34	0.0000	123.0000	152.0000	End	-Y3 Local Edge	Reference Line	No Curve			

TENDON S3-T6R

Point Type	Reference Object Type	Reference Object or Range	Offset X (ft)	Offset Y (in)	Offset Z (in)	X Reference	Y Reference	Z Reference	Curvature Type			Width
geometry	member	22	0.0000	123.0000	143.0000	Start	-Y3 Local Edge	Reference Line	No Curve			
path	member	23										
path	member	24										
path	member	25										
path	member	26										
geometry	member	27	5.0000	11.0000	98.5000	Start	-Y3 Local Edge	Reference Line	No Curve			
geometry	member	27	15.0000	11.0000	90.5000	Start	-Y3 Local Edge	Reference Line	No Curve			
path	member	28										
geometry	member	29	5.0000	11.0000	90.5000	Start	-Y3 Local Edge	Reference Line	No Curve			
geometry	member	29	15.0000	11.0000	98.5000	Start	-Y3 Local Edge	Reference Line	No Curve			
path	member	30										
path	member	31										
path	member	32										
path	member	33										
geometry	member	34	0.0000	123.0000	134.0000	End	-Y3 Local Edge	Reference Line	No Curve			

TENDON S3-T7R

Point Type	Reference Object Type	Reference Object or Range	Offset X (ft)	Offset Y (in)	Offset Z (in)	X Reference	Y Reference	Z Reference	Curvature Type			Width
geometry	member	22	0.0000	123.0000	125.0000	Start	-Y3 Local Edge	Reference Line	No Curve			
path	member	23										
path	member	24										
path	member	25										
path	member	26										
geometry	member	27	15.0000	11.0000	98.5000	Start	-Y3 Local Edge	Reference Line	No Curve			
path	member	28										
geometry	member	29	5.0000	11.0000	98.5000	Start	-Y3 Local Edge	Reference Line	No Curve			
path	member	30										
path	member	31										
path	member	32										
path	member	33										
geometry	member	34	0.0000	123.0000	116.0000	End	-Y3 Local Edge	Reference Line	No Curve			

TENDON S3-T8R

Point Type	Reference Object Type	Reference Object or Range	Offset X (ft)	Offset Y (in)	Offset Z (in)	X Reference	Y Reference	Z Reference	Curvature Type			Width
geometry	member	22	0.0000	21.0000	98.5000	Start	-Y3 Local Edge	Reference Line	No Curve			
geometry	member	23	1.5000	11.0000	98.5000	Start	-Y3 Local Edge	Reference Line	No Curve			
path	member	24										
geometry	member	25	5.0000	11.0000	98.5000	Start	-Y3 Local Edge	Reference Line	No Curve			
geometry	member	26	5.0000	11.0000	90.5000	Start	-Y3 Local Edge	Reference Line	No Curve			
geometry	member	26	15.0000	11.0000	82.5000	Start	-Y3 Local Edge	Reference Line	No Curve			
geometry	member	27	5.0000	11.0000	74.5000	Start	-Y3 Local Edge	Reference Line	No Curve			
geometry	member	27	15.0000	11.0000	74.5000	Start	-Y3 Local Edge	Reference Line	No Curve			
path	member	28										
geometry	member	29	5.0000	11.0000	74.5000	Start	-Y3 Local Edge	Reference Line	No Curve			
geometry	member	29	15.0000	11.0000	74.5000	Start	-Y3 Local Edge	Reference Line	No Curve			
geometry	member	30	5.0000	11.0000	82.5000	Start	-Y3 Local Edge	Reference Line	No Curve			
geometry	member	30	15.0000	11.0000	90.5000	Start	-Y3 Local Edge	Reference Line	No Curve			
geometry	member	31	15.0000	11.0000	90.5000	Start	-Y3 Local Edge	Reference Line	No Curve			
path	member	32										
geometry	member	33	2.0000	11.0000	90.5000	Start	-Y3 Local Edge	Reference Line	No Curve			
geometry	member	34	0.0000	21.0000	90.5000	End	-Y3 Local Edge	Reference Line	No Curve			

TENDON S4-T5L

Point Type	Reference Object Type	Reference Object	Offset X	Offset Y	Offset Z	X Reference	Y Reference	Z Reference	Curvature Type			Width
geometry	member	33	0.0000	123.0000	-161.0000	Start	-Y3 Local Edge	Reference Line	No Curve			
path	member	34										
path	member	35										
path	member	36										
geometry	member	37	15.0000	11.0000	-98.5000	Start	-Y3 Local Edge	Reference Line	No Curve			
geometry	member	38	5.0000	11.0000	-90.5000	Start	-Y3 Local Edge	Reference Line	No Curve			
geometry	member	38	15.0000	11.0000	-82.5000	Start	-Y3 Local Edge	Reference Line	No Curve			
path	member	39										
geometry	member	40	5.0000	11.0000	-82.5000	Start	-Y3 Local Edge	Reference Line	No Curve			
geometry	member	40	15.0000	11.0000	-90.5000	Start	-Y3 Local Edge	Reference Line	No Curve			
geometry	member	41	5.0000	11.0000	-98.5000	Start	-Y3 Local Edge	Reference Line	No Curve			
path	member	42										
path	member	43										
path	member	44										
geometry	member	45	0.0000	123.0000	-152.0000	End	-Y3 Local Edge	Reference Line	No Curve			

TENDON S4-T6L

Point Type	Reference Object Type	Reference Object or Range	Offset X (ft)	Offset Y (in)	Offset Z (in)	X Reference	Y Reference	Z Reference	Curvature Type			Width
geometry	member	33	0.0000	123.0000	-143.0000	Start	-Y3 Local Edge	Reference Line	No Curve			
path	member	34										
path	member	35										
path	member	36										
path	member	37										
geometry	member	38	5.0000	11.0000	-98.5000	Start	-Y3 Local Edge	Reference Line	No Curve			
geometry	member	38	15.0000	11.0000	-90.5000	Start	-Y3 Local Edge	Reference Line	No Curve			
path	member	39										
geometry	member	40	5.0000	11.0000	-90.5000	Start	-Y3 Local Edge	Reference Line	No Curve			
geometry	member	40	15.0000	11.0000	-98.5000	Start	-Y3 Local Edge	Reference Line	No Curve			
path	member	41										
path	member	42										
path	member	43										
path	member	44										
geometry	member	45	0.0000	123.0000	-134.0000	End	-Y3 Local Edge	Reference Line	No Curve			

TENDON S4-T7L

Point Type	Reference Object Type	Reference Object or Range	Offset X (ft)	Offset Y (in)	Offset Z (in)	X Reference	Y Reference	Z Reference	Curvature Type			Width
geometry	member	33	0.0000	123.0000	-125.0000	Start	-Y3 Local Edge	Reference Line	No Curve			
path	member	34										
path	member	35										
path	member	36										
path	member	37										
geometry	member	38	15.0000	11.0000	-98.5000	Start	-Y3 Local Edge	Reference Line	No Curve			
path	member	39										
geometry	member	40	5.0000	11.0000	-98.5000	Start	-Y3 Local Edge	Reference Line	No Curve			
path	member	41										
path	member	42										
path	member	43										
path	member	44										
geometry	member	45	0.0000	123.0000	-116.0000	End	-Y3 Local Edge	Reference Line	No Curve			

TENDON S4-T8L

Point Type	Reference Object Type	Reference Object or Range	Offset X (ft)	Offset Y (in)	Offset Z (in)	X Reference	Y Reference	Z Reference	Curvature Type			Width
geometry	member	33	0.0000	21.0000	-98.5000	Start	-Y3 Local Edge	Reference Line	No Curve			
geometry	member	34	1.5000	11.0000	-98.5000	Start	-Y3 Local Edge	Reference Line	No Curve			
path	member	35										
geometry	member	36	5.0000	11.0000	-98.5000	Start	-Y3 Local Edge	Reference Line	No Curve			
geometry	member	37	5.0000	11.0000	-90.5000	Start	-Y3 Local Edge	Reference Line	No Curve			
geometry	member	37	15.0000	11.0000	-82.5000	Start	-Y3 Local Edge	Reference Line	No Curve			
geometry	member	38	5.0000	11.0000	-74.5000	Start	-Y3 Local Edge	Reference Line	No Curve			
geometry	member	38	15.0000	11.0000	-74.5000	Start	-Y3 Local Edge	Reference Line	No Curve			
path	member	39										
geometry	member	40	5.0000	11.0000	-74.5000	Start	-Y3 Local Edge	Reference Line	No Curve			
geometry	member	40	15.0000	11.0000	-74.5000	Start	-Y3 Local Edge	Reference Line	No Curve			
geometry	member	41	5.0000	11.0000	-82.5000	Start	-Y3 Local Edge	Reference Line	No Curve			
geometry	member	41	15.0000	11.0000	-90.5000	Start	-Y3 Local Edge	Reference Line	No Curve			
geometry	member	42	15.0000	11.0000	-90.5000	Start	-Y3 Local Edge	Reference Line	No Curve			
path	member	43										
geometry	member	44	2.0000	11.0000	-90.5000	Start	-Y3 Local Edge	Reference Line	No Curve			
geometry	member	45	0.0000	21.0000	-90.5000	End	-Y3 Local Edge	Reference Line	No Curve			

TENDON S4-T5R

Point Type	Reference Object Type	Reference Object or Range	Offset X (ft)	Offset Y (in)	Offset Z (in)	X Reference	Y Reference	Z Reference	Curvature Type			Width
geometry	member	33	0.0000	123.0000	161.0000	Start	-Y3 Local Edge	Reference Line	No Curve			
path	member	34										
path	member	35										
path	member	36										
geometry	member	37	15.0000	11.0000	98.5000	Start	-Y3 Local Edge	Reference Line	No Curve			
geometry	member	38	5.0000	11.0000	90.5000	Start	-Y3 Local Edge	Reference Line	No Curve			
geometry	member	38	15.0000	11.0000	82.5000	Start	-Y3 Local Edge	Reference Line	No Curve			
path	member	39										
geometry	member	40	5.0000	11.0000	82.5000	Start	-Y3 Local Edge	Reference Line	No Curve			
geometry	member	40	15.0000	11.0000	90.5000	Start	-Y3 Local Edge	Reference Line	No Curve			
geometry	member	41	5.0000	11.0000	98.5000	Start	-Y3 Local Edge	Reference Line	No Curve			
path	member	42										
path	member	43										
path	member	44										
geometry	member	45	0.0000	123.0000	152.0000	End	-Y3 Local Edge	Reference Line	No Curve			

TENDON S4-T6R

Point Type	Reference Object Type	Reference Object or Range	Offset X (ft)	Offset Y (in)	Offset Z (in)	X Reference	Y Reference	Z Reference	Curvature Type			Width
geometry	member	33	0.0000	123.0000	143.0000	Start	-Y3 Local Edge	Reference Line	No Curve			
path	member	34										
path	member	35										
path	member	36										
path	member	37										
geometry	member	38	5.0000	11.0000	98.5000	Start	-Y3 Local Edge	Reference Line	No Curve			

geometry	member	38	15.0000	11.0000	90.5000	Start	-Y3 Local Edge	Reference Line	No Curve			
path	member	39										
geometry	member	40	5.0000	11.0000	90.5000	Start	-Y3 Local Edge	Reference Line	No Curve			
geometry	member	40	15.0000	11.0000	98.5000	Start	-Y3 Local Edge	Reference Line	No Curve			
path	member	41										
path	member	42										
path	member	43										
path	member	44										
geometry	member	45	0.0000	123.0000	134.0000	End	-Y3 Local Edge	Reference Line	No Curve			

TENDON S4-T7R

Point Type	Reference Object Type	Reference Object or Range	Offset X (ft)	Offset Y (in)	Offset Z (in)	X Reference	Y Reference	Z Reference	Curvature Type			Width
geometry	member	33	0.0000	123.0000	125.0000	Start	-Y3 Local Edge	Reference Line	No Curve			
path	member	34										
path	member	35										
path	member	36										
path	member	37										
geometry	member	38	15.0000	11.0000	98.5000	Start	-Y3 Local Edge	Reference Line	No Curve			
path	member	39										
geometry	member	40	5.0000	11.0000	98.5000	Start	-Y3 Local Edge	Reference Line	No Curve			
path	member	41										
path	member	42										
path	member	43										
path	member	44										
geometry	member	45	0.0000	123.0000	116.0000	End	-Y3 Local Edge	Reference Line	No Curve			

TENDON S4-T8R

Point Type	Reference Object Type	Reference Object or Range	Offset X (ft)	Offset Y (in)	Offset Z (in)	X Reference	Y Reference	Z Reference	Curvature Type			Width
geometry	member	33	0.0000	21.0000	98.5000	Start	-Y3 Local Edge	Reference Line	No Curve			
geometry	member	34	1.5000	11.0000	98.5000	Start	-Y3 Local Edge	Reference Line	No Curve			
path	member	35										
geometry	member	36	5.0000	11.0000	98.5000	Start	-Y3 Local Edge	Reference Line	No Curve			
geometry	member	37	5.0000	11.0000	90.5000	Start	-Y3 Local Edge	Reference Line	No Curve			
geometry	member	37	15.0000	11.0000	82.5000	Start	-Y3 Local Edge	Reference Line	No Curve			
geometry	member	38	5.0000	11.0000	74.5000	Start	-Y3 Local Edge	Reference Line	No Curve			
geometry	member	38	15.0000	11.0000	74.5000	Start	-Y3 Local Edge	Reference Line	No Curve			
path	member	39										
geometry	member	40	5.0000	11.0000	74.5000	Start	-Y3 Local Edge	Reference Line	No Curve			
geometry	member	40	15.0000	11.0000	74.5000	Start	-Y3 Local Edge	Reference Line	No Curve			
geometry	member	41	5.0000	11.0000	82.5000	Start	-Y3 Local Edge	Reference Line	No Curve			
geometry	member	41	15.0000	11.0000	90.5000	Start	-Y3 Local Edge	Reference Line	No Curve			
geometry	member	42	15.0000	11.0000	90.5000	Start	-Y3 Local Edge	Reference Line	No Curve			
path	member	43										
geometry	member	44	2.0000	11.0000	90.5000	Start	-Y3 Local Edge	Reference Line	No Curve			
geometry	member	45	0.0000	21.0000	90.5000	End	-Y3 Local Edge	Reference Line	No Curve			

TENDON S5-T5L

Point Type	Reference Object Type	Reference Object or Range	Offset X (ft)	Offset Y (in)	Offset Z (in)	X Reference	Y Reference	Z Reference	Curvature Type			Width
geometry	member	44	0.0000	123.0000	-161.0000	Start	-Y3 Local Edge	Reference Line	No Curve			
path	member	45										
path	member	46										

path	member	47										
geometry	member	48	15.0000	11.0000	-98.5000	Start	-Y3 Local Edge	Reference Line	No Curve			
geometry	member	49	5.0000	11.0000	-90.5000	Start	-Y3 Local Edge	Reference Line	No Curve			
geometry	member	49	15.0000	11.0000	-82.5000	Start	-Y3 Local Edge	Reference Line	No Curve			
path	member	50										
geometry	member	51	5.0000	11.0000	-82.5000	Start	-Y3 Local Edge	Reference Line	No Curve			
geometry	member	51	15.0000	11.0000	-90.5000	Start	-Y3 Local Edge	Reference Line	No Curve			
geometry	member	52	5.0000	11.0000	-98.5000	Start	-Y3 Local Edge	Reference Line	No Curve			
path	member	53										
path	member	54										
path	member	55										
geometry	member	56	0.0000	123.0000	-152.0000	End	-Y3 Local Edge	Reference Line	No Curve			

TENDON S5-T6L

Point Type	Reference Object Type	Reference Object or Range	Offset X (ft)	Offset Y (in)	Offset Z (in)	X Reference	Y Reference	Z Reference	Curvature Type			Width
geometry	member	44	0.0000	123.0000	-143.0000	Start	-Y3 Local Edge	Reference Line	No Curve			
path	member	45										
path	member	46										
path	member	47										
path	member	48										
geometry	member	49	5.0000	11.0000	-98.5000	Start	-Y3 Local Edge	Reference Line	No Curve			
geometry	member	49	15.0000	11.0000	-90.5000	Start	-Y3 Local Edge	Reference Line	No Curve			
path	member	50										
geometry	member	51	5.0000	11.0000	-90.5000	Start	-Y3 Local Edge	Reference Line	No Curve			
geometry	member	51	15.0000	11.0000	-98.5000	Start	-Y3 Local Edge	Reference Line	No Curve			
path	member	52										
path	member	53										
path	member	54										
path	member	55										
geometry	member	56	0.0000	123.0000	-134.0000	End	-Y3 Local Edge	Reference Line	No Curve			

TENDON S5-T7L

Point Type	Reference Object Type	Reference Object or Range	Offset X (ft)	Offset Y (in)	Offset Z (in)	X Reference	Y Reference	Z Reference	Curvature Type			Width
geometry	member	44	0.0000	123.0000	-125.0000	Start	-Y3 Local Edge	Reference Line	No Curve			
path	member	45										
path	member	46										
path	member	47										
path	member	48										
geometry	member	49	15.0000	11.0000	-98.5000	Start	-Y3 Local Edge	Reference Line	No Curve			
path	member	50										
geometry	member	51	5.0000	11.0000	-98.5000	Start	-Y3 Local Edge	Reference Line	No Curve			
path	member	52										
path	member	53										
path	member	54										
path	member	55										
geometry	member	56	0.0000	123.0000	-116.0000	End	-Y3 Local Edge	Reference Line	No Curve			

TENDON S5-T8L

Point Type	Reference Object Type	Reference Object or Range	Offset X (ft)	Offset Y (in)	Offset Z (in)	X Reference	Y Reference	Z Reference	Curvature Type			Width
geometry	member	44	0.0000	21.0000	-98.5000	Start	-Y3 Local Edge	Reference Line	No Curve			
geometry	member	45	1.5000	11.0000	-98.5000	Start	-Y3 Local Edge	Reference Line	No Curve			

path	member	46										
geometry	member	47	5.0000	11.0000	-98.5000	Start	-Y3 Local Edge	Reference Line	No Curve			
geometry	member	48	5.0000	11.0000	-90.5000	Start	-Y3 Local Edge	Reference Line	No Curve			
geometry	member	48	15.0000	11.0000	-82.5000	Start	-Y3 Local Edge	Reference Line	No Curve			
geometry	member	49	5.0000	11.0000	-74.5000	Start	-Y3 Local Edge	Reference Line	No Curve			
geometry	member	49	15.0000	11.0000	-74.5000	Start	-Y3 Local Edge	Reference Line	No Curve			
path	member	50										
geometry	member	51	5.0000	11.0000	-74.5000	Start	-Y3 Local Edge	Reference Line	No Curve			
geometry	member	51	15.0000	11.0000	-74.5000	Start	-Y3 Local Edge	Reference Line	No Curve			
geometry	member	52	5.0000	11.0000	-82.5000	Start	-Y3 Local Edge	Reference Line	No Curve			
geometry	member	52	15.0000	11.0000	-90.5000	Start	-Y3 Local Edge	Reference Line	No Curve			
geometry	member	53	15.0000	11.0000	-90.5000	Start	-Y3 Local Edge	Reference Line	No Curve			
path	member	54										
geometry	member	55	2.0000	11.0000	-90.5000	Start	-Y3 Local Edge	Reference Line	No Curve			
geometry	member	56	0.0000	21.0000	-90.5000	End	-Y3 Local Edge	Reference Line	No Curve			

TENDON S5-T5R

Point Type	Reference Object Type	Reference Object or Range	Offset X (ft)	Offset Y (in)	Offset Z (in)	X Reference	Y Reference	Z Reference	Curvature Type			Width
geometry	member	44	0.0000	123.0000	161.0000	Start	-Y3 Local Edge	Reference Line	No Curve			
path	member	45										
path	member	46										
path	member	47										
geometry	member	48	15.0000	11.0000	98.5000	Start	-Y3 Local Edge	Reference Line	No Curve			
geometry	member	49	5.0000	11.0000	90.5000	Start	-Y3 Local Edge	Reference Line	No Curve			
geometry	member	49	15.0000	11.0000	82.5000	Start	-Y3 Local Edge	Reference Line	No Curve			
path	member	50										
geometry	member	51	5.0000	11.0000	82.5000	Start	-Y3 Local Edge	Reference Line	No Curve			
geometry	member	51	15.0000	11.0000	90.5000	Start	-Y3 Local Edge	Reference Line	No Curve			
geometry	member	52	5.0000	11.0000	98.5000	Start	-Y3 Local Edge	Reference Line	No Curve			
path	member	53										
path	member	54										
path	member	55										
geometry	member	56	0.0000	123.0000	152.0000	End	-Y3 Local Edge	Reference Line	No Curve			

TENDON S5-T6R

Point Type	Reference Object Type	Reference Object	Offset X	Offset Y	Offset Z	X Reference	Y Reference	Z Reference	Curvature Type			Width
geometry	member	44	0.0000	123.0000	143.0000	Start	-Y3 Local Edge	Reference Line	No Curve			
path	member	45										
path	member	46										
path	member	47										
path	member	48										
geometry	member	49	5.0000	11.0000	98.5000	Start	-Y3 Local Edge	Reference Line	No Curve			
geometry	member	49	15.0000	11.0000	90.5000	Start	-Y3 Local Edge	Reference Line	No Curve			
path	member	50										
geometry	member	51	5.0000	11.0000	90.5000	Start	-Y3 Local Edge	Reference Line	No Curve			
geometry	member	51	15.0000	11.0000	98.5000	Start	-Y3 Local Edge	Reference Line	No Curve			
path	member	52										
path	member	53										
path	member	54										
path	member	55										
geometry	member	56	0.0000	123.0000	134.0000	End	-Y3 Local Edge	Reference Line	No Curve			

TENDON S5-T7R

Point Type	Reference Object Type	Reference Object or Range	Offset X (ft)	Offset Y (in)	Offset Z (in)	X Reference	Y Reference	Z Reference	Curvature Type			Width
geometry	member	44	0.0000	123.0000	125.0000	Start	-Y3 Local Edge	Reference Line	No Curve			
path	member	45										
path	member	46										
path	member	47										
path	member	48										
geometry	member	49	15.0000	11.0000	98.5000	Start	-Y3 Local Edge	Reference Line	No Curve			
path	member	50										
geometry	member	51	5.0000	11.0000	98.5000	Start	-Y3 Local Edge	Reference Line	No Curve			
path	member	52										
path	member	53										
path	member	54										
path	member	55										
geometry	member	56	0.0000	123.0000	116.0000	End	-Y3 Local Edge	Reference Line	No Curve			

TENDON S5-T8R

Point Type	Reference Object Type	Reference Object or Range	Offset X (ft)	Offset Y (in)	Offset Z (in)	X Reference	Y Reference	Z Reference	Curvature Type			Width
geometry	member	44	0.0000	21.0000	98.5000	Start	-Y3 Local Edge	Reference Line	No Curve			
geometry	member	45	1.5000	11.0000	98.5000	Start	-Y3 Local Edge	Reference Line	No Curve			
path	member	46										
geometry	member	47	5.0000	11.0000	98.5000	Start	-Y3 Local Edge	Reference Line	No Curve			
geometry	member	48	5.0000	11.0000	90.5000	Start	-Y3 Local Edge	Reference Line	No Curve			
geometry	member	48	15.0000	11.0000	82.5000	Start	-Y3 Local Edge	Reference Line	No Curve			
geometry	member	49	5.0000	11.0000	74.5000	Start	-Y3 Local Edge	Reference Line	No Curve			
geometry	member	49	15.0000	11.0000	74.5000	Start	-Y3 Local Edge	Reference Line	No Curve			
path	member	50										
geometry	member	51	5.0000	11.0000	74.5000	Start	-Y3 Local Edge	Reference Line	No Curve			
geometry	member	51	15.0000	11.0000	74.5000	Start	-Y3 Local Edge	Reference Line	No Curve			
geometry	member	52	5.0000	11.0000	82.5000	Start	-Y3 Local Edge	Reference Line	No Curve			
geometry	member	52	15.0000	11.0000	90.5000	Start	-Y3 Local Edge	Reference Line	No Curve			
geometry	member	53	15.0000	11.0000	90.5000	Start	-Y3 Local Edge	Reference Line	No Curve			
path	member	54										
geometry	member	55	2.0000	11.0000	90.5000	Start	-Y3 Local Edge	Reference Line	No Curve			
geometry	member	56	0.0000	21.0000	90.5000	End	-Y3 Local Edge	Reference Line	No Curve			

TENDON S6-T9L

Point Type	Reference Object Type	Reference Object or Range	Offset X (ft)	Offset Y (in)	Offset Z (in)	X Reference	Y Reference	Z Reference	Curvature Type			Width
geometry	member	55	0.0000	123.0000	-161.0000	Start	-Y3 Local Edge	Reference Line	No Curve			
path	member	56										
path	member	57										
path	member	58										
path	member	59										
geometry	member	60	5.0000	11.0000	-98.5000	Start	-Y3 Local Edge	Reference Line	No Curve			
geometry	member	60	15.0000	11.0000	-90.5000	Start	-Y3 Local Edge	Reference Line	No Curve			
geometry	member	61	5.0000	11.0000	-82.5000	Start	-Y3 Local Edge	Reference Line	No Curve			
geometry	member	62	15.0000	11.0000	-82.5000	Start	-Y3 Local Edge	Reference Line	No Curve			
geometry	member	63	5.0000	11.0000	-90.5000	Start	-Y3 Local Edge	Reference Line	No Curve			
geometry	member	63	15.0000	11.0000	-98.5000	Start	-Y3 Local Edge	Reference Line	No Curve			
path	member	64										

path	member	65										
geometry	member	66	0.0000	60.0000	-128.6900	End	-Y3 Local Edge	Reference Line	No Curve			

TENDON S6-T10L

Point Type	Reference Object Type	Reference Object or Range	Offset X (ft)	Offset Y (in)	Offset Z (in)	X Reference	Y Reference	Z Reference	Curvature Type			Width
geometry	member	55	0.0000	123.0000	-143.0000	Start	-Y3 Local Edge	Reference Line	No Curve			
path	member	56										
path	member	57										
path	member	58										
path	member	59										
geometry	member	60	15.0000	11.0000	-98.5000	Start	-Y3 Local Edge	Reference Line	No Curve			
geometry	member	61	5.0000	11.0000	-90.5000	Start	-Y3 Local Edge	Reference Line	No Curve			
geometry	member	62	15.0000	11.0000	-90.5000	Start	-Y3 Local Edge	Reference Line	No Curve			
geometry	member	63	5.0000	11.0000	-98.5000	Start	-Y3 Local Edge	Reference Line	No Curve			
path	member	64										
path	member	65										
geometry	member	66	0.0000	84.0000	-142.9400	End	-Y3 Local Edge	Reference Line	No Curve			

TENDON S6-T11L

Point Type	Reference Object Type	Reference Object or Range	Offset X (ft)	Offset Y (in)	Offset Z (in)	X Reference	Y Reference	Z Reference	Curvature Type			Width
geometry	member	55	0.0000	123.0000	-125.0000	Start	-Y3 Local Edge	Reference Line	No Curve			
path	member	56										
path	member	57										
path	member	58										
path	member	59										
path	member	60										
geometry	member	61	5.0000	11.0000	-98.5000	Start	-Y3 Local Edge	Reference Line	No Curve			
geometry	member	62	15.0000	11.0000	-98.5000	Start	-Y3 Local Edge	Reference Line	No Curve			
path	member	63										
path	member	64										
path	member	65										
geometry	member	66	0.0000	108.0000	-157.1250	End	-Y3 Local Edge	Reference Line	No Curve			

TENDON S6-T12L

Point Type	Reference Object Type	Reference Object or Range	Offset X (ft)	Offset Y (in)	Offset Z (in)	X Reference	Y Reference	Z Reference	Curvature Type			Width
geometry	member	55	0.0000	21.0000	-98.5000	Start	-Y3 Local Edge	Reference Line	No Curve			
geometry	member	56	2.0000	11.0000	-98.5000	Start	-Y3 Local Edge	Reference Line	No Curve			
path	member	57										
geometry	member	58	5.0000	11.0000	-98.5000	Start	-Y3 Local Edge	Reference Line	No Curve			
geometry	member	59	5.0000	11.0000	-98.0000	Start	-Y3 Local Edge	Reference Line	No Curve			
geometry	member	59	15.0000	11.0000	-90.5000	Start	-Y3 Local Edge	Reference Line	No Curve			
geometry	member	60	5.0000	11.0000	-82.5000	Start	-Y3 Local Edge	Reference Line	No Curve			
geometry	member	60	15.0000	11.0000	-74.5000	Start	-Y3 Local Edge	Reference Line	No Curve			
geometry	member	61	5.0000	11.0000	-74.5000	Start	-Y3 Local Edge	Reference Line	No Curve			
geometry	member	62	15.0000	11.0000	-74.5000	Start	-Y3 Local Edge	Reference Line	No Curve			
geometry	member	63	5.0000	11.0000	-74.5000	Start	-Y3 Local Edge	Reference Line	No Curve			
geometry	member	63	15.0000	11.0000	-82.5000	Start	-Y3 Local Edge	Reference Line	No Curve			

geometry	member	64	5.0000	11.0000	-90.5000	Start	-Y3 Local Edge	Reference Line	No Curve			
geometry	member	64	15.0000	11.0000	-98.5000	Start	-Y3 Local Edge	Reference Line	No Curve			
path	member	65										
geometry	member	66	0.0000	24.0000	-107.3750	End	-Y3 Local Edge	Reference Line	No Curve			

TENDON S6-T9R

Point Type	Reference Object Type	Reference Object or Range	Offset X (ft)	Offset Y (in)	Offset Z (in)	X Reference	Y Reference	Z Reference	Curvature Type			Width
geometry	member	55	0.0000	123.0000	161.0000	Start	-Y3 Local Edge	Reference Line	No Curve			
path	member	56										
path	member	57										
path	member	58										
path	member	59										
geometry	member	60	5.0000	11.0000	98.5000	Start	-Y3 Local Edge	Reference Line	No Curve			
geometry	member	60	15.0000	11.0000	90.5000	Start	-Y3 Local Edge	Reference Line	No Curve			
geometry	member	61	5.0000	11.0000	82.5000	Start	-Y3 Local Edge	Reference Line	No Curve			
geometry	member	62	15.0000	11.0000	82.5000	Start	-Y3 Local Edge	Reference Line	No Curve			
geometry	member	63	5.0000	11.0000	90.5000	Start	-Y3 Local Edge	Reference Line	No Curve			
geometry	member	63	15.0000	11.0000	98.5000	Start	-Y3 Local Edge	Reference Line	No Curve			
path	member	64										
path	member	65										
geometry	member	66	0.0000	60.0000	128.6900	End	-Y3 Local Edge	Reference Line	No Curve			

TENDON S6-T10R

Point Type	Reference Object Type	Reference Object or Range	Offset X (ft)	Offset Y (in)	Offset Z (in)	X Reference	Y Reference	Z Reference	Curvature Type			Width
geometry	member	55	0.0000	123.0000	143.0000	Start	-Y3 Local Edge	Reference Line	No Curve			
path	member	56										
path	member	57										
path	member	58										
path	member	59										
geometry	member	60	15.0000	11.0000	98.5000	Start	-Y3 Local Edge	Reference Line	No Curve			
geometry	member	61	5.0000	11.0000	90.5000	Start	-Y3 Local Edge	Reference Line	No Curve			
geometry	member	62	15.0000	11.0000	90.5000	Start	-Y3 Local Edge	Reference Line	No Curve			
geometry	member	63	5.0000	11.0000	98.5000	Start	-Y3 Local Edge	Reference Line	No Curve			
path	member	64										
path	member	65										
geometry	member	66	0.0000	84.0000	142.9400	End	-Y3 Local Edge	Reference Line	No Curve			

TENDON S6-T11R

Point Type	Reference Object Type	Reference Object or Range	Offset X (ft)	Offset Y (in)	Offset Z (in)	X Reference	Y Reference	Z Reference	Curvature Type			Width
geometry	member	55	0.0000	123.0000	125.0000	Start	-Y3 Local Edge	Reference Line	No Curve			
path	member	56										
path	member	57										
path	member	58										
path	member	59										
path	member	60										
geometry	member	61	5.0000	11.0000	98.5000	Start	-Y3 Local Edge	Reference Line	No Curve			
geometry	member	62	15.0000	11.0000	98.5000	Start	-Y3 Local Edge	Reference Line	No Curve			
path	member	63										
path	member	64										
path	member	65										
geometry	member	66	0.0000	108.0000	157.1250	End	-Y3 Local Edge	Reference Line	No Curve			

TENDON S6-T12R

Point Type	Reference Object Type	Reference Object or Range	Offset X (ft)	Offset Y (in)	Offset Z (in)	X Reference	Y Reference	Z Reference	Curvature Type			Width
geometry	member	55	0.0000	21.0000	98.5000	Start	-Y3 Local Edge	Reference Line	No Curve			
geometry	member	56	2.0000	11.0000	98.5000	Start	-Y3 Local Edge	Reference Line	No Curve			
path only	member	57										
geometry	member	58	5.0000	11.0000	98.5000	Start	-Y3 Local Edge	Reference Line	No Curve			
geometry	member	59	5.0000	11.0000	98.0000	Start	-Y3 Local Edge	Reference Line	No Curve			
geometry	member	59	15.0000	11.0000	90.5000	Start	-Y3 Local Edge	Reference Line	No Curve			
geometry	member	60	5.0000	11.0000	82.5000	Start	-Y3 Local Edge	Reference Line	No Curve			
geometry	member	60	15.0000	11.0000	74.5000	Start	-Y3 Local Edge	Reference Line	No Curve			
geometry	member	61	5.0000	11.0000	74.5000	Start	-Y3 Local Edge	Reference Line	No Curve			
geometry	member	62	15.0000	11.0000	74.5000	Start	-Y3 Local Edge	Reference Line	No Curve			
geometry	member	63	5.0000	11.0000	74.5000	Start	-Y3 Local Edge	Reference Line	No Curve			
geometry	member	63	15.0000	11.0000	82.5000	Start	-Y3 Local Edge	Reference Line	No Curve			
geometry	member	64	5.0000	11.0000	90.5000	Start	-Y3 Local Edge	Reference Line	No Curve			
geometry	member	64	15.0000	11.0000	98.5000	Start	-Y3 Local Edge	Reference Line	No Curve			
path only	member	65										
geometry	member	66	0.0000	24.0000	107.3750	End	-Y3 Local Edge	Reference Line	No Curve			

Stage Summary

Stage 1 'Span 1' Day = 88 Temp = 72°F Rel Hum = 70 %

Step 1 : Step 1

Construct Structure Groups

span 1

NO Support Activity.

NO Slave/Master Activity.

NO Tendon Activity.

NO Displacement Initialization Activity.

Load Activity

1 SW 1

2 S1 GrdRls/deviators 1

Step 2 : Step 2

No Construction activity

NO Support Activity.

NO Slave/Master Activity.

Tendon Activity

S1-T1L Stress

NO Displacement Initialization Activity.

NO Load Activity.

Step 3 : Step 3

No Construction activity

NO Support Activity.

NO Slave/Master Activity.

Tendon Activity

S1-T2L Stress

NO Displacement Initialization Activity.

NO Load Activity.

Step 4 : Step 4

No Construction activity

NO Support Activity.

NO Slave/Master Activity.

Tendon Activity

S1-T3L Stress

NO Displacement Initialization Activity.

NO Load Activity.

Step 5 : Step 5

No Construction activity

NO Support Activity.

NO Slave/Master Activity.

Tendon Activity

S1-T4L Stress

NO Displacement Initialization Activity.

NO Load Activity.

Step 6 : Step 6

No Construction activity

NO Support Activity.

NO Slave/Master Activity.

Tendon Activity

S1-T1R Stress

NO Displacement Initialization Activity.

NO Load Activity.

Step 7 : Step 7

No Construction activity

NO Support Activity.

NO Slave/Master Activity.

Tendon Activity

S1-T2R Stress

NO Displacement Initialization Activity.

NO Load Activity.

Step 8 : Step 8

No Construction activity

NO Support Activity.

NO Slave/Master Activity.

Tendon Activity

S1-T3R Stress

NO Displacement Initialization Activity.

NO Load Activity.

Step 9 : Step 9

No Construction activity

NO Support Activity.

NO Slave/Master Activity.

Tendon Activity

S1-T4R Stress

NO Displacement Initialization Activity.

NO Load Activity.

Stage 2 'Span 2' Day = 121 Temp = 72°F Rel Hum = 70 %

Step 1 : Step 1

Construct Structure Groups

span 2

NO Support Activity.

NO Slave/Master Activity.

NO Tendon Activity.

NO Displacement Initialization Activity.

Load Activity

1 SW 1

7 S2 GrdRls/deviators 1

Step 2 : Step 2

No Construction activity

NO Support Activity.

NO Slave/Master Activity.

Tendon Activity

S2-T5L Stress

NO Displacement Initialization Activity.

NO Load Activity.

Step 3 : Step 3

No Construction activity

NO Support Activity.

NO Slave/Master Activity.

Tendon Activity

S2-T6L Stress

NO Displacement Initialization Activity.

NO Load Activity.

Step 4 : Step 4

No Construction activity

NO Support Activity.

NO Slave/Master Activity.

Tendon Activity

S2-T7L Stress

NO Displacement Initialization Activity.

NO Load Activity.

Step 5 : Step 5

No Construction activity

NO Support Activity.

NO Slave/Master Activity.

Tendon Activity

S2-T8L Stress

NO Displacement Initialization Activity.

NO Load Activity.

Step 6 : Step 6

No Construction activity

NO Support Activity.

NO Slave/Master Activity.

Tendon Activity

S2-T5R Stress

NO Displacement Initialization Activity.

NO Load Activity.

Step 7 : Step 7

No Construction activity

NO Support Activity.

NO Slave/Master Activity.

Tendon Activity

S2-T6R Stress

NO Displacement Initialization Activity.

NO Load Activity.

Step 8 : Step 8

No Construction activity

NO Support Activity.

NO Slave/Master Activity.

Tendon Activity

S2-T7R Stress

NO Displacement Initialization Activity.

NO Load Activity.

Step 9 : Step 9

No Construction activity

NO Support Activity.

NO Slave/Master Activity.

Tendon Activity

S2-T8R Stress

NO Displacement Initialization Activity.

NO Load Activity.

Stage 3 'Span 3' Day = 130 Temp = 72°F Rel Hum = 70 %

Step 1 : Step 1

Construct Structure Groups

span 3

NO Support Activity.

NO Slave/Master Activity.

NO Tendon Activity.

NO Displacement Initialization Activity.

Load Activity

1 SW 1

3 S3 GrdRls/deviators 1

Step 2 : Step 2

No Construction activity

NO Support Activity.

NO Slave/Master Activity.

Tendon Activity

S3-T5L Stress

NO Displacement Initialization Activity.

NO Load Activity.

Step 3 : Step 3

No Construction activity

NO Support Activity.

NO Slave/Master Activity.

Tendon Activity

S3-T6L Stress

NO Displacement Initialization Activity.

NO Load Activity.

Step 4 : Step 4

No Construction activity

NO Support Activity.

NO Slave/Master Activity.

Tendon Activity

S3-T7L Stress

NO Displacement Initialization Activity.

NO Load Activity.

Step 5 : Step 5

No Construction activity

NO Support Activity.

NO Slave/Master Activity.

Tendon Activity

S3-T8L Stress

NO Displacement Initialization Activity.

NO Load Activity.

Step 6 : Step 6

No Construction activity

NO Support Activity.

NO Slave/Master Activity.

Tendon Activity

S3-T5R Stress

NO Displacement Initialization Activity.

NO Load Activity.

Step 7 : Step 7

No Construction activity

NO Support Activity.

NO Slave/Master Activity.

Tendon Activity

S3-T6R Stress

NO Displacement Initialization Activity.

NO Load Activity.

Step 8 : Step 8

No Construction activity

NO Support Activity.

NO Slave/Master Activity.

Tendon Activity

S3-T7R Stress

NO Displacement Initialization Activity.

NO Load Activity.

Step 9 : Step 9

No Construction activity

NO Support Activity.

NO Slave/Master Activity.

Tendon Activity

S3-T8R Stress

NO Displacement Initialization Activity.

NO Load Activity.

Stage 4 'Span 4' Day = 142 Temp = 72°F Rel Hum = 70 %

Step 1 : Step 1

Construct Structure Groups

span 4

NO Support Activity.

NO Slave/Master Activity.

NO Tendon Activity.

NO Displacement Initialization Activity.

Load Activity

1 SW 1

9 S4 GrdRls/deviators 1

Step 2 : Step 2

No Construction activity

NO Support Activity.

NO Slave/Master Activity.

Tendon Activity

S4-T5L Stress

NO Displacement Initialization Activity.

NO Load Activity.

Step 3 : Step 3

No Construction activity

NO Support Activity.

NO Slave/Master Activity.

Tendon Activity

S4-T6L Stress

NO Displacement Initialization Activity.

NO Load Activity.

Step 4 : Step 4

No Construction activity

NO Support Activity.

NO Slave/Master Activity.

Tendon Activity

S4-T7L Stress

NO Displacement Initialization Activity.

NO Load Activity.

Step 5 : Step 5

No Construction activity

NO Support Activity.

NO Slave/Master Activity.

Tendon Activity

S4-T8L Stress

NO Displacement Initialization Activity.

NO Load Activity.

Step 6 : Step 6

No Construction activity

NO Support Activity.

NO Slave/Master Activity.

Tendon Activity

S4-T5R Stress

NO Displacement Initialization Activity.

NO Load Activity.

Step 7 : Step 7

No Construction activity

NO Support Activity.

NO Slave/Master Activity.

Tendon Activity

S4-T6R Stress

NO Displacement Initialization Activity.

NO Load Activity.

Step 8 : Step 8

No Construction activity

NO Support Activity.

NO Slave/Master Activity.

Tendon Activity

S4-T7R Stress

NO Displacement Initialization Activity.

NO Load Activity.

Step 9 : Step 9

No Construction activity

NO Support Activity.

NO Slave/Master Activity.

Tendon Activity

S4-T8R Stress

NO Displacement Initialization Activity.

NO Load Activity.

Stage 5 'Span 5' Day = 164 Temp = 72°F Rel Hum = 70 %

Step 1 : Step 1

Construct Structure Groups

span 5

NO Support Activity.

NO Slave/Master Activity.

NO Tendon Activity.

NO Displacement Initialization Activity.

Load Activity

1 SW 1

10 S5 GrdRls/deviators 1

Step 2 : Step 2

No Construction activity

NO Support Activity.

NO Slave/Master Activity.

Tendon Activity

S5-T5L Stress

NO Displacement Initialization Activity.

NO Load Activity.

Step 3 : Step 3

No Construction activity

NO Support Activity.

NO Slave/Master Activity.

Tendon Activity

S5-T6L Stress

NO Displacement Initialization Activity.

NO Load Activity.

Step 4 : Step 4

No Construction activity

NO Support Activity.

NO Slave/Master Activity.

Tendon Activity

S5-T7L Stress

NO Displacement Initialization Activity.

NO Load Activity.

Step 5 : Step 5

No Construction activity

NO Support Activity.

NO Slave/Master Activity.

Tendon Activity

S5-T8L Stress

NO Displacement Initialization Activity.

NO Load Activity.

Step 6 : Step 6

No Construction activity

NO Support Activity.

NO Slave/Master Activity.

Tendon Activity

S5-T5R Stress

NO Displacement Initialization Activity.

NO Load Activity.

Step 7 : Step 7

No Construction activity

NO Support Activity.

NO Slave/Master Activity.

Tendon Activity

S5-T6R Stress

NO Displacement Initialization Activity.

NO Load Activity.

Step 8 : Step 8

No Construction activity

NO Support Activity.

NO Slave/Master Activity.

Tendon Activity

S5-T7R Stress

NO Displacement Initialization Activity.

NO Load Activity.

Step 9 : Step 9

No Construction activity

NO Support Activity.

NO Slave/Master Activity.

Tendon Activity

S5-T8R Stress

NO Displacement Initialization Activity.

NO Load Activity.

Stage 6 'Span 6' Day = 184 Temp = 72°F Rel Hum = 70 %

Step 1 : Step 1

Construct Structure Groups

span 6

NO Support Activity.

NO Slave/Master Activity.

NO Tendon Activity.

NO Displacement Initialization Activity.

Load Activity

1 SW 1

8 S6 GrdRls/deviators 1

Step 2 : Step 2

No Construction activity

NO Support Activity.

NO Slave/Master Activity.

Tendon Activity

S6-T9L Stress

NO Displacement Initialization Activity.

NO Load Activity.

Step 3 : Step 3

No Construction activity

NO Support Activity.

NO Slave/Master Activity.

Tendon Activity

S6-T10L Stress

NO Displacement Initialization Activity.

NO Load Activity.

Step 4 : Step 4

No Construction activity

NO Support Activity.

NO Slave/Master Activity.

Tendon Activity

S6-T11L Stress

NO Displacement Initialization Activity.

NO Load Activity.

Step 5 : Step 5

No Construction activity

NO Support Activity.

NO Slave/Master Activity.

Tendon Activity

S6-T12L Stress

NO Displacement Initialization Activity.

NO Load Activity.

Step 6 : Step 6

No Construction activity

NO Support Activity.

NO Slave/Master Activity.

Tendon Activity

S6-T9R Stress

NO Displacement Initialization Activity.

NO Load Activity.

Step 7 : Step 7

No Construction activity

NO Support Activity.

NO Slave/Master Activity.

Tendon Activity

S6-T10R Stress

NO Displacement Initialization Activity.

NO Load Activity.

Step 8 : Step 8

No Construction activity

NO Support Activity.

NO Slave/Master Activity.

Tendon Activity

S6-T11R Stress

NO Displacement Initialization Activity.

NO Load Activity.

Step 9 : Step 9

No Construction activity

NO Support Activity.

NO Slave/Master Activity.

Tendon Activity

S6-T12R Stress

NO Displacement Initialization Activity.

NO Load Activity.

Stage 7 'Stage 7' Day = 200 Temp = 72°F Rel Hum = 70 %

Currently NO Step in this Stage.

Stage 8 'Stage 8' Day = 300 Temp = 72°F Rel Hum = 70 %

Currently NO Step in this Stage.

Stage 9 'Stage 9' Day = 400 Temp = 72°F Rel Hum = 70 %

Currently NO Step in this Stage.

Stage 10 'Stage 9.5' Day = 500 Temp = 72°F Rel Hum = 70 %

Currently NO Step in this Stage.

Stage 11 'Stage 10' Day = 1000 Temp = 72°F Rel Hum = 70 %

Currently NO Step in this Stage.

Stage 12 'Stage 11' Day = 2000 Temp = 72°F Rel Hum = 70 %

Currently NO Step in this Stage.

Stage 13 'Stage 12' Day = 3000 Temp = 72°F Rel Hum = 70 %

Currently NO Step in this Stage.

Stage 14 'Stage 13' Day = 4000 Temp = 72°F Rel Hum = 70 %

Currently NO Step in this Stage.

Stage 15 'Stage 14' Day = 5000 Temp = 72°F Rel Hum = 70 %

Currently NO Step in this Stage.

Stage 16 'Stage 15 (2013)' Day = 9500 Temp = 72°F Rel Hum = 70 %

Step 1 : Step 1

No Construction activity

NO Support Activity.

NO Slave/Master Activity.

NO Tendon Activity.

NO Displacement Initialization Activity.

Load Activity

23 Unit Load (Section F) 1

Step 2 : Step 2

No Construction activity

NO Support Activity.

NO Slave/Master Activity.

NO Tendon Activity.

NO Displacement Initialization Activity.

Load Activity

24 Unit Load (Section E) 1

Appendix C. Original Drawings of Sections and Tendon Profiles

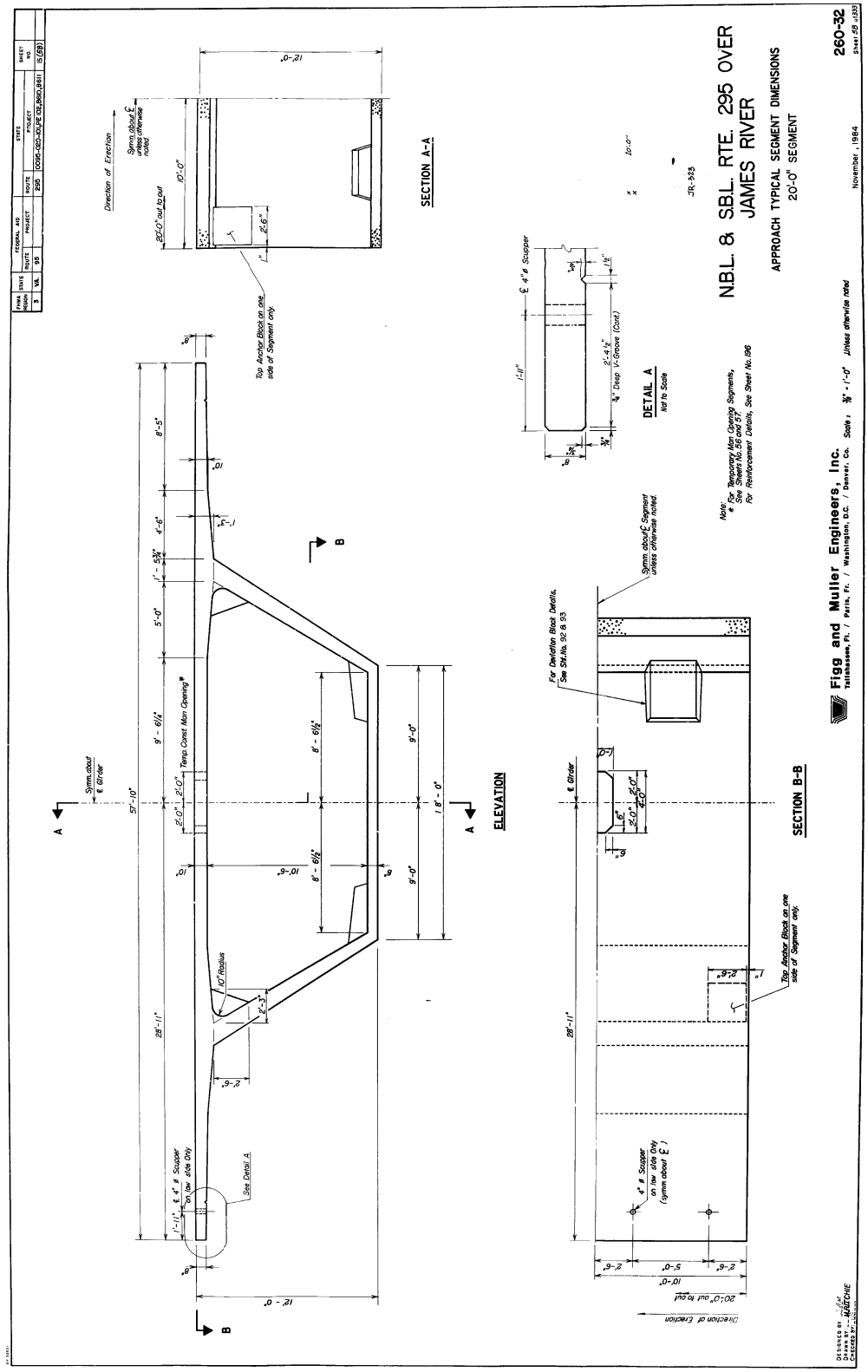

FHWA REGION	STATE	FEDERAL AID ROUTE	FEDERAL AID PROJECT	STATE ROUTE	STATE PROJECT	SHEET NO.
3	VA.	95		295	0095-020-101,PE 102,B610,B611	15 (61)

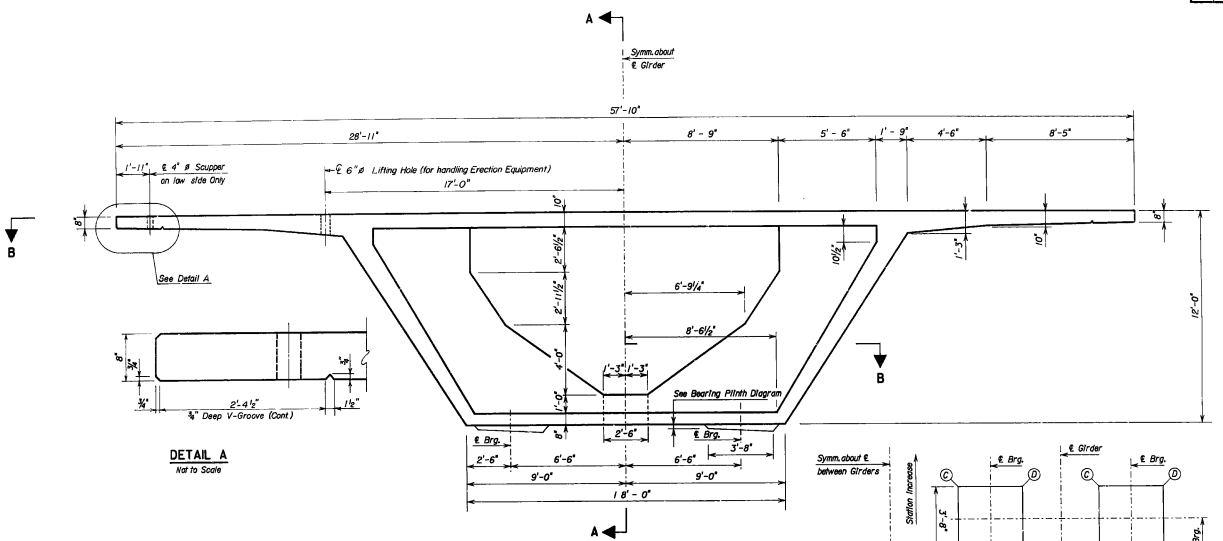

Pier	A	B	C	D
2-6	1 15/16"	1"	3 1/4"	2 5/16"
21	2 11/16"	2"	1 15/16"	1"
22	3 1/8"	2 3/16"	1 15/16"	1"
23-24	3 1/4"	2 5/16"	1 15/16"	1"
26-28	3 1/4"	2 5/16"	1 15/16"	1"

N.B.L. & S.B.L. RTE. 295 OVER JAMES RIVER

APPROACH PIER SEGMENT DIMENSIONS (9'-0" SEGMENT)

DESIGNED BY YG
DRAWN BY GLC
CHECKED BY

Figg and Muller Engineers, Inc.
Tallahassee, Fl. / Paris, Fr. / Washington, D.C. / Denver, Co.

Scale: 3/8" = 1'-0" Unless otherwise noted

November, 1984

260-32

Sheet 61 of 333

FHWA REGION	STATE	FEDERAL AID ROUTE	FEDERAL AID PROJECT	STATE ROUTE	STATE PROJECT	SHEET NO.
3	VA.	95		295	0095-020-101,PE 102,B610,B611	15(80)

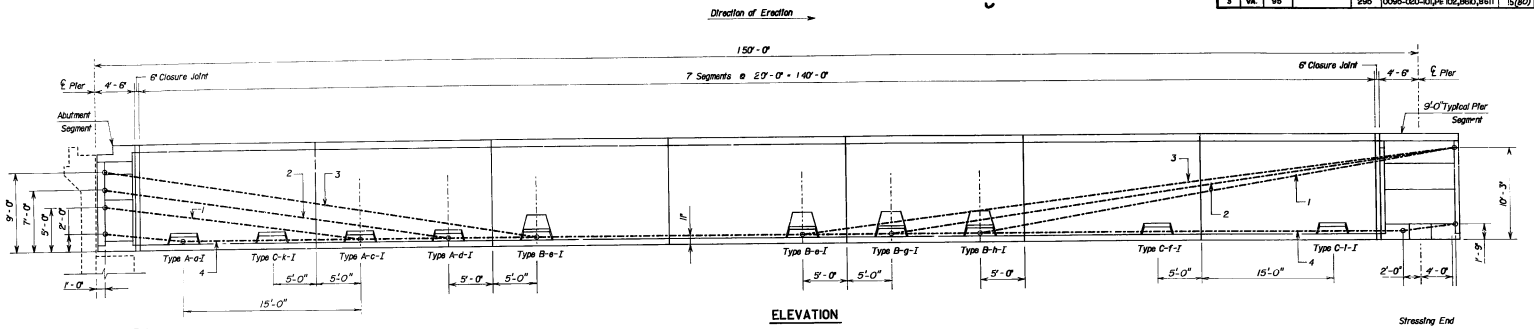

ELEVATION

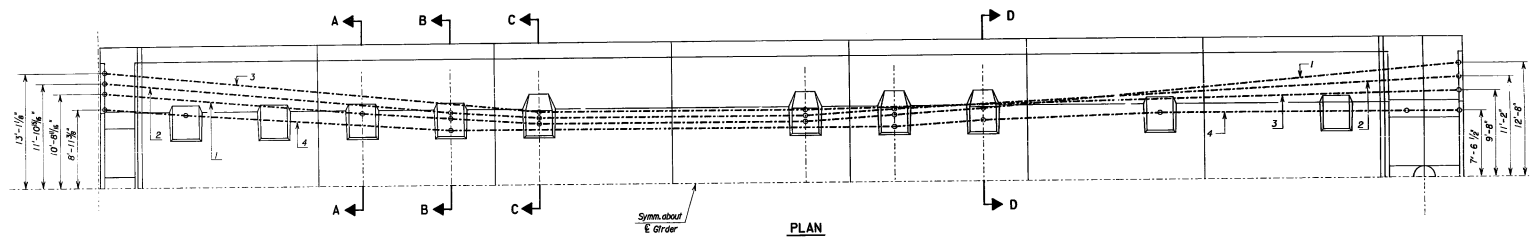

PLAN

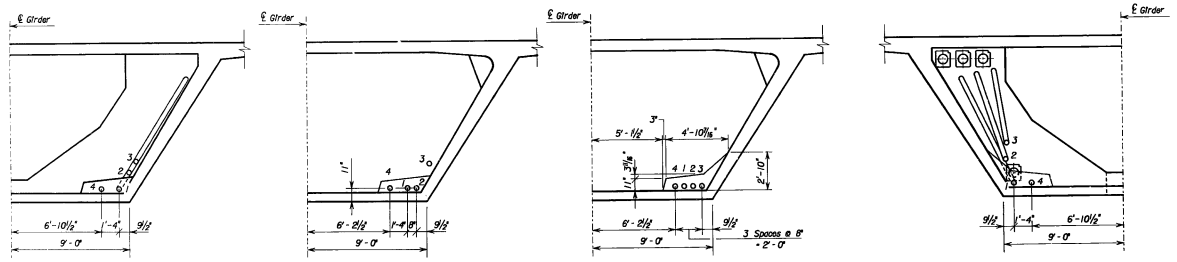

SECTION A - A

SECTION B - B

SECTION C - C

SECTION D - D

Note:
All Tendons are 19 - 0.6" ø Strands Each.

× 20'-0" Typ. Int. Segs.
40'-0" Typ. Pier Segs.

N.B.L. & S.B.L. RTE. 295 OVER JAMES RIVER

APPROACH END SPAN POST-TENSIONING LAYOUT I SPANS 1 & 28

Note: Geometric dimensions of Approach Deviation Blocks were revised by the Contractor.

DESIGNED BY C.C.
DRAWN BY M.R.
CHECKED BY

Figg and Muller Engineers, Inc.
Tallahassee, Fl. / Paris, Fr. / Washington, D.C. / Denver, Co.

Scale: 3/16" = 1'-0" Unless otherwise noted

November, 1984

260-32

Sheet 80 of 339

FHWA REGION	STATE	FEDERAL AID ROUTE	FEDERAL AID PROJECT	STATE ROUTE	STATE PROJECT	SHEET NO.
3	VA.	95		295	0095-020-101,PE102,B610,B611	15(81)

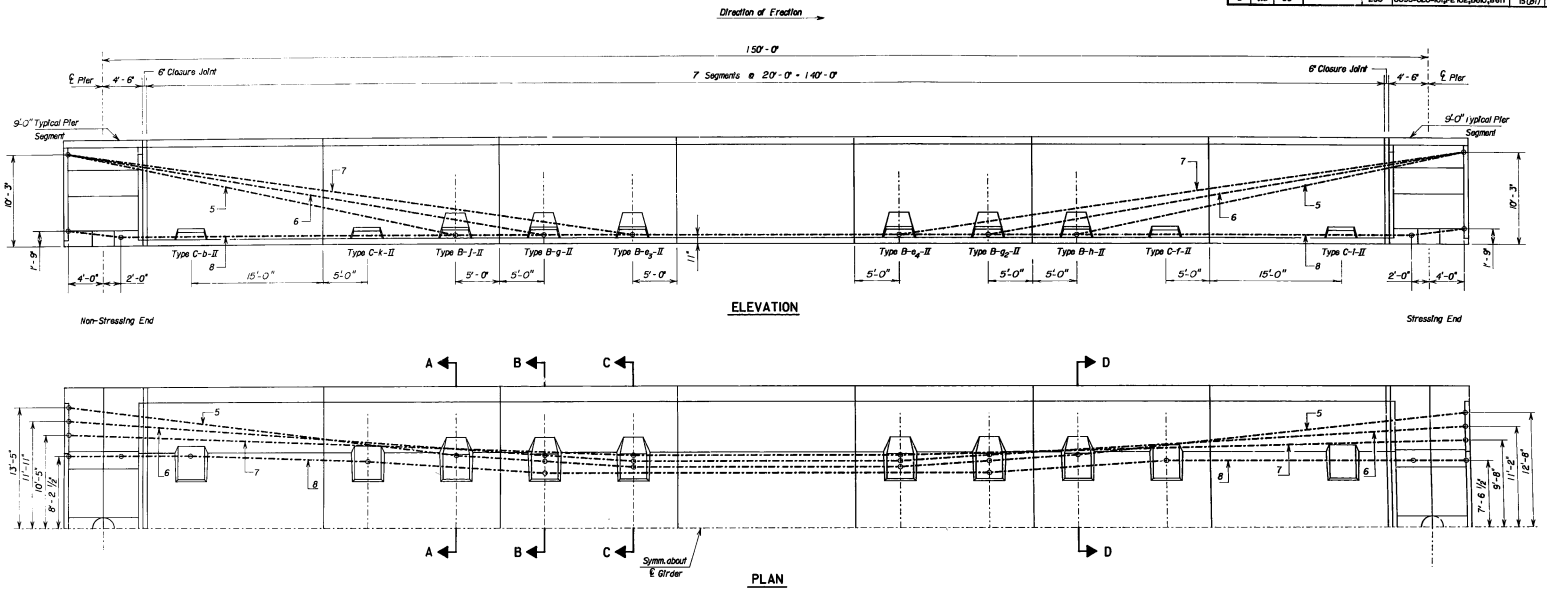

ELEVATION

PLAN

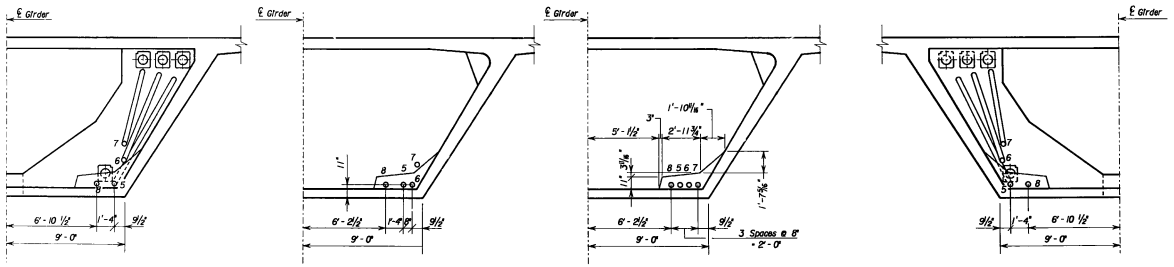

SECTION A - A

SECTION B - B

SECTION C - C

SECTION D - D

Note:
All Tendons are 13 - 0.6" ø Strands Each.

20'-0" Typ. Apt. Sec.
4'-0" Typ. Pier Sec.

N.B.L. & S.B.L. RTE. 295 OVER JAMES RIVER

APPROACH TYPICAL SPAN POST-TENSIONING LAYOUT II SPANS 2-5, 8-11, 21-23, 26 AND 27

Note: Geometric dimensions of Approach Deviation Blocks were revised by the Contractor.

Figg and Muller Engineers, Inc.
Tallahassee, Fl. / Paris, Fr. / Washington, D.C. / Denver, Co.

Scale: 3/16" = 1'-0" Unless otherwise noted

November, 1984

260-32

Sheet 81 of 333

DESIGNED BY
DRAWN BY JJC
CHECKED BY

FHWA REGION	STATE	FEDERAL AID ROUTE	FEDERAL AID PROJECT	STATE ROUTE	STATE PROJECT	SHEET NO.
3	VA.	95		295	0095-020-101,PE 102,B610,B611	15(82)

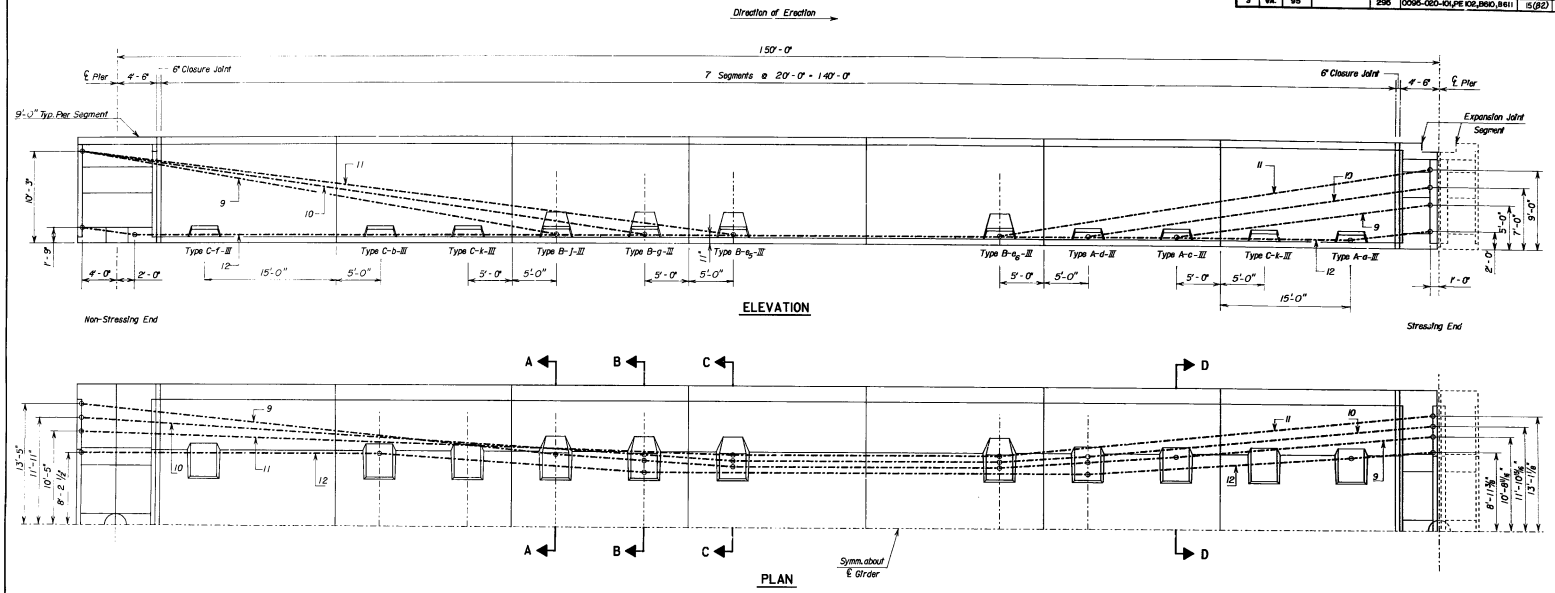

N.B.L. & S.B.L. RTE. 295 OVER JAMES RIVER

APPROACH EXPANSION JOINT SPAN POST-TENSIONING LAYOUT III SPANS 6, 12, 20 & 25

DESIGNED BY R.P.
DRAWN BY
CHECKED BY

Note: Geometric dimensions of Approach Deviation Blocks were revised by the Contractor.

Figg and Muller Engineers, Inc.
Tallahassee, Fl. / Paris, Fr. / Washington, D.C. / Denver, Co.

Scale: ⅜" = 1'-0" Unless otherwise noted

November, 1984

260-32

Sheet 82 of 333

FHWA REGION	STATE	FEDERAL AID ROUTE	FEDERAL AID PROJECT	STATE ROUTE	STATE PROJECT	SHEET NO.
3	VA.	95		295	0096-020-101,PE 102,B610,B611	15 (97)

LONGITUDINAL POST TENSIONING QUANTITIES APPROACH SUPERSTRUCTURE

Span No.	Tendon No.	Tendon Type	Tendon Length (ft)	Tendon Weight (lbs)	Number of Tendons / Girder	Total Weight (lbs)	Stressing Force (kips)
1,28	1	19-0.6" ϕ	153.99	2165	4	8,660	861
	2	19-0.6" ϕ	153.96	2164	4	8,658	865
	3	19-0.6" ϕ	154.03	2165	4	8,662	871
	4	19-0.6" ϕ	152.78	2148	4	8,592	861
2,3,4,5, 8,9,10,11, 21,22,23, 26,27,	5	19-0.6" ϕ	159.74	2245	26	58,370	879
	6	19-0.6" ϕ	159.03	2236	26	58,136	871
	7	19-0.6" ϕ	158.58	2229	26	57,954	865
	8	19-0.6" ϕ	157.30	2211	26	57,486	854
6,12 20,25,	9	19-0.6" ϕ	153.99	2165	8	17,320	889
	10	19-0.6" ϕ	153.96	2164	8	17,317	883
	11	19-0.6" ϕ	154.03	2165	8	17,325	874
	12	19-0.6" ϕ	152.78	2148	8	17,184	868
7,24	13	19-0.6" ϕ	153.99	2165	4	8,660	861
	14	19-0.6" ϕ	153.96	2164	4	8,656	865
	15	19-0.6" ϕ	154.03	2165	4	8,660	871
	16	19-0.6" ϕ	152.78	2148	4	8,592	861

TOTAL WEIGHT BOTH GIRDERS = 740,464 Lbs.

POST TENSIONING QUANTITIES APPROACH SUPERSTRUCTURE

Pier	Bar Size	Length	Weight (Lbs.)	Number of Anchorages	Number of Bars	Total Weight (Lbs.)	Stressing Force (kips)
8	1 3/8" ϕ	11.90	66	32	16	1058	1668
9	↓	↓	↓	↓	↓	↓	↓
10							
11							
12	1 3/8" ϕ	11.90	66	32	16	1058	1668
Totals	—	—	—	160	80	5291	—

Note: Totals shown are for One Girder only.

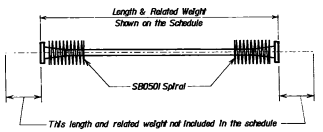

Note : All mild steel reinforcement for Post-tensioning shall be incidental to the system.

VERTICAL POST TENSIONING QUANTITIES APPROACH SUPERSTRUCTURE

Segment	Tendon No.	Number of Segs./ Girder	Tendon Type	Tendon Length (ft)	Tendon Weight (lbs)	Total Weight (lbs)	Stressing Force (kips)
Typical* Pier	A	34	4 x 0.6" ϕ	28.05	83	2823	185k
	B	34	4 x 0.6" ϕ	26.79	79	2696	↓
	C	34	4 x 0.6" ϕ	26.14	77	2630	
	D	34	4 x 0.6" ϕ	25.50	75	2566	
	A'	34	4 x 0.6" ϕ	28.01	83	2824	
	B'	34	4 x 0.6" ϕ	26.80	79	2696	
	C'	34	4 x 0.6" ϕ	26.14	77	2630	
	D'	34	4 x 0.6" ϕ	25.49	75	2565	
Exp.Jt. Pier	A	6	4 x 0.6" ϕ	28.47	84	505	
	B	6	4 x 0.6" ϕ	26.13	77	464	
	C	6	4 x 0.6" ϕ	26.55	79	474	
	D	6	4 x 0.6" ϕ	26.54	79	474	
	A'	6	4 x 0.6" ϕ	28.46	84	505	
	B'	6	4 x 0.6" ϕ	26.12	77	463	
	C'	6	4 x 0.6" ϕ	26.56	79	474	
	D'	6	4 x 0.6" ϕ	26.53	79	474	
Abut.	A	2	4 x 0.6" ϕ	28.47	84	168	
	B	2	4 x 0.6" ϕ	26.13	77	154	
	C	2	4 x 0.6" ϕ	26.55	79	158	
	D	2	4 x 0.6" ϕ	26.54	79	158	
	A'	2	4 x 0.6" ϕ	28.46	84	168	
	B'	2	4 x 0.6" ϕ	26.12	77	154	
	C'	2	4 x 0.6" ϕ	26.56	79	158	
	D'	2	4 x 0.6" ϕ	26.53	79	158	185k

TOTAL WEIGHT BOTH GIRDERS = 53,078 Lbs.

* 9'0" SEGMENTS
SIZE 8"

N.B.L. & S.B.L. RTE. 295 OVER JAMES RIVER

SUPERSTRUCTURE POST-TENSIONING QUANTITIES AND STRESSING SCHEDULE

DESIGNED BY
DRAWN BY
CHECKED BY

Figg and Muller Engineers, Inc.
Tallahassee, Fl. / Paris, Fr. / Washington, D.C. / Denver, Co.

Scale : N / A Unless otherwise noted

November, 1984

260-32

Sheet 97 of 133

Appendix D. Sample Calculation of Effective Prestress

Example Effective Prestress Calculation - Event 5/2/2013 6:25 PM

Introduction: The following calculations highlight and explain the method of calculating effective prestress from data gathered with the long-term monitoring system. For the purpose of this example one event from May 2, 2013 at 18:25 it taken, and all calculations are conducted.

$ORIGIN := 1$ Initialize vector origin designation

1. Material Property Definition

$E_c := 5000ksi$ Modulus of elasticity of concrete

$\alpha_c := 0.000011$ strain/degree C Coeficient of thermal expansion

2. Geometry Definition

$I_{tr} := 36807560in^4$ Transformed moment of inertia

$I_{cr} := 16346893in^4$ Transformed cracked moment inertia

$A_{tr} := 14037in^2$ Transformed gross sectional area

$A_{cr} := 12268in^2$ Cracked transformed sectional area. Taken as the gross stransformed section minus the bottom flange.

$n_{ps} := 8$ Number of prestressing tendons

$A_s := 0.217in^2 \cdot 19$ Area of one tendon.

$A_{ps} := n_{ps} \cdot A_s = 32.984\,in^2$ Area of prestressing tendons in span 6

$e_{cr} := 89.59in$ Eccentricity off tendons from cracked centroid

$y_{bar} := 107in$ Distance from bottom of section to centroid (uncracked)

$y := 98.5in$ Distance from uncracked transformed centroid to the top of the bottom flange

$y_{cr} := 112.67in$ Distance from cracked transformed centroid to the top of the bottom flange

$d_b := 145.5in$

3. Thermocouple locations,

Thermocouple distance from the bottom of the section

$$y_{TC} := (5.5\ \ 3.2\ \ 1\ \ 36.7\ \ 34.7\ \ 67.5\ \ 64.9\ \ 97\ \ 94.4\ \ 129.7\ \ 131.7\ \ 133.7\ \ 135.7\ \ 137.7\ \ 139\ \ 140\ \ 141\ \ 142\ \ 136\ \ 143\ \ 144.75)^T$$

Thermocouple distance from the centroid of the section

$y_{bar\_TC} := y_{bar} - y_{TC}$

Thermocouple Tributary Areas

$A_1 := 2 \cdot (543.4 \quad 248.3 \quad 228.8 \quad 188.7 \quad 188.7 \quad 212.1 \quad 212.1 \quad 257.5 \quad 257.5 \quad 333.8 \quad 158.6)^T \, in^2$: for clarity the vector of s is borken into two vectors, and combined afterwards

$A_2 := 2 \cdot (336.6 \quad 356.9 \quad 520.5 \quad 399 \quad 347 \quad 347 \quad 347 \quad 346 \quad 478.9 \quad 565)^T \, in^2$

$A_{tc} := stack(A_1, A_2)$ Vector of Thermocouple tributary areas.

4. Readings from the Long-Term Monitoring System

Reading from thermocouple at event

$TC_1 := (17.94 \quad 18.08 \quad 18.21 \quad 17.85 \quad 18.04 \quad 17.76 \quad 18.12 \quad 17.61 \quad 18.08 \quad 19.97)^T$ Note: for clarity the vector of temperatures is borken into two vectors, and combined afterwards

$TC_2 := (20.49 \quad 21.33 \quad 22.38 \quad 23.65 \quad 24.36 \quad 24.69 \quad 24.91 \quad 25.37 \quad 22.72 \quad 25.61)^T$

$TC := stack(TC_1, TC_2)$ Full tempertature vector

$\varepsilon_{ST01} := 14.47 \times 10^{-6} \frac{in}{in}$

5. Calculation of temperature in Deck overlay

$T_{cool} := \min(TC) = 17.61$ degree C Minimum temperature

$y_{cool} := 49.8in = 49.8\,in$ Depth of the minimum temperature

$TC_{deck} := \frac{(TC_{20} - T_{cool})}{\left[y_{cool} - \left(d_b - y_{TC_{20}}\right)\right]^5} \cdot (y_{cool} - 0.75in)^5 + T_{cool} = 27.204$ Tempertature in the deck overlay calculated by a fifth order approximation

$TC := stack(TC, TC_{deck})$ Full vector of temperatures, including deck temperature

6. Demands at section A-A gathered from FE model

$M_{2nd} := 15487.6kip \cdot ft$ Secondary moment. iterated from FE mode

$M_{cr} := 1274.8kip \cdot ft$ Moment due to creep on the redundant structure. Iterated from the FE model.

$M_{sh} := -100.7kip \cdot ft$ Moment due to shrinkage on the redundant structure. Iterate from the FE model.

$M_d := 20978kip \cdot ft$ Moment due to the dead load.

$P_{2nd} := 16.5kip$ Secondary axial forces. Iterated from FE model

$P_{cr} := -60.3kip$ Axial force due to creep on the redundant structure. Iterate from FE model.

$P_{sh} := 135kip$ Axial force due to shrinkage on the redundant structure. Iterate from FE model.

$P_{d} := -27kip$ Axial force due to the dead load.

7. Thermal Restraining Loads

$TC_{norm} := TC - T_{cool}$ Thermocouple data normalized to the coolest temp

$P_{th} := \left(A_{tc} \cdot TC_{norm}\right) \cdot \alpha_c \cdot E_c = 3.252 \times 10^{3}\,kip$ Restraining axial force from thermal gradient

$M_{th} := \overrightarrow{\left(TC_{norm} \cdot A_{tc}\right)} \cdot y_{bar\_TC} \cdot \alpha_c \cdot E_c = -9.77 \times 10^{4}\,kip \cdot in$ Restraining moment from thermal gradient

$r_{Pth\_AA} := -0.00535$ Coefficient relating restraining moment to moment at section AA. Found via FE model

$r_{Mth\_AA} := 0.878$ Coefficient relating restrain axial force to axial force at section AA. Found via FE model.

$P_{th\_AA} := r_{Pth\_AA} \cdot P_{th} = -17.396\,kip$ Axial force at section A due to restrained thermal movement by bearing stiffness.

$M_{th\_AA} := r_{Mth\_AA} \cdot M_{th} + y \cdot P_{th\_AA} = -8.749 \times 10^{4}\,kip \cdot in$ Moment at section AA due to thermal moment and eccentricity of the axial force imposed by the bearing stiffness.

8. Live load moment

$r_{\varepsilon AA} := 0.6889$ Coefficient relating the strain at section BB to the strain at section AA due to live loads.

$\varepsilon_{AA} := r_{\varepsilon AA} \cdot \varepsilon_{ST01}$ strain at the top of the bottom flange at section AA due to live load

$M_{live} := \frac{\varepsilon_{AA} \cdot E_c \cdot I_{tr}}{y} = 1.862 \times 10^{4}\,kip \cdot in$ Moment at section AA due to live load

9. Self-Equilibrating Stresses

$\sigma_{th} := -\left(TC_1 - T_{cool}\right)\cdot\alpha_c\cdot E_c = -18.15\ psi$

Stress at the top of the bottom flange of section A-A due to the thermal gradient applied to a fixed-fixed beam

$\sigma_{Pth} := \frac{P_{th}}{A_{tr}} = 231.638\ psi$

Stress due to the release of the restraining axial force

$\sigma_{Mth} := \frac{M_{th}\cdot y}{I_{tr}} = -261.447\ psi$

Stress at the top of the bottom flange of section A-A due to the release of the restraining moment

$\sigma_{SE} := \sigma_{th} + \sigma_{Pth} + \sigma_{Mth} = -47.959\ psi$

Total self-equilibrating stress at the top of the bottom flange at section A-A

10. Total External force on sectin A-A

$M_{total} := M_{live} + M_d + \left|M_{th\_AA}\right| + M_{2nd} + M_{cr} + M_{sh}$

Total moments acting on the beam at section A-A

$P_{total} := P_d + P_{th\_AA} + P_{2nd} + P_{cr} + P_{sh}$

Total axial force acting on the beam at section A-A

11. Effective Prestressing Force

$P_e := \left(\frac{M_{total}\cdot y_{cr}}{I_{cr}} + \frac{P_{total}}{A_{cr}} + \sigma_{SE}\right) \div \left(\frac{1}{A_{cr}} + \frac{e_{cr}\cdot y_{cr}}{I_{cr}}\right) = 5.437 \times 10^3\ kip$

$\sigma_{ps} := \frac{P_e}{A_{ps}} = 164.834\ ksi$

Average remaining prestress in span 6 tendons.

Appendix E. Sample Calculation of Flexural Capacity

Flexural Capacity Design of Span 6 of the Varina Enon Bridge

ORIGIN := 1

1. Material Property Definition

$E_c := 5000\text{ksi}$ — Modulus of elasticity of concrete

$E_{ps} := 27400\text{ksi}$ — Modulus of elasticity of prestressing strands

$f_{c28} := 5.5\text{ksi}$ — 28 day strength of concrete

$\beta_1 := \max\left[0.65, .85 - .15\cdot\left(\frac{f_{c28} - 4000\text{psi}}{1000\text{psi}}\right)\right] = 0.65$ — Beta Factor from AASHTO § 5.7.2.2

$f_{pu} := 270\text{ksi}$ — Ultimate tensile strength of prestressing strands

$f_{py} := 0.9\cdot f_{pu} = 243\cdot\text{ksi}$ — Yield stress of prestressing strands by ACI Table R20.3.2.3.1

$f_{pe} := 153.9\text{ksi}$ — Effective prestress from Field calculations

$\varepsilon_{cu} := .003$ — assumed crussing strain of unconfined concrete.

2. Geometry Definition

$L := 150\text{ft}$ — Span 6 length

$A_g := 13855.9\text{in}^2$ — Secion Area (uncracked, untransformed, no guardrail)

$I_g := 35725223\text{in}^4$ — Gross moment of inertial (uncracked, untransformed, no guardrail)

$n_{ps} := 8$ — Number of prestressing tendons

$A_{tendon} := 19\cdot 0.217\text{in}^2 = 4.123\cdot\text{in}^2$ — Area of steel in each tendon: (19) 0.6" diam strands

$A_{ps} := n_{ps}\cdot A_{tendon} = 32.984\text{in}^2$ — Area of prestressing steel

$h_{beam} := 145.5\text{in}$ — Depth of the section including topping slab.

$t_{tf} := 9.5\text{in}$ — Thickness of top flange before camfer

$b_{tf} := 57\text{ft} + 10\text{in}$ — Width of top flange

$t_{bf} := 8\text{in}$ — Thickness of bottom flange

$b_{bf} := 18\text{ft}$ — Smallest width of the bottom flange

$y_{bar} := 145.5\text{in} - 39.99\text{in} = 105.51\text{ in}$ — Distance from centroid to extreme fiber in tension

3. Check slenderness of the top flange by AASHTO § 5.7.4.7

$X_u := 27ft + 8.75in$ Width of the top flange between webs

$t := 11.5in$ Thickness of top flange between webs

$\lambda_t := \frac{X_u}{t} = 28.935$

4. Calculation of Positive Moment capcity at the critical section (60 ft south of pier 7)

$d_{p\_B} := h_{beam} - t_{bf} - 3in = 134.5\ in$ Distance from extreme compression fiber to centroid of prestressing @ 60ft from Pier 7.

$f_{ps1} := f_{pe} + 15ksi$ First iteration of stress in strand at ultimate

$L_i := (154.25 + 154 + 154 + 153)\cdot ft\cdot\frac{1}{4} = 1.846 \times 10^3\ in$ Average tendon length between anchorages.

$N_s := 0$ No bonded points because not bonded at deviators

$L_e := \frac{2\cdot L_i}{2 + N_s} = 1.846 \times 10^3\ in$ Effective tendon length between anchorages

Iterative procedure is performed to Solve to f.ps and c.

I.1 $a := \frac{A_{ps}\cdot f_{ps1}}{0.85\cdot f'_{c28}\cdot b_{tf}} = 1.717\ in$ Effective compression block (iteration 1)

$c := \frac{a}{\beta_1} = 2.642\ in$ Thus, the compression block is in the top flange

$f_{ps} := \min\left[f_{pe} + 900ksi\frac{(d_{p\_B} - c)}{(L_e)}, f_{py}\right] = 218.195\cdot ksi$ Resulting stress in strands at ultimate (iteration 1)

I.2 $a := \frac{A_{ps}\cdot f_{ps}}{0.85\cdot f'_{c28}\cdot b_{tf}} = 2.218\ in$ Effective compression block (iteration 2)

$c := \frac{a}{\beta_1} = 3.413\ in$ Thus, the compression block is in the top flange

$f_{ps} := \min\left[f_{pe} + 900ksi\frac{(d_{p\_B} - c)}{(L_e)}, f_{py}\right] = 217.819\cdot ksi$ Resulting stress in strands at ultimate (iteration 2)

I.3 $a := \frac{A_{ps}\cdot f_{ps}}{0.85\cdot f'_{c28}\cdot b_{tf}} = 2.214\ in$ Effective compression block (iteration 3)

$c := \frac{a}{\beta_1} = 3.407\ in$ Thus, the compression block is in the top flange

$f_{ps} := \min\left[f_{pe} + 900ksi\frac{(d_{p\_B} - c)}{(L_e)}, f_{py}\right] = 217.822\cdot ksi$ Resulting stress in strands at ultimate (iteration 3)

Calculate nominal flexural capacity

$$M_{n\_pos} := A_{ps} \cdot f_{ps} \cdot \left(d_{p\_B} - \frac{a}{2} \right) = 7.986 \times 10^{4} \cdot kip \cdot ft$$ Nominal Flexural strength at Section B-B at 9,500 days

Check the strain in most extreme steel in tension.

$$\varepsilon_{ps} := \frac{\varepsilon_{cu}}{c} \cdot \left(d_{p\_B} - \frac{c}{2} \right) = 0.117$$ > 0.005, so tension conctrolled, use Φ=0.90 $\Phi_f := 0.9$

Factored Flexural Capacity

$$\Phi M_{n\_pos} := \Phi_f \cdot M_{n\_pos} = 7.188 \times 10^{4} \cdot kip \cdot ft$$

5. Calculation of Negative Moment capacity at South end of pier 6

$$d_{p\_supp} := (11in + 8ft + 10.5in + 9ft + 9ft + 4in) \cdot \frac{1}{4} = 84.375\,in$$ Average depth to centroid of tendons at pier 6 Calculated from AutoCAD drawings

$d_t := 9ft + 3in$ Depth to the most extreme strand in tension

Iterative procedure is performed to Solve to f.ps and c.

$$a := \frac{A_{ps} \cdot f_{ps1}}{0.85 \cdot f_{c28} \cdot b_{bf}} = 5.517\,in$$ Effective compression block (iteration 1)

Thus, the compression block is in the bottom flange

$$c := \frac{a}{\beta_1} = 8.488\,in$$

$$f_{pss} := \min\left[f_{pe} + 900ksi \frac{(d_{p\_supp} - c)}{(L_e)}, f_{py} \right] = 190.903 \cdot ksi$$ Resulting stress in strands at ultimate (iteration 1)

$$a := \frac{A_{ps} \cdot f_{ps}}{0.85 \cdot f_{c28} \cdot b_{bf}} = 6.236\,in$$ Effective compression block (iteration 2)

Thus, the compression block is in the bottom flange

$$c := \frac{a}{\beta_1} = 9.593\,in$$

$$f_{pss} := \min\left[f_{pe} + 900ksi \frac{(d_{p\_supp} - c)}{(L_e)}, f_{py} \right] = 190.364 \cdot ksi$$ Resulting stress in strands at ultimate (iteration 2)

$$a := \frac{A_{ps} \cdot f_{ps}}{0.85 \cdot f_{c28} \cdot b_{bf}} = 6.218\,in$$ Effective compression block (iteration 3)

Thus, the compression block is in the bottom flange

$$c := \frac{a}{\beta_1} = 9.566\,in$$

$$f_{pss} := \min\left[f_{pe} + 900ksi \frac{(d_{p\_supp} - c)}{(L_e)}, f_{py} \right] = 190.377 \cdot ksi$$ Resulting stress in strands at ultimate (iteration 3)

Calculate nominal flexural capacity

$$M_{n\_supp} := A_{ps} \cdot f_{ps} \cdot \left(d_{p\_supp} - \frac{a}{2} \right) = 4.253 \times 10^{4} \cdot kip \cdot ft$$ Nominal Flexural strength at Section B-B at 9,500 days

Check the strain in most extreme steel in tension.

$$\varepsilon_{ps} := \frac{\varepsilon_{cu}}{c} \cdot \left(d_t - \frac{c}{2} \right) = 0.033$$ < 0.005, so Tension controlled $\Phi_f := 0.9$

Factored Flexural Capacity

$$\Phi M_{n\_supp} := \Phi_f \cdot M_{n\_supp} = 3.827 \times 10^{4} \cdot kip \cdot ft$$

6. Positive moment demand at the critical section (60 ft. South of pier 7)

$\eta_D := 1.00$ AASHTO 1.3.3: Ductility load modifier for conventional designs and details complying with these specifications

$\eta_R := 1.00$ AASHTO 1.3.4 Redundancy load modifier for conventional levels of redundancy.

$\eta_i := 1.05$ AASHTO 1.3.5 Operational Importance load modifier for critical, or essential bridges.

$M_{u\_pos\_S1} := \eta_i \cdot 64730 kip \cdot ft = 6.797 \times 10^{4} \cdot kip \cdot ft$ Demand taken for Strength I linear combination from FEM analysis

$$DCR_{pos} := \frac{M_{u\_pos\_S1}}{\Phi M_{n\_pos}} = 0.946$$ < 1.0 Demand capacity ratio at the critical section is less than 1, so the design checks for Strength 1

6. Negative moment demand at the critical section (South end of pier 6)

$M_{u\_supp\_S1} := -5373 kip \cdot ft \cdot \eta_i = -5.642 \times 10^{3} \cdot kip \cdot ft$ Demand taken for Strength I linear combination from FEM analysis

$$DCR := \frac{|M_{u\_supp\_S1}|}{\Phi M_{n\_supp}} = 0.147$$ < 1.0 Demand capacity ratio at the critical negative moment section is less than 1, so the design checks for strength 1